1966

Continuously tapered dielectric matching transitions for waveguides

William E. Hord

Department: Electrical and Computer Engineering

CONTINUOUSLY TAPERED DIELECTRIC MATCHING TRANSITIONS FOR WAVEGUIDES

A Dissertation

Presented to

the Faculty of the Graduate School

The University of Missouri at Rolla

In Partial Fulfillment

of the Requirements for the Degree

Doctor of Philosophy

---

by

William Eugene Hord - 1938

August 1966

Professor G. G. Skitek Dissertation Supervisor

ABSTRACT

Dielectric matching transitions at microwave frequencies are used for matching air filled waveguides into dielectric filled waveguides for maser work or into dielectric rod antennas. Also dielectric loading has been shown to improve the performance of the ferrite isolators.

The dielectric matching transitions that have been analyzed in the literature are of the stepped type. The continuously tapered dielectric matching transitions investigated in this dissertation provide increased bandwidth with very little increase of physical complexity.

The dissertation provides an analytical method for analysis and design for the continuously tapered dielectric matching transition. First-order and second-order approximate solutions for both symmetrical cross section and unsymmetrical cross section linearly tapered matching transitions are given. In addition other continuous tapers which promise lower reflection coefficients than the linear tapers are analyzed using the first-order approximation.

ACKNOWLEDGEMENTS

The author would like to acknowledge the guidance of Professor G. G. Skitek throughout his graduate education. The author would also like to acknowledge the most helpful comments Dr. E. C. Bertnolli has given him regarding this dissertation.

The author is appreciative of the help given by Mr. Robert Peirson in running the computer and helpful comments on the programming.

Thanks go to Mrs. Sharra Hinz for typing the manuscript.

Finally the author would like to acknowledge the patience and understanding of his family during the preparation of this dissertation.

TABLE OF CONTENTS

	Page
ABSTRACT	ii
ACKNOWLEDGEMENTS	iii
LIST OF FIGURES	v
LIST OF SYMBOLS	ix
I. INTRODUCTION TO DIELECTRIC MATCHING TRANSITIONS	1
II. APPLICATION OF THE GENERALIZED TELEGRAPHIST'S EQUATIONS TO CONTINUOUSLY TAPERED DIELECTRIC MATCHING TRANSITIONS	5
III. APPROXIMATE SOLUTIONS OF THE TELEGRAPHIST'S EQUATIONS	26
IV. LINEAR DIELECTRIC TAPERS	34
V. NONLINEAR UNSYMMETRICAL CONTINUOUSLY TAPERED TRANSITIONS	59
VI. EXPERIMENTAL PROCEDURES AND RESULTS	72
VII. CONCLUSIONS AND SUGGESTIONS FOR FURTHER DEVELOPMENT	87
BIBLIOGRAPHY	89
APPENDIX A PROOF OF THEOREM I AND ITS COROLLARY	91
APPENDIX B COMPUTER PROGRAMS	98
VITA	107

LIST OF FIGURES

Figure		Page
1	Rectangular Waveguide Orientation	10
2	Unsymmetrical Continuously Tapered Matching Transition	12
3	Symmetrical Side Continuously Tapered Matching Transition	15
4	Symmetrical Center Continuously Tapered Matching Transition	17
5	Transfer Admittances for UCT of Figure 2	20
6	Transfer Admittances for SSCT of Figure 3	21
7	Transfer Admittances for SCCT of Figure 4	22
8	Transfer Admittances for UCT of Figure 2	23
9	Transfer Admittances for SSCT of Figure 3	24
10	Transfer Admittances for SCCT of Figure 4	25
11	$\lvert\Gamma(0)\rvert$ Versus L/a for the Linear UCT with ω as Parameter	38
12	$\lvert\Gamma(0)\rvert$ Versus L/a for the Linear UCT with ϵ_r as Parameter	39
13	Comparison of First-Order and Second-Order Approximations for the Linear UCT with ω as Parameter	40
14	Comparison of First-Order and Second-Order Approximations for the Linear UCT with ϵ_r as Parameter	41
15	$\lvert\Gamma(0)\rvert$ Versus L/a for the Linear SSCT with ω as Parameter	44

Figure		Page
16	$\|\Gamma(0)\|$ Versus L/a for the Linear SSCT with ϵ_r as Parameter	45
17	Comparison of First-Order and Second-Order Approximations for the Linear SSCT with ω as Parameter	46
18	Comparison of First-Order and Second-Order Approximations for the Linear SSCT with ϵ_r as Parameter	47
19	$\|\Gamma(0)\|$ Versus L/a for the Linear SCCT with ω as Parameter	49
20	$\|\Gamma(0)\|$ Versus L/a for the Linear SCCT with ϵ_r as Parameter	50
21	Comparison of First-Order and Second-Order Approximations for the Linear SCCT with ω as Parameter	51
22	Comparison of First-Order and Second-Order Approximations for the Linear SCCT with ϵ_r as Parameter	52
23	$\|\Gamma(0)\|$ Versus L/a for the Three Linear Tapers for $\epsilon_r = 1.7$	53
24	$\|\Gamma(0)\|$ Versus L/a for the Three Linear Tapers for $\epsilon_r = 4.0$	54
25	Plot of Complex Integrand for the Linear UCT	56
26	Plot of Complex Integrand for the Linear SSCT	57
27	Plot fo Complex Integrand for the Linear SCCT	58
28	$\|\Gamma(0)\|$ Versus L/a for Bessel Line	64

Figure		Page
29	$\|\Gamma(0)\|$ Versus L/a for Parabolic Line	66
30	$\|\Gamma(0)\|$ Versus L/a for the Three Unsymmetrical Continuously Tapered Lines	68
31	Taper Shape for Bessel and Parabolic Lines	70
32	Variation of Z_o with Length for Bessel Line with ω as Parameter	71
33	Dielectric Slotted Line	74
34	Block Diagram of Experimental Equipment	75
35	VSWR Versus Frequency for an Abrupt Junction (L/a = 0)	77
36	VSWR Versus Frequency for the Linear UCT for L/a = 0.5	78
37	VSWR Versus Frequency for the Linear UCT for L/a = 1.0	79
38	VSWR Versus Frequency for the Linear UCT for L/a = 1.5	80
39	VSWR Versus Frequency for the Linear SSCT for L/a = 0.5	81
40	VSWR Versus Frequency for the Linear SSCT for L/a = 1.0	82
41	VSWR Versus Frequency for the Linear SCCT for L/a = 0.5	83
42	VSWR Versus Frequency for the Linear SCCT for L/a = 0.75	84
43	VSWR Versus Frequency for the Linear SCCT for L/a = 1.0	85

Figure		Page
44	VSWR Versus Frequency for the Linear SCCT for L/a = 1.5	86

LIST OF SYMBOLS

ω - radian frequency

μ - permeability

μ_o - free space permeability

ϵ - permittivity

ϵ_r - relative permittivity

ϵ_o - free space permittivity

TE - transverse electric

TEM - transverse electric and magnetic

TM - transverse magnetic

T_n^e - scalar mode function of n^{th} TE mode

T_n^h - scalar mode function of n^{th} TM mode

j - $\sqrt{-1}$

V_n^e - mode voltage of n^{th} TE mode

I_n^e - mode current of n^{th} TE mode

V_n^h - mode voltage of n^{th} TM mode

I_n^h - mode current of n^{th} TM mode

x,y,z - rectangular coordinates

$I_{z_n}^e$ - longitudinal current of n^{th} TE mode

$V_{z_n}^e$ - longitudinal current of n^{th} TM mode

Ω_n^e - cutoff constant of n^{th} TE mode

Ω_n^h - cutoff constant of n^{th} TM mode

δ_{mn} - Kronecker delta

a - waveguide width

b - waveguide height

Y_n - transfer admittance per unit length of n^{th} TE mode

Y_{mn} - transfer admittance per unit length between n^{th} and m^{th} TE modes

k_o - intrinsic wave number of free space

k - intrinsic wave number of dielectric

V - voltage along transmission line

I - current along transmission line

Z_o - characteristic impedance of transmission line

β - propagation constant of transmission line

Z - series impedance per unit length of transmission line

Y - shunt admittance per unit length of transmission line

Γ - reflection coefficeint

$\Gamma(0)$- input reflection coefficient

Z_{11} - impedance per unit length of all TE modes

VSWR- voltage standing wave ratio

CHAPTER I

INTRODUCTION TO DIELECTRIC MATCHING TRANSITIONS

A. Introduction

Dielectric matching transitions are used for matching from air filled waveguides into dielectric filled waveguides for maser application (1) or for dielectric rod antennas (2). Dielectric loading is also used to improve the performance of ferrite isolators (3,4) and, consequently, matching from an air filled waveguide into a waveguide of this kind is necessary.

Since microwave components and systems are being used more and more in both military and commerical applications it is very probable that the continuously tapered dielectric matching transitions will find considerable use.

B. Review of the Literature

The dielectric matching transitions reported in the literature (1,2,3) are all of the stepped type. This is natural since the stepped transition is quite easy to handle analytically. The use of the stepped transition permits one to ignore the effects of higher order waveguide modes at the discontinuities and treat the problem as the junction of two transmission lines having different characteristic impedances and propagation constants. This approach was used sucessfully by Collin (2) for matching into a dielectric filled waveguide. Sullivan and Parkes (3) used an approach similar to this to design a matching transition for a dielectric-loaded ferrite

device. Goodwin and Moss (1) analyzed a step transition for matching into a dielectric filled waveguide of different dimensions than the main waveguide for use in a traveling wave maser.

All stepped transitions suffer a common drawback. They are limited to a particular frequency band due to the resonances associated with the step dimensions. Although this may mot be a serious limitation now, it will become a restriction on the bandwidth of microwave systems since more and more broadband components are being developed. For this reason an investigation of continuously tapered matching transitions was deemed necessary.

Early in the investigation it was discovered that the results of nonuniform transmission line theory would give results which were quite useful as a first-order approximation. For this reason a review of some of the literature in this field is worthwhile.

The first to investigate a nonuniform transmission line was Heaviside (5) who studied a particular line in the family of lines called Bessel lines. Starr (6) later studied the complete family of Bessel lines. The hyperbolic line introduced by Scott (7) started a flood of literature on nonuniform transmission lines for TEM (transverse electric and magnetic) modes. Ghose (8), Klopfenstein (9), Willis and Sinha (10), Bolinder (11) and Yang (12) all contributed to the theory and various type lines appeared. Some of the more important lines were the parabolic line, the exponential line

and the Dolph-Chebyshev line. This work was culminated by Collin (13) who described a synthesis procedure for an optimum line. The line was optimum in the sense that the input reflection coefficient fell below a prescribed value in minimum length. An exact analysis of any type transmission line was formulated by Bertnolli (14).

C. Scope of the Investigation

Since previous work on nonuniform transmission lines dealt with the TEM mode (propagation constant is independent of z) these results cannot be used for waveguide modes (propagation constant is dependent on z). The first objective of this dissertation is to develop a method of dealing with waveguides which are filled nonhomogeneously with the nonhomogeneity being nonuniform in the direction of propagation.

The method described in the dissertation uses the generalized telegraphist's equations which convert the field equations into an infinite system of coupled transmission line equations. A first-order approximation considering only the dominant mode was investigated. A second-order approximation taking the next higher mode into account was also investigated. Numerical results were obtained for linearly tapered dielectric transitions both of symmetrical and unsymmetrical cross section.

Unsymmetrical transitions capable of producing a Bessel line and a parabolic line were investigated. Numerical results using the first-order approximation of both these lines

are presented and compared with the linearly tapered unsymmetrical transition.

CHAPTER II

APPLICATION OF THE GENERALIZED TELEGRAPHIST'S EQUATIONS TO CONTINUOUSLY TAPERED DIELECTRIC MATCHING TRANSITIONS

A. Generalized Telegraphist's Equations

The propagation of electromagnetic energy in a waveguide is determined by the solution of Maxwell's equations with the appropriate boundary conditions applied. Under certain sets of conditions, such as a rectangular waveguide filled with a homogeneous dielectric, the problem is solved using the method of separation of variables. This same method may be used whenever the waveguide boundary is circular or elliptic. The method will also work for a rectangular waveguide filled with two homogeneous dielectrics providing the dielectric interface is parallel to one of the sides of the waveguide. In general the method fails if the dielectric medium is nonhomegeneous.

The generalized telegraphist's equations as derived by Schelkunoff (15) may be used to obtain approximate solutions for a nonhomogeneous waveguide. The word approximate is used since the general equations contain an infinity of terms most of which can be safely ignored for an approximate analysis. The generalized telegraphist's equations expand the solution of a problem in a series of orthogonal functions. The orthogonal functions may be any set but the most practical set is provided by the solutions for waveguides which are filled with homogeneous media. These functions already satisfy the boundary conditions and the problem then is to obtain a series of

these solutions which also satisfy Maxwell's equations for the nonhomogeneous filled waveguide.

Schelkunoff's work provides such a series for any rectangular waveguide problem. This series then presents the solution in the form of coupled waveguide modes, and the solution of any particular problem will depend upon evaluating coupling coefficients between modes. Approximate analytic techniques take into account the dominant mode and those modes that are most tightly coupled to the dominant mode. This technique has yielded good results for a nonisotropic ferrite waveguide when only two modes are considered (15).

The generalized telegraphist's equations (15) in linear, isotropic, and nonhomogeneous media reduce to the following form.

$$V_m^e = -j\omega \sum_n I_{z_n}^e \iint_s \mu \, \Omega_n^e \, T_n^e \, T_m^e \, ds \qquad (1)$$

$$I_m^h = -j\omega \sum_n V_{z_n}^h \iint_s \epsilon \, \Omega_n^h \, T_n^h \, T_m^h \, ds \qquad (2)$$

$$\frac{dV_m^h}{dz} = j\omega \sum_n I_n^h \iint_s \left[-\mu \frac{\partial T_n^h}{\partial y} \frac{\partial T_m^h}{\partial y} - \mu \frac{\partial T_n^h}{\partial x} \frac{\partial T_m^h}{\partial x} \right] ds$$

$$+ j\omega \sum_n I_n^e \iint_s \left[\mu \frac{\partial T_n^e}{\partial x} \frac{\partial T_m^h}{\partial y} - \mu \frac{\partial T_n^e}{\partial y} \frac{\partial T_m^h}{\partial x} \right] ds$$

$$+ \Omega_m^h V_{z_m}^h \tag{3}$$

$$\frac{dV_m^e}{dz} = -j\omega \sum_n I_n^h \iint_s \left[-\mu \frac{\partial T_n^h}{\partial y} \frac{\partial T_m^e}{\partial x} + \mu \frac{\partial T_n^h}{\partial x} \frac{\partial T_m^e}{\partial y}\right] ds$$

$$-j\omega \sum_n I_n^e \iint_s \left[\mu \frac{\partial T_n^e}{\partial x} \frac{\partial T_m^e}{\partial x} + \mu \frac{\partial T_n^e}{\partial y} \frac{\partial T_m^e}{\partial y}\right] ds \tag{4}$$

$$\frac{dI_m^e}{dz} = j\omega \sum_n V_n^h \iint_s \left[-\epsilon \frac{\partial T_n^h}{\partial x} \frac{\partial T_m^e}{\partial y} + \epsilon \frac{\partial T_n^h}{\partial y} \frac{\partial T_m^e}{\partial x}\right] ds$$

$$+ j\omega \sum_n V_n^e \iint_s \left[-\epsilon \frac{\partial T_n^e}{\partial y} \frac{\partial T_m^e}{\partial y} - \epsilon \frac{\partial T_n^e}{\partial x} \frac{\partial T_m^e}{\partial x}\right] ds$$

$$+ \Omega_m^e I_{z_m}^e \tag{5}$$

$$\frac{dI_m^h}{dz} = -j\omega \sum_n V_n^h \iint_s \left[\epsilon \frac{\partial T_n^h}{\partial x} \frac{\partial T_m^h}{\partial x} + \epsilon \frac{\partial T_n^h}{\partial y} \frac{\partial T_m^h}{\partial y}\right] ds$$

$$-j\omega \sum_n V_n^e \iint_s \left[\epsilon \frac{\partial T_n^e}{\partial y} \frac{\partial T_m^h}{\partial x} - \epsilon \frac{\partial T_n^e}{\partial x} \frac{\partial T_m^h}{\partial y}\right] ds \tag{6}$$

The T's in all the above equations stand for scalar mode functions in an air filled waveguide. Each subscript denotes mode. The mode whose cutoff frequency is the lowest being numbered n = 1, the next lowest n = 2, etc. The

superscript e stands for a TE (transverse electric) mode and the superscript h stands for a TM (transverse magnetic) mode. Ω_m is the cutoff constant of the m^{th} mode. The surface s for all integrations is the waveguide cross section. μ and ϵ characterize the nonhomogeneity of the material in the waveguide.

The V_n's and I_n's in the equations are equivalent voltages and currents for the waveguide modes. These voltages and currents represent the variation of the transverse components of the electric and magnetic field intensities with z the direction of propagation. The V_{z_n}'s and I_{z_n}'s represent the variation of the longitudinal component of electric or magnetic field intensity in the direction of propagation.

Other relations helpful in simplying equations (1) through (6) are listed in the set of equations (7). The reader is referred to Schelkunoff (16) for proof of these. These relationships result from the orthogonality of the mode functions and their partial derivatives. δ_{mn} in equation (7) is the Kronecker delta equal to zero for $m \neq n$ and equal to 1 for $n = m$.

$$\Omega_m^e \, \Omega_n^e \iint_s T_n^e \, T_m^e \, ds = \Omega_m^h \, \Omega_n^h \iint_s T_n^h \, T_m^h \, ds = \delta_{mn} \qquad (a)$$

$$\iint_s T_n^e \, T_m^h \, ds = 0 \qquad (b)$$

$$\iint_s \left[\frac{\partial T_n^e}{\partial x} \frac{\partial T_m^e}{\partial x} + \frac{\partial T_n^e}{\partial y} \frac{\partial T_m^e}{\partial y} \right] ds = \delta_{mn} \qquad (c)$$

$$\iint_s \left[\frac{\partial T_n^e}{\partial x} \frac{\partial T_m^h}{\partial x} + \frac{\partial T_n^e}{\partial y} \frac{\partial T_m^h}{\partial y} \right] ds = 0 \qquad (d)$$

$$\iint_s \left[\frac{\partial T_n^e}{\partial x} \frac{\partial T_m^h}{\partial y} - \frac{\partial T_n^e}{\partial y} \frac{\partial T_m^h}{\partial x} \right] ds = 0 \qquad (e) \quad (7)$$

The following mode functions apply to the rectangular waveguide shown in Figure 1.

$$T_{pq}^h = N_{pq} \sin \frac{p\pi}{a} x \sin \frac{q\pi}{b} y$$

$$T_{po}^h = N_{po} \sin \frac{p\pi}{a} x$$

$$T_{oq}^h = N_{oq} \sin \frac{q\pi}{b} y$$

$$T_{pq}^e = N_{pq} \cos \frac{p\pi}{a} x \cos \frac{q\pi}{b} y$$

$$T_{p0}^e = N_{p0} \cos \frac{p\pi}{a} a$$

$$T_{0q}^e = N_{0q} \cos \frac{q\pi}{a} y \qquad (8)$$

$$N_{pq} = \frac{2}{\sqrt{ab}\ \Omega_{pq}}$$

$$N_{p0} = \sqrt{\frac{2}{ab}}\ \frac{1}{\Omega_{p0}}$$

$$N_{0q} = \sqrt{\frac{2}{ab}}\ \frac{1}{\Omega_{0q}}$$

$$\Omega_{pq}^h = \Omega_{pq}^e = \sqrt{\left(\frac{p\pi}{a}\right)^2 + \left(\frac{q\pi}{b}\right)^2}$$

p and q are integers 1, 2, 3, . . .

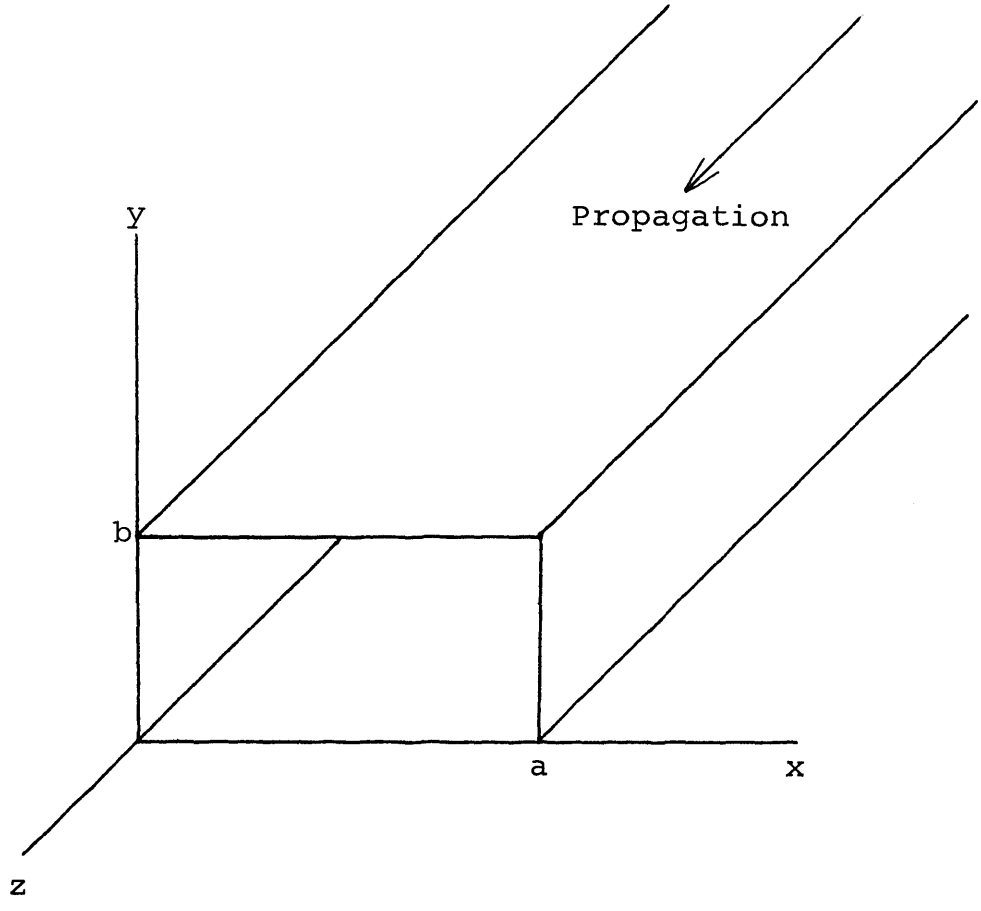

Figure 1. Rectangular Waveguide Orientation

A quite useful theorem will now be stated. Proof of this theorem is found in Appendix A.

Theorem I: Consider a dielectric matching transition consisting of a continuously tapered dielectric of constant permeability in a uniform rectangular waveguide. If the dielectric constant is independent of y only TE_{n0} modes where n = 1, 2, 3, ... exist in the transition when it is excited by the dominant TE_{10} mode.

B. Unsymmetrical Continuously Tapered Dielectric Matching Section

An unsymmetrical continuously tapered dielectric matching section (referred to as UCT hereafter) for matching an air filled waveguide to a dielectric filled waveguide is shown in Figure 2. At a typical cross section the nonhomogenenous region may be described by

$$\epsilon_r(x,y,z,t) = \epsilon_r(x) = \begin{cases} \epsilon_r & 0 < x < d(z) \\ 1 & d(z) < x < a \end{cases} \tag{9}$$

$$\mu(x,y,z,t) = \mu_0 \qquad 0 < x < a. \tag{10}$$

The incident mode on the transition section will be assumed to be a TE_{10} mode. From Theorem I the only modes which will be excited will be TE_{n0} modes. Only equations (1), (4) and (5) relate the TE modes and may be rewritten in the form

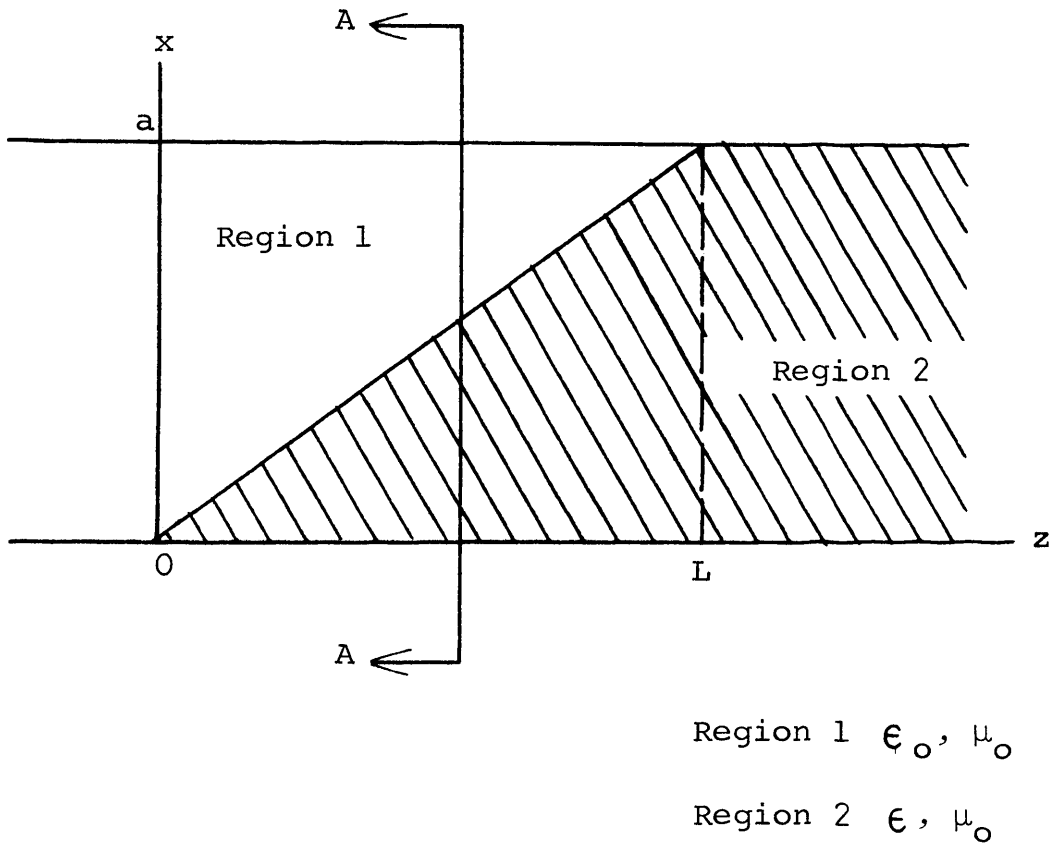

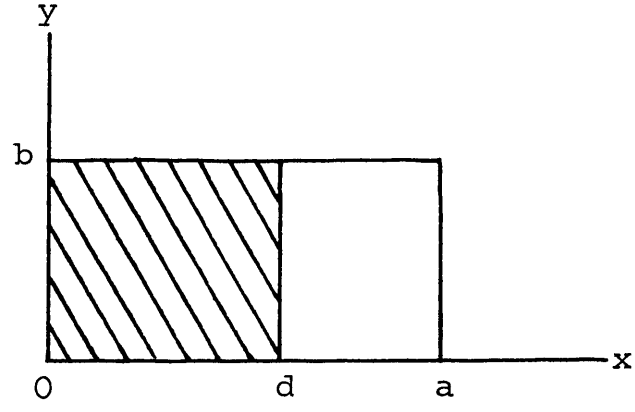

Section A-A

Figure 2. Unsymmetrical Continuously Tapered Matching Transition

$$\frac{dV_m^e}{dz} = -j\omega\mu_o I_m^e \tag{11}$$

$$\frac{dI_m^e}{dz} = -j\left[Y_m V_m^e + \sum_{n'} Y_{mn} V_n\right] \tag{12}$$

where

$$Y_m = \frac{-(\Omega_m^e)^2}{\omega \mu_o} + \omega \epsilon_o \iint_s \epsilon_r(x) \left[\left(\frac{\partial T_m^e}{\partial x}\right)^2 + \left(\frac{\partial T_m^e}{\partial y}\right)^2\right] ds \tag{13}$$

$$Y_{mn} = \omega \epsilon_o \iint_s \epsilon_r(x) \left[\frac{\partial T_m^e}{\partial x}\frac{\partial T_n^e}{\partial x} + \frac{\partial T_m^e}{\partial y}\frac{\partial T_n^e}{\partial y}\right] ds \tag{14}$$

and the n' indicates summation over all n except n = m. Y_m and Y_{mn} are transfer admittances expressed per unit length along the waveguide.

Substitution of the appropriate mode functions into equations (13) and (14) give for the transfer admittances upon integration

$$Y_m = \frac{k_o^2 - \left(\frac{m\pi}{a}\right)^2}{\omega \mu_o} + \frac{\omega \epsilon_o (\epsilon_r - 1)}{m\pi}\left(\frac{m\pi d}{a} - \frac{1}{2}\sin\frac{2m\pi d}{a}\right) \tag{15}$$

$$Y_{mn} = \frac{\omega \epsilon_o (\epsilon_r - 1)}{\pi}\left[\frac{\sin (n-m)\frac{\pi d}{a}}{n-m} - \frac{\sin (n+m)\frac{\pi d}{a}}{n+m}\right] \tag{16}$$

where $k_o = \omega\sqrt{\mu_o \epsilon_o}$ is the intrinsic wave number of free space.

The e superscript will be dropped from here on since only TE modes are under consideration.

C. Symmetrical Side Continuously Tapered Dielectric Section

A symmetrical side continuously tapered transition (SSCT) for matching into a dielectric filled waveguide is shown in Figure 3. For this configuration the nonhomogeneous region is described by

$$\epsilon_r(x,y,z,t) = \epsilon_r(x) = \begin{cases} \epsilon_r & 0 < x < d(z) \\ 1 & d(z) < x < a-d(z) \\ \epsilon_r & a-d(z) < x < a. \end{cases} \tag{17}$$

$$\mu(x,y,z,t) = \mu_o \qquad 0 < x < a. \tag{18}$$

A corollary of the theorem on page 9 will now be stated. The proof of this corollary is given in Appendix A.

Corollary: Consider a dielectric matching transition consisting of a continuously tapered dielectric of constant permeability in a uniform rectangular waveguide. If the dielectric constant is independent of y and in addition is symmetrical in x about the center of the waveguide only $TE_{(2n-1),0}$ modes where n = 1, 2, 3, . . . exist in the transition when it is excited by the dominant TE_{10} mode.

The generalized telegraphist's equations reduce to

$$\frac{dV_m}{dz} = -j\omega \mu_o I_m \tag{19}$$

$$\frac{dI_m}{dz} = -j \left[Y_m V_m + \sum_{n'} Y_{mn} V_n \right] \tag{20}$$

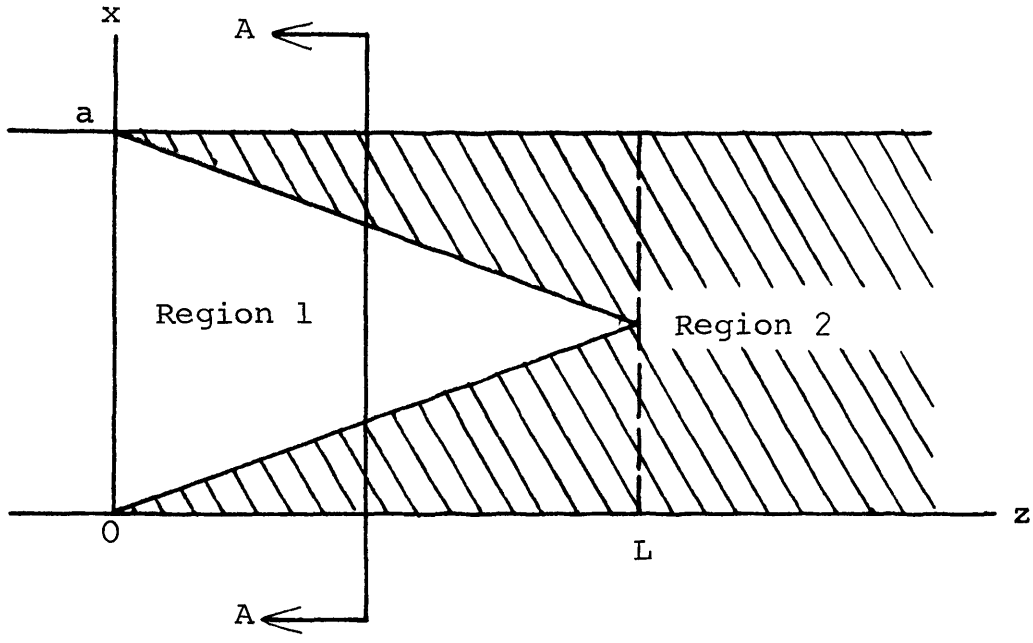

Region 1 ϵ_o, μ_o

Region 2 ϵ, μ_o

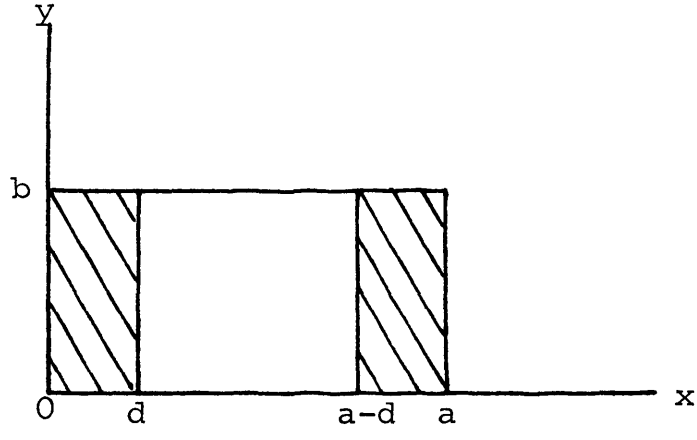

Section A-A

Figure 3. Symmetrical Side Continuously Tapered Matching Transition

where Y_m and Y_{mn} are defined by equations (13) and (14).

Substitution of the mode functions and use of equations (17) and (18) into (13) and (14) yields

$$Y_m = \frac{k_o^2 - (\frac{m\pi}{a})^2}{\omega \mu_o} + \frac{2\omega \epsilon_o(\epsilon_r - 1)}{m\pi}\left[\frac{m\pi d}{a} - \frac{1}{2}\sin\frac{2m\pi d}{a}\right] \tag{21}$$

$$Y_{mn} = \frac{\omega \epsilon_o(\epsilon_r - 1)}{\pi}\left[1 + (-1)^{m+n}\right]\left[\frac{\sin(n-m)\frac{\pi d}{a}}{n-m} - \frac{\sin(n+m)\frac{\pi d}{a}}{n+m}\right] \tag{22}$$

Substitution of m = 1 in equation (22) gives $Y_{mn} = 0$ for n even which satisfies the corollary.

D. Symmetrical Center Continuously Tapered Dielectric Matching Section

Another symmetrical method (SCCT) of matching into a dielectric filled waveguide is shown in Figure 4. The non-homogeneous region is described by

$$\epsilon_r(x,y,z,t) = \epsilon_r(x) = \begin{cases} 1 & 0 < x < d(z) \\ \epsilon_r & d(z) < x < a-d(z) \\ 1 & a-d(z) < x < a \end{cases} \tag{23}$$

and

$$\mu(x,y,z,t) = \mu_o \qquad 0 < x < a. \tag{24}$$

The generalized telegraphist's equations again reduce to

$$\frac{dV_m}{dz} = -j\omega \mu_o I_m \tag{25}$$

$$\frac{dI_m}{dz} = -j\left[Y_m V_m + \sum_{n'} Y_{mn} V_n\right] \tag{26}$$

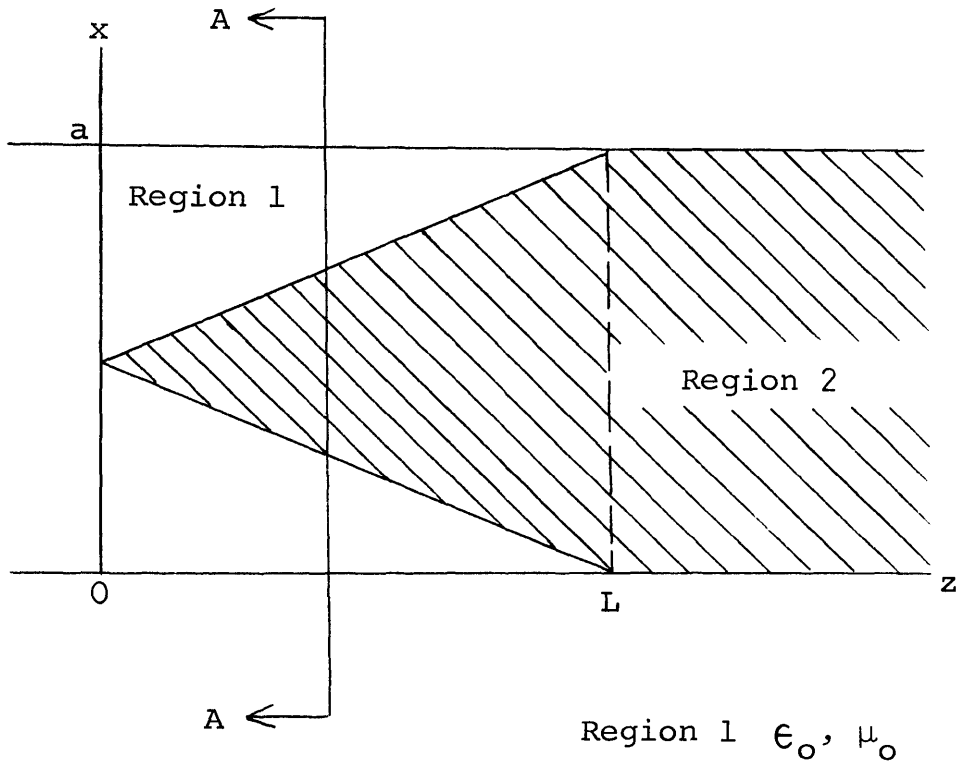

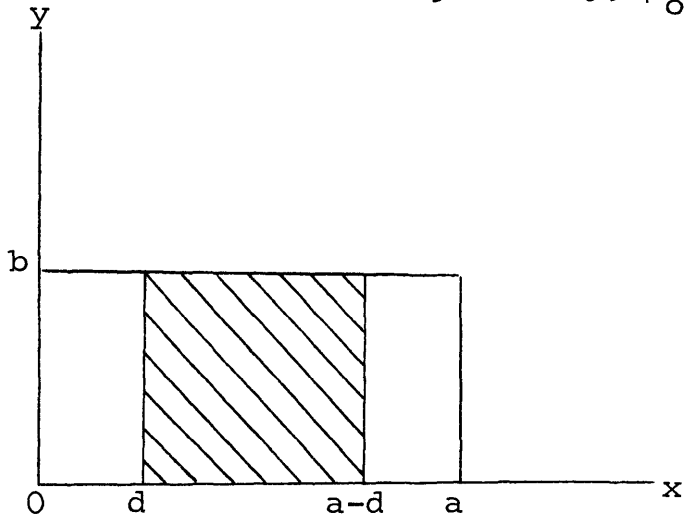

Section A-A

Figure 4. Symmetrical Center Continuously Tapered Matching Transition

where Y_m and Y_{mn} are given by equations (13) and (14).

Substitution of the mode functions and use of equations (23) and (24) into (13) and (14) yield

$$Y_m = \frac{k^2 - (\frac{m\pi}{a})^2}{\omega \mu_o} - \frac{2\omega \epsilon_o(\epsilon_r - 1)}{m\pi} \left[\frac{m\pi d}{a} - \frac{1}{2} \sin \frac{2m\pi d}{a}\right] \qquad (27)$$

$$Y_{mn} = \frac{\omega \epsilon_o(1 - \epsilon_r)}{\omega \mu_o} \left[1 + (-1)^{m+n}\right] \left[\frac{\sin(n-m)\frac{\pi d}{a}}{n-m} - \frac{\sin(n+m)\frac{\pi d}{a}}{n+m}\right] \qquad (28)$$

where $k = \omega \sqrt{\mu_o \epsilon_r \epsilon_o}$.

Two general conclusions may be drawn at this point. The first is that the transfer admittances are symmetrical, i.e. $Y_{12} = Y_{21}$. The second is that symmetrical tapers have an advantage over the unsymmetrical tapers since the coupling between the TE_{10} and the TE_{20} modes is zero for the symmetrical taper from the corollary. This means the symmetrical taper could be used at frequencies for which the TE_{20} mode is above cutoff and still have single mode propagation.

E. Transfer Admittances

The transfer admittances Y_{mn} give rise to coupling between the TE_{m0} mode and the TE_{n0} mode. Examination of the equations for Y_{mn} indicates that the coupling from the n^{th} mode to the m^{th} mode decrease as $1/n$ for $n >> m$. The higher order modes then are coupled only lightly to the dominant mode ($m = 1$).

For the unsymmetrical taper with the TE_{10} mode incident on the transition the TE_{20} mode is the mode coupled most tightly to the dominant mode. Since both Y_1 and Y_{12} are

monotonically increasing functions fo frequency any comparison of mode amplitudes should be made at the lowest frequency to be investigated. This comparison is shown in Figure 5 for $\epsilon_r = 1.7$ and f = 8.2 ghz. The computed transfer admittances are plotted versus d/a.

For both symmetrical transitions (see Figures 3 and 4) with the TE_{10} mode incident on the transition the TE_{20} mode is not excited and the TE_{30} mode is the most tightly coupled mode to the dominant mode. Figure 6 and 7 give mode amplitude comparisons for the symmetric side and center taper respectively for $\epsilon_r = 1.7$ and f = 8.2 ghz. Again the transfer admittances are plotted versus d/a.

The coupling between modes exist because of the nonhomogeneity of the cross section of the transition. The permittivity of the dielectric will effect the transfer admittances. Figures 8, 9, and 10 show the effect of the relative dielectric constants on the mode amplitudes for the different tapers. The value d/a was chosen so that Y_{1n} had a maximum or near maximum value.

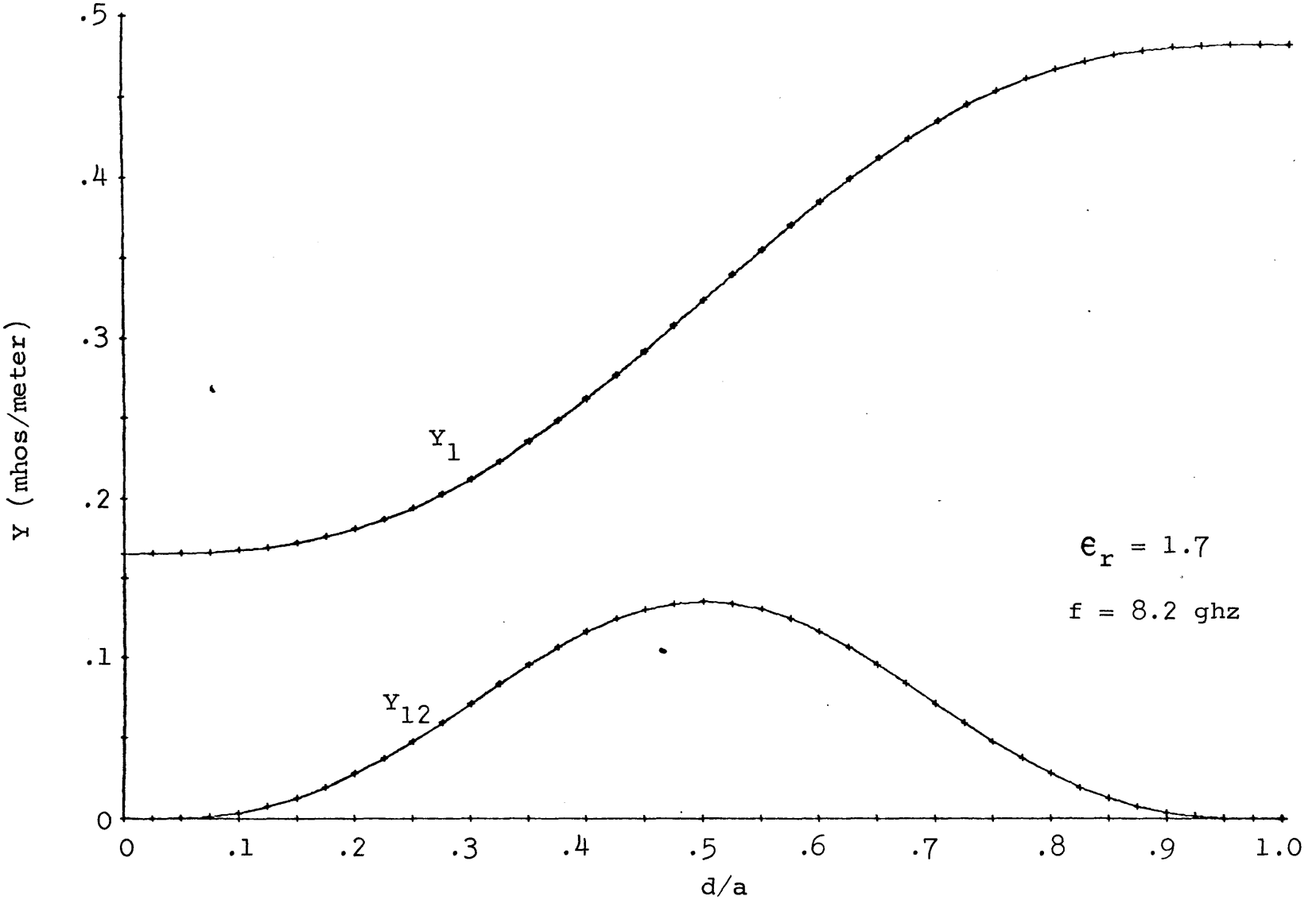

Figure 5. Transfer Admittances For UCT of Figure 2

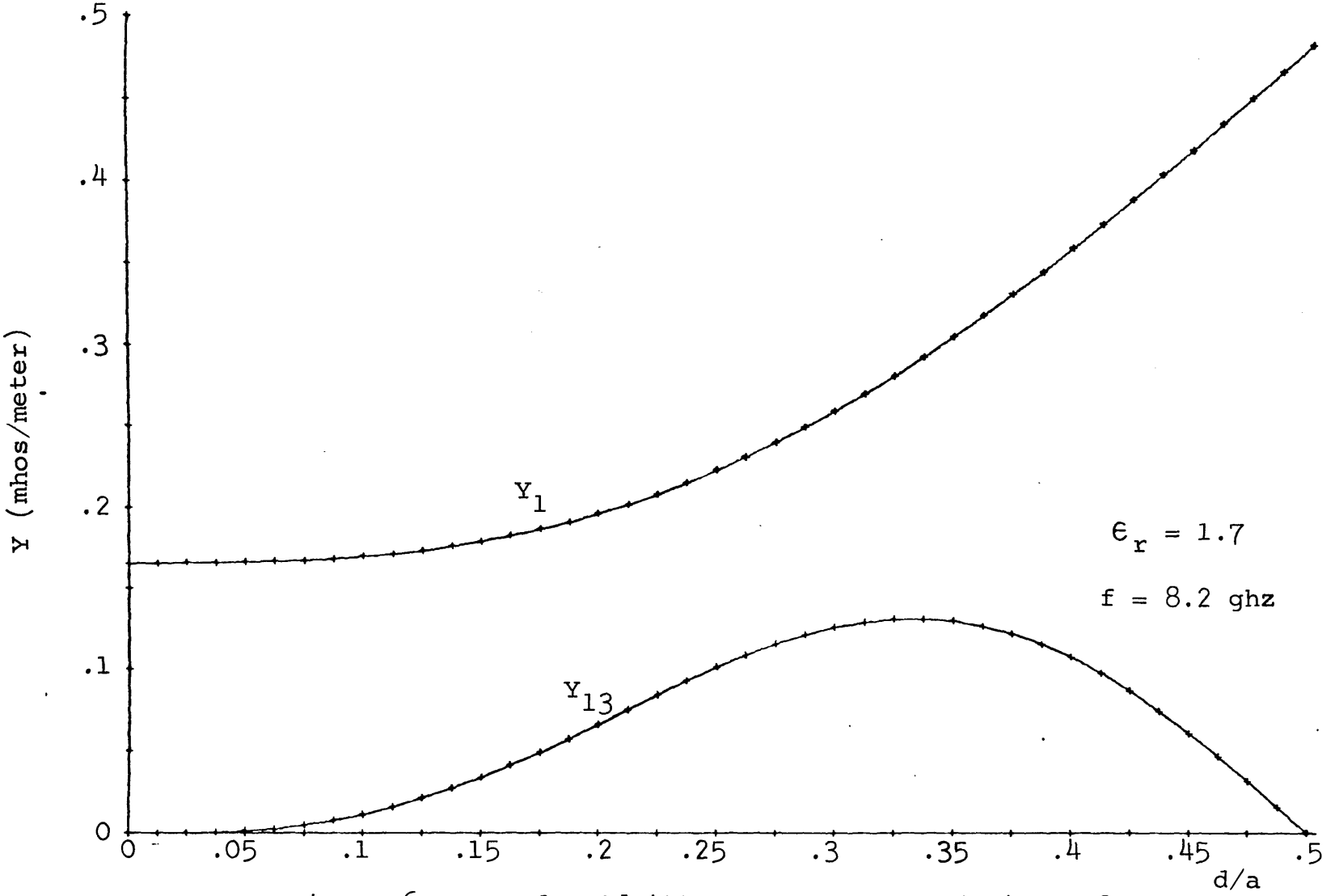

Figure 6. Transfer Admittances For SSCT of Figure 3

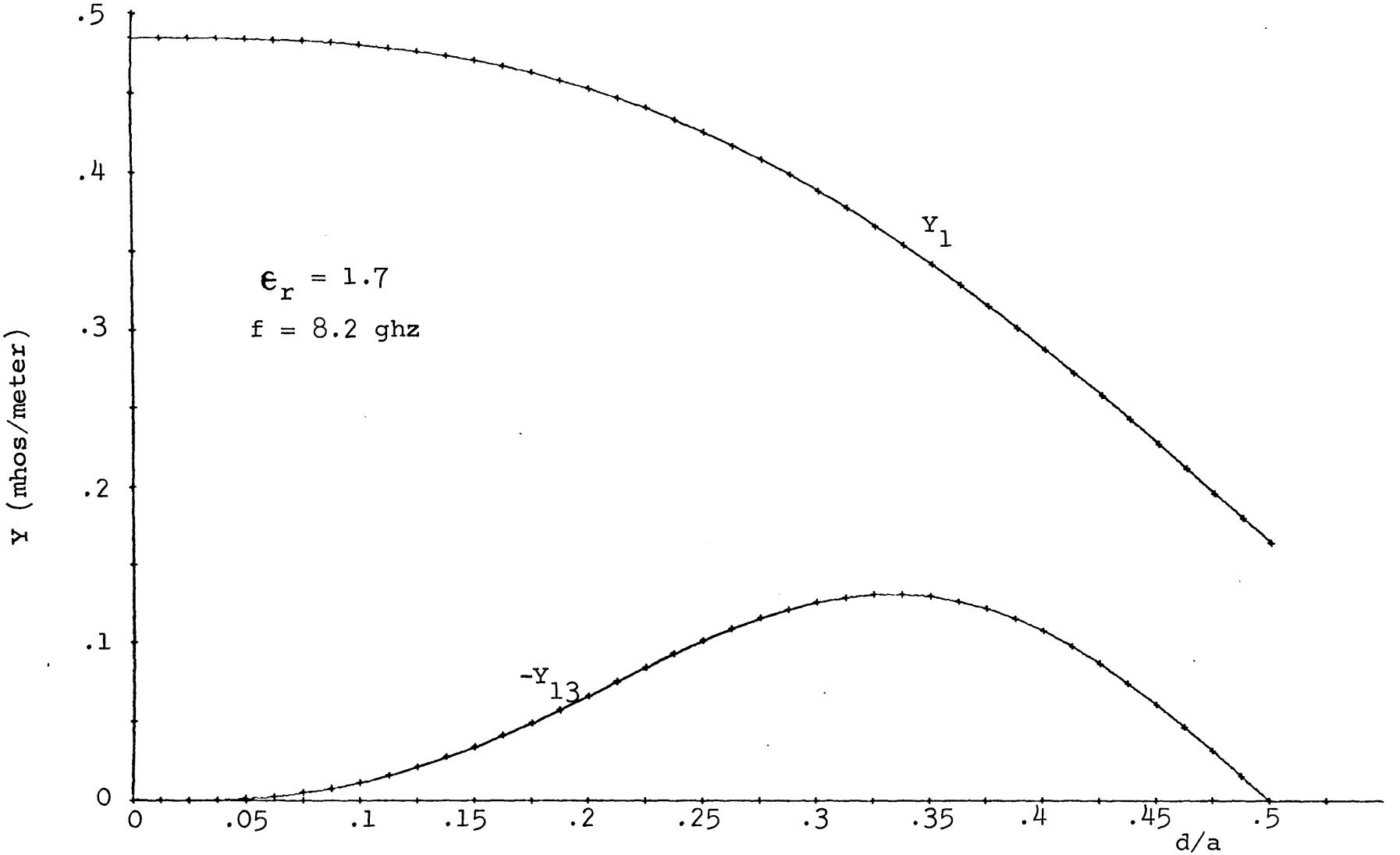

Figure 7. Transfer Admittances For SCCT of Figure 4

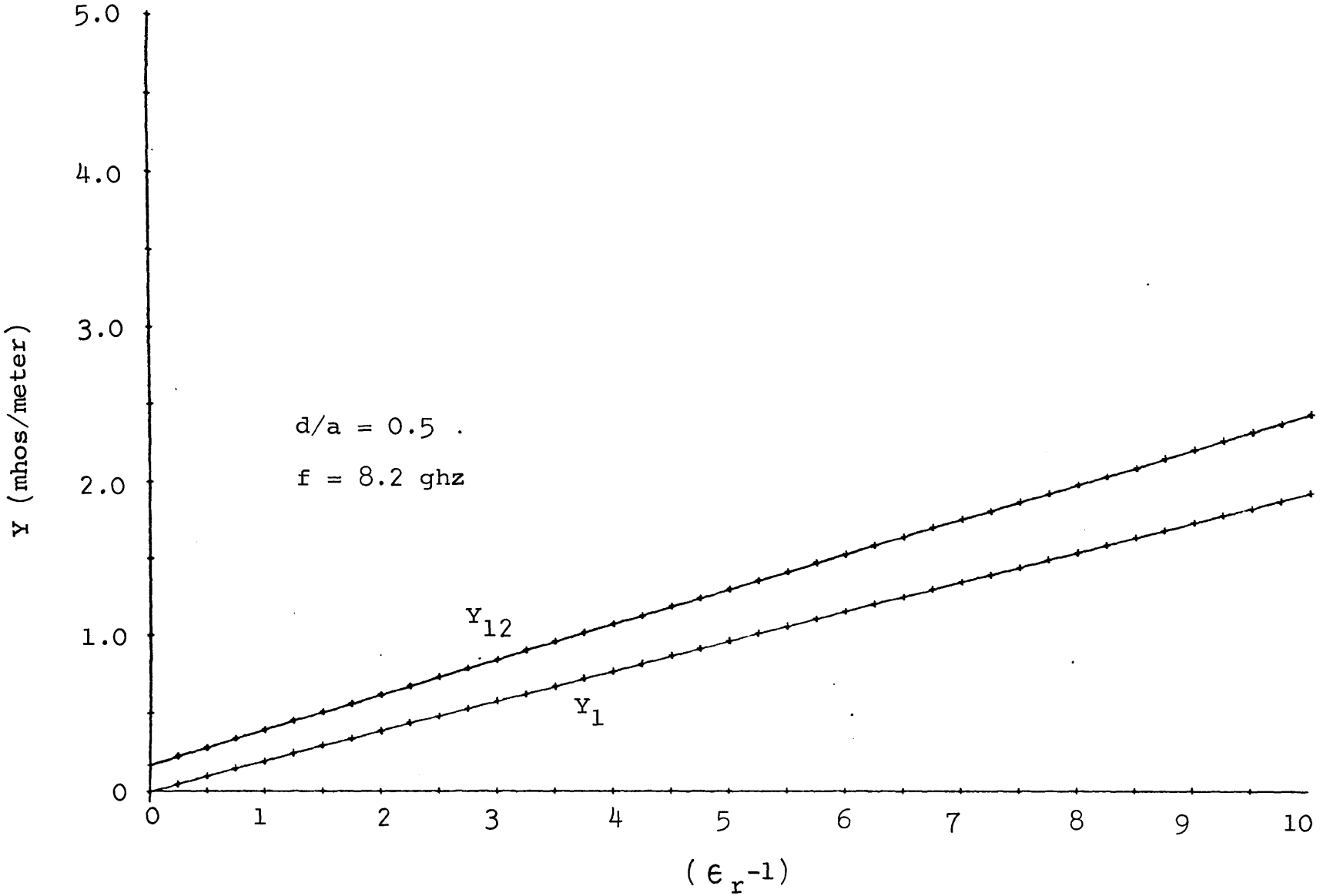

Figure 8. Transfer Admittances For UCT of Figure 2

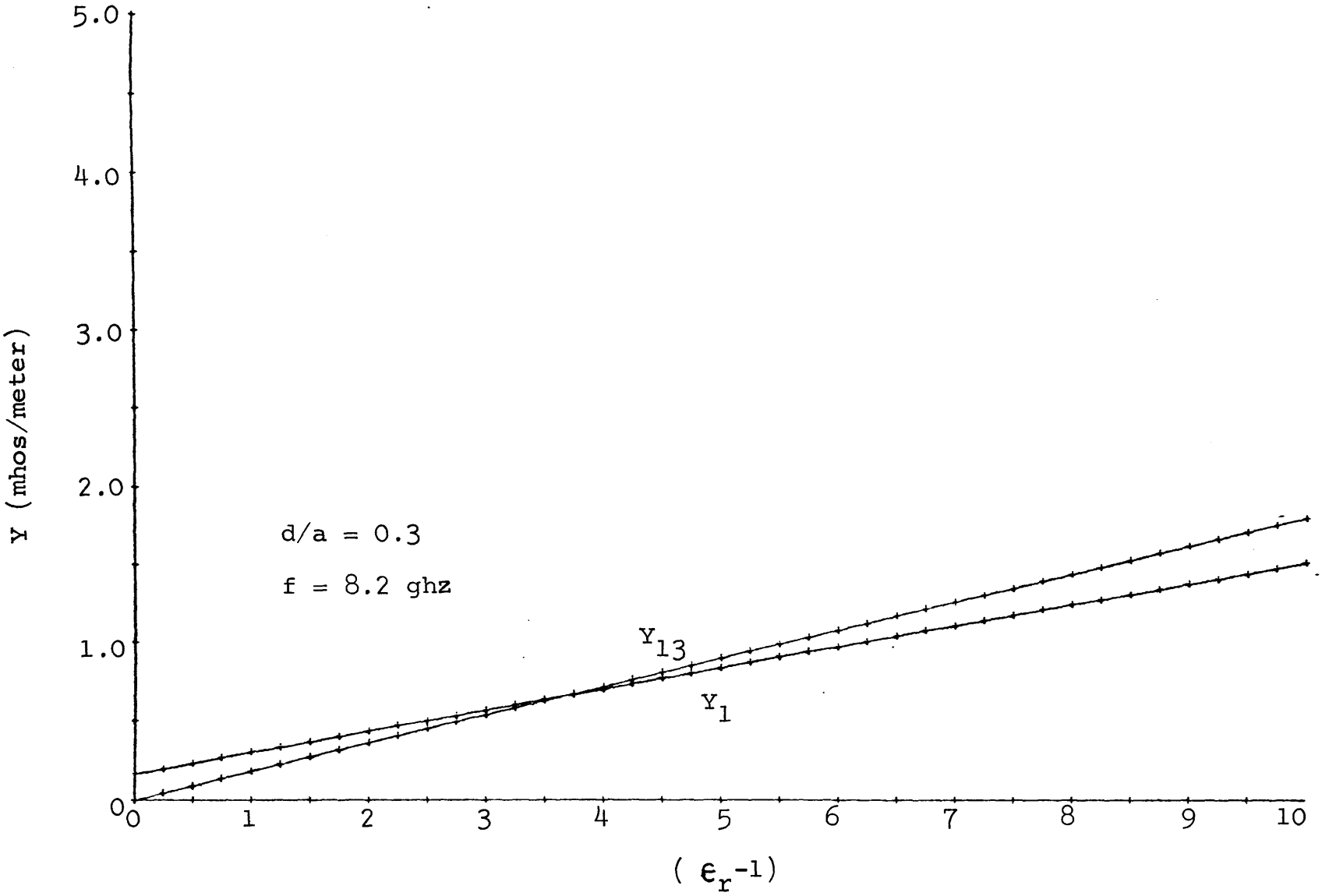

Figure 9. Transfer Admittances For SSCT of Figure 3

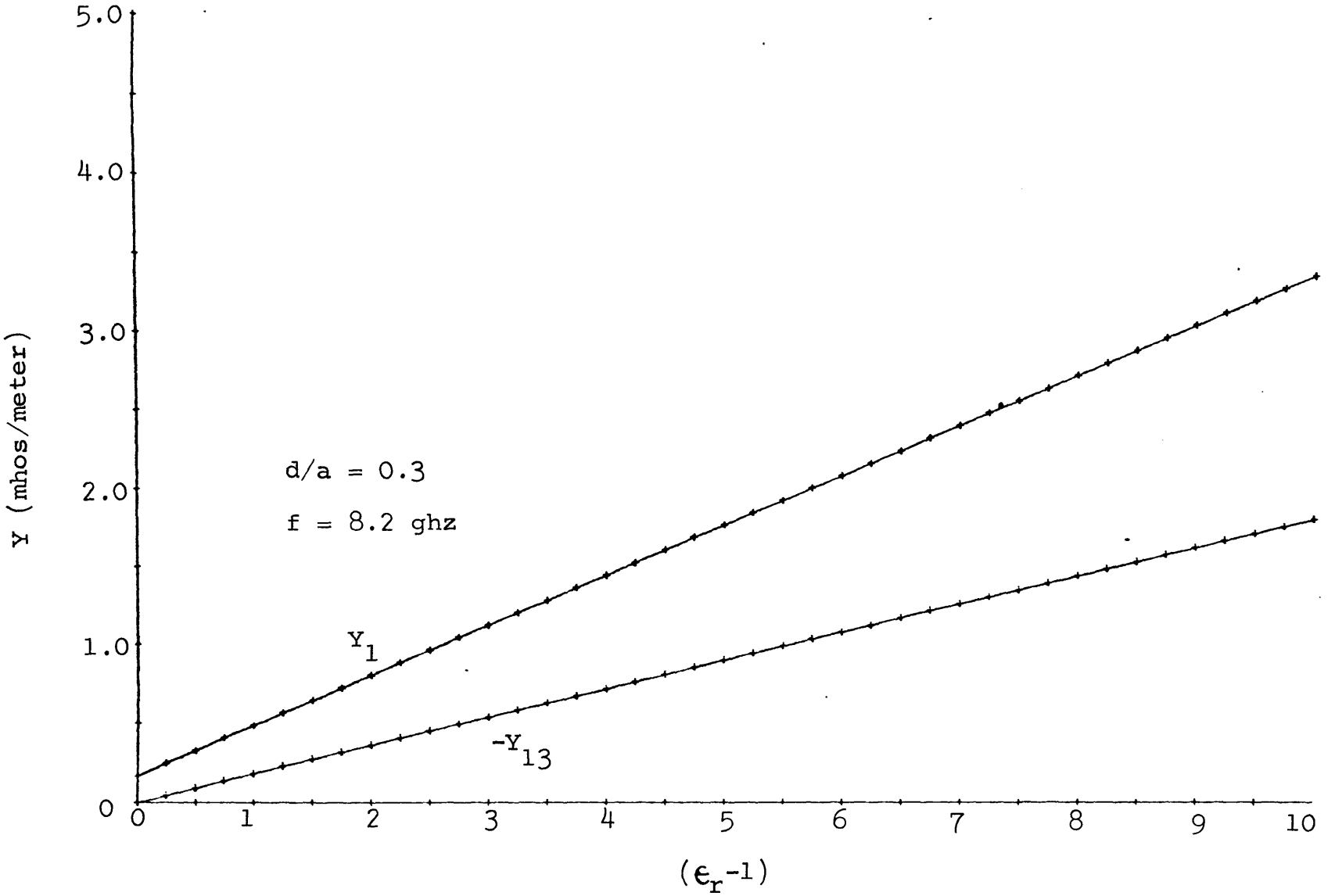

Figure 10. Transfer Admittances For SCCT of Figure 4

CHAPTER III

APPROXIMATE SOLUTIONS OF THE TELEGRAPHIST'S EQUATIONS

A. First-Order Approximation

Since the transitions described in the previous chapter are intended to be used for matching, the quantity of primary interest is the reflection coefficient at the transition section input plane ($z = 0$). A first-order approximation to the solution for the relection coefficient can be found by assuming only the TE_{10} mode exists in the transition. For this solution to be of value the coupling from the TE_{10} mode to other modes must be low. If this coupling is low the problem may be solved using nonuniform transmission line theory.

The differential equations which are satisfied by the voltage V and the current I along any transmission line are

$$\frac{dV}{dz} = -Z(z)\ I(z) \tag{29}$$

$$\frac{dI}{dz} = -Y(z)\ V(z) \tag{30}$$

where harmonic time variation has been assumed, $Z(z)$ is the series impedance, and $Y(z)$ is the shunt admittance both per unit length along the line. The characteristic impedance and propagation constant in terms of $Z(z)$ and $Y(z)$ are

$$Z_o(z) = \sqrt{\frac{Z(z)}{Y(z)}} \tag{31}$$

$$j\beta(z) = \sqrt{Z(z)\ Y(z)}. \tag{32}$$

The definition of the voltage reflection coefficient $\Gamma(z)$ is

$$\Gamma(z) = \frac{\frac{V(z)}{I(z)} - Z_o(z)}{\frac{V(z)}{I(z)} + Z_o(z)} . \qquad (33)$$

If equations (31), (32) and (33) are substituted into equations (29) and (30) it may be shown that $\Gamma(z)$ satisfies the nonlinear differential equation

$$\frac{d\Gamma(z)}{dz} - 2j\beta\Gamma(z) + \frac{1}{2}\frac{d\left[\ln Z_o(z)\right]}{dz}\left[1 - \Gamma(z)^2\right] = 0. \qquad (34)$$

For matching applications it is desirable to keep $\Gamma(z)^2 << 1$. If this restriction is placed on Γ, equation (34) may be linearized to give

$$\frac{d\Gamma(z)}{dz} - 2j\beta\Gamma(z) + \frac{1}{2}\frac{d\left[\ln Z_o(z)\right]}{dz} = 0. \qquad (35)$$

The solution (8) of this equation at the input plane ($z = 0$) is

$$\Gamma(0) = \frac{1}{2}\int_0^L \frac{d(\ln Z_o)}{dz}\, e^{-2\int_o^z j\beta dw}\, dz. \qquad (36)$$

For certain variations of Z_o and β this equation may be solved exactly as will be shown later. However for the general case an exact solution of equation (36) is very difficult and may even be impossible. For difficult cases resort will have to be made to numerical solutions to obtain results.

Equations (29) and (30) may be rewritten as follows

$$\frac{dV}{dz} = -j\beta\, Z_o\, I(z) \qquad (37)$$

$$\frac{dI}{dz} = -j \frac{\beta}{Z_o} V(z). \tag{38}$$

The general equations for the voltage and current of the TE_{10} mode were

$$\frac{dV_{10}}{dz} = -j\omega \mu_o I_{10} \tag{39}$$

$$\frac{dI_{10}}{dz} = -j Y_1 V_{10}. \tag{40}$$

Comparison of equations (37) and (39) show that

$$\beta Z_o = \omega \mu_o \tag{41}$$

and comparison of equations (38) and (40) show

$$Y_1 = \beta/Z_o. \tag{42}$$

Solving for β and Z_o yields

$$\beta = \sqrt{\omega \mu_o Y_1} \tag{43}$$

$$Z_o = \sqrt{\frac{\omega \mu_o}{Y_1}} \tag{44}$$

For the purposes of numerical calculation another method exists which is better adapted for computer solution than evaluating equation (36) numerically. The transition section is divided into a number of small steps each of length ΔL. At each step β and Z_o are considered to be constant. Each section then acts as a transmission line of length ΔL with constants β_n and Z_{o_n}. The input impedances of the n^{th} section may then be written

$$\frac{Z_{i_n}}{Z_{o_n}} = \frac{Z_{i_{n+1}} \cos(\beta_n \Delta L) + jZ_{o_n} \sin(\beta_n \Delta L)}{Z_{o_n} \cos(\beta_n \Delta L) + jZ_{i_{n+1}} \sin(\beta_n \Delta L)} \tag{45}$$

where Z_{o_n} is the characteristic impedance of the n^{th} section and β_n is the propagation constant of the n^{th} section. If the total number of steps is m then

$$Z_{i_{m+1}} = Z_{o_{\text{dielectric filled line}}} . \tag{46}$$

Using equation (46) as a starting point the input impedance of the first section may be found. From this the input reflection coefficient may be calculated.

B. Second-Order Approximation

A second-order approximation to the solution for the reflection coefficient can be found by including coupling from the dominant mode to the next excited mode, i.e. the TE_{20} mode for the unsymmetrical taper and the TE_{30} mode for the symmetrical taper. Letting Y_{1n} be the transfer admittance for either the TE_{20} or TE_{30} mode gives the generalized telegraphist's equations in the following form

$$\frac{dV_{10}}{dz} = -j\omega \mu_o I_{10}$$

$$\frac{dI_{10}}{dz} = -j Y_1 V_{10} - j Y_{1n} V_{n0}$$

$$\frac{dV_{n0}}{dz} = -j\omega \mu_o I_{n0}$$

$$\frac{dI_{n0}}{dz} = -j Y_n V_{n0} - j Y_{n1} V_{10}$$

where n is either 2 or 3. If Z_{11} is defined to be $\omega \mu_o$ the equations may be put in matrix form as

$$\begin{bmatrix} \frac{dV_{10}}{dz} \\ \frac{dI_{10}}{dz} \\ \frac{dV_{n0}}{dz} \\ \frac{dI_{n0}}{dz} \end{bmatrix} = -j \begin{bmatrix} 0 & Z_{11} & 0 & 0 \\ Y_1 & 0 & Y_{1n} & 0 \\ 0 & 0 & 0 & Z_{11} \\ Y_{n1} & 0 & Y_n & 0 \end{bmatrix} \begin{bmatrix} V_{10} \\ I_{10} \\ V_{n0} \\ I_{n0} \end{bmatrix} \tag{47}$$

where the Y's are defined in Chapter II. All the elements of the above matrix are real although some may be negative.

The derivatives in (47) may be approximated by

$$\frac{dV}{dz} \doteq \frac{V(z) - V(z - \Delta z)}{\Delta z} .$$

The backward derivative is used since the output quantities will be known and the input quantities are unknown. If the coefficient matrix is denoted by K in equation (47) an approximate incremental solution may be written

$$\begin{bmatrix} V_{10} \\ I_{10} \\ V_{n0} \\ I_{n0} \end{bmatrix}_{z-\Delta z} \doteq \begin{bmatrix} V_{10} \\ I_{10} \\ V_{20} \\ I_{20} \end{bmatrix}_{z} + j\left[K(z)\ \Delta z\right] \begin{bmatrix} V_{10} \\ I_{10} \\ V_{n0} \\ I_{n0} \end{bmatrix}_{z} \tag{48}$$

The matrix on the left can be taken to be the input voltages and currents of a network of length Δz and the matrix common to both terms on the right hand side of (48) is the repre-

sentation of the output voltages and currents. The transfer matrix of the n^{th} section is then

$$T_n = \left[I + K\,\Delta z\right]_{n\Delta z} \tag{49}$$

Equation (49) is simply the first two terms of the infinite series expansion of the true solution the matrizant (17). To solve for the transfer matrix of the transition section the section may be divided into small sections each of length Δz. The transfer matrix of each section may be found and multiplication of the individual transfer matrices gives the overall transfer matrix.

The transfer matrix of the transition does not contain all the necessary information to solve for the input reflection coefficeint. The output voltages and currents must be specified. The dielectric filled waveguide will be assumed to extend to infinity. This means that no reflected waves will occur in this part of the line and as a result the voltages and currents of each mode are related by the characteristic impedance of the mode. Any one of the output quantities may arbitrarily set to unity and the current I_{10} will be chosen for this. The voltage V_{10} is then equal to the characteristic impedance of the TE_{10} mode.

$$I_{10} = 1 \tag{50}$$

$$V_{10} = \frac{\omega \mu_o}{\sqrt{\omega^2 \mu_o \epsilon_o \epsilon_r - (\pi/a)^2}}$$

For the voltage and current of the coupled mode two separate cases arise depending on whether the waveguide is above or below the cutoff frequency of the coupled mode. In either case the input voltage and current of the coupled mode may be assumed to be zero since only frequencies for which this mode is cutoff in the air filled waveguide are under investigation.

If the frequency is such that the dielectric-filled waveguide is below cutoff for the coupled mode, the voltage and current of this mode may be assumed to be zero at the output. This is justified since the transfer admittance to this mode is zero at the output of the transition and any voltages and currents of the mode established in the transition will attenuate very quickly since the waveguide is below cutoff. For this case only a portion of the transfer matrix is required and the input voltage and current may be written

$$\begin{bmatrix} V_{10} \\ I_{10} \end{bmatrix}_{input} = \begin{bmatrix} T_{11} & T_{12} \\ T_{21} & T_{22} \end{bmatrix} \begin{bmatrix} V_{10} \\ I_{10} \end{bmatrix}_{output} \tag{52}$$

where V_{10} and I_{10} at the output are defined by equations (50) and (51).

If the frequency is such that the dielectric-filled waveguide can propagate the coupled mode, the voltage and current at the output of the transition of the coupled mode must be taken into account. The voltage may be written in terms of the current as

$$V_{n0} = \frac{\omega \mu_o}{\sqrt{\omega^2 \mu_o \epsilon_o \epsilon_r - (n\pi/a)^2}} \tag{53}$$

where n is either 2 or 3. The dominant mode input voltage and current may now be written.

$$\begin{bmatrix} V_{10} \\ I_{10} \\ 0 \\ 0 \end{bmatrix}_{\text{input}} = \begin{bmatrix} T_{11} & T_{12} & T_{13} & T_{14} \\ T_{21} & T_{22} & T_{23} & T_{24} \\ T_{31} & T_{32} & T_{33} & T_{34} \\ T_{41} & T_{42} & T_{43} & T_{44} \end{bmatrix} \begin{bmatrix} V_{10} \\ I_{10} \\ V_{n0} \\ I_{n0} \end{bmatrix}_{\text{output}} \tag{54}$$

Using either the third or fourth equation of the above matrix allows solution of I_{n0} in terms of I_{10}. The output matrix is then known and V_{10} and I_{10} at the output may be found.

CHAPTER IV

LINEAR DIELECTRIC TAPERS

A. The Linear UCT

For the first-order approximation the characteristic impedance in terms of the admittance from equation (44) was found to be

$$Z_o = \sqrt{\frac{\omega \mu_o}{Y_1}}$$

and for the unsymmetrical taper

$$Y_1 = \frac{k_o^2 - (\frac{\pi}{a})^2}{\omega \mu_o} + \frac{\omega \epsilon_o (\epsilon_r - 1)}{\pi} \left[\frac{\pi d}{a} - \frac{1}{2} \sin \frac{2\pi d}{a}\right]$$

from equation (13). Y_1 may be expressed as a function of z by substituting

$$\frac{d}{a} = z/L$$

to give

$$Y_1 = \frac{k_o^2 - (\frac{\pi}{a})^2}{\omega \mu_o} + \frac{\omega \epsilon_o (\epsilon_r - 1)}{\pi} \left[\frac{\pi}{L} z - \frac{1}{2} \sin \frac{2\pi}{L} z\right] \quad (55)$$

The derivative of Z_o with z may be written as

$$\frac{dZ_o}{dz} = - \frac{\sqrt{\omega \mu_o}}{2} Y_1(z)^{-3/2} \frac{dY_1}{dz} \quad (56)$$

where

$$\frac{dY_1}{dz} = \frac{\omega \epsilon_o (\epsilon_r - 1)}{L} \left[1 - \cos \frac{2\pi}{L} z\right]. \quad (57)$$

Substitution shows that

$$\left.\frac{dZ_o}{dz}\right|_{z = 0} = 0$$

$$\left.\frac{dZ_o}{dz}\right|_{z = L} = 0.$$

Thus no reflection occurs due to first-order variation of impedance at the input and output ends of this particular taper. These are the same conditions imposed on the characteristic impedance of the parabolic line. However, this does not mean that the unsymmetrical taper is a parabolic line.

Equation (55) states that Y_1 is not dependent upon the absolute length of the transition section but depends only on the normalized distance along the line z/L. The derivative of the admittance does depend upon the absolute length of the transition section varying inversely with L. The modulus of the integrand of equation (36) for the input reflection coefficient was

$$\frac{1}{2}\frac{d\,(\ln Z_o)}{dz} .$$

Writing this in terms of admittance gives

$$\frac{1}{2}\frac{d(\ln Z_o)}{dz} = -\frac{1}{4}\,\frac{\frac{dY_1}{dz}}{Y_1} = -\frac{1}{4}\,\frac{d(\ln Y_1)}{dz} . \qquad (58)$$

From this it is seen that the modulus of the integrand of equation (36) decreases as 1/L. Since the length of the integration interval increases as L, the overall effect of these two combined is to hold the integral constant. Any improvement in the reflection coefficient due to tapering is thus due to the phase term in the integrand of equation (36).

The shape of the taper then affects primarily the phase term of equation (36) which may be written

$$e^{-2\int_0^z j\sqrt{\omega \mu_o Y_1}\, d\tau} . \qquad (59)$$

It was decided to use the computer to investigate the behavior of the matching transitions. It was desirable to know how the reflection coefficient varied when the dielectric constant, frequency and length of the transition were varied. The length of the transition was normalized to the width of the waveguide (a) and is used as the independent variable. The frequency was used as a parameter and varied from 8.2 ghz to 9.8 ghz in 400 mhz steps. This allows a wide enough bandwidth to adequately test the theory. The dielectric constant was selected to have three values of 1.7, 2.5 and 4.0. The value of 1.7 was picked since the experimental work was to be done using this value. The value 2.5 was picked so that the waveguide would be just below the cutoff frequency of the TE_{20} mode in the dielectric-filled waveguide when the frequency was 8.2 ghz. The value of 4.0 was chosen so that the dielectric-filled waveguide could propagate the TE_{20} mode at a frequency of 8.2 ghz.

Figure 11 shows the variation of $\Gamma(0)$ versus L/a for $\epsilon_r = 1.7$ and with ω as a parameter. These curves and all other curves unless stated otherwise were obtained using the first-order approximation of Chapter III and were computed using the step approximation of the taper. The number of steps was chosen to be 20 which does not ensure the highest

accuracy but does keep the computing time down. This set of curves required about one half hour computing time on the IBM 1620 Model II computer. Figure 12 gives the variation of $\Gamma(0)$ versus L/a for f = 8.2 ghz and with ϵ_r as a parameter.

The second-order approximation was then used to check the validity of the first-order approximation. Again the number of steps was chosen to be 20 to minimize the computer time. The second-order approximation requires about five times as much computer time as does the first-order approximation. Figure 13 gives both approximations for the case $\epsilon_r = 1.7$ and f = 8.2 ghz and $\epsilon_r = 1.7$ and f = 9.8 ghz. Figure 14 gives both approximations for f = 8.2 ghz with $\epsilon_r = 1.7, 2.5, 4.0$.

B. The Linear SSCT

Much of what was said in the preceeding section on the UCT is also applicable to the SSCT. The difference between the two will be pointed out in this section.

The admittance function was from equation (21)

$$Y_1 = \frac{k_o^2 - (\frac{\pi}{a})^2}{\omega \mu_o} + \frac{2\omega \epsilon_o (\epsilon_r - 1)}{\pi} (\frac{\pi d}{a} - \frac{1}{2} \sin \frac{2\pi d}{a})$$

and may be expressed as a function of z by the substitution

$$\frac{d}{a} = \frac{z}{2L} .$$

Making this substitution gives

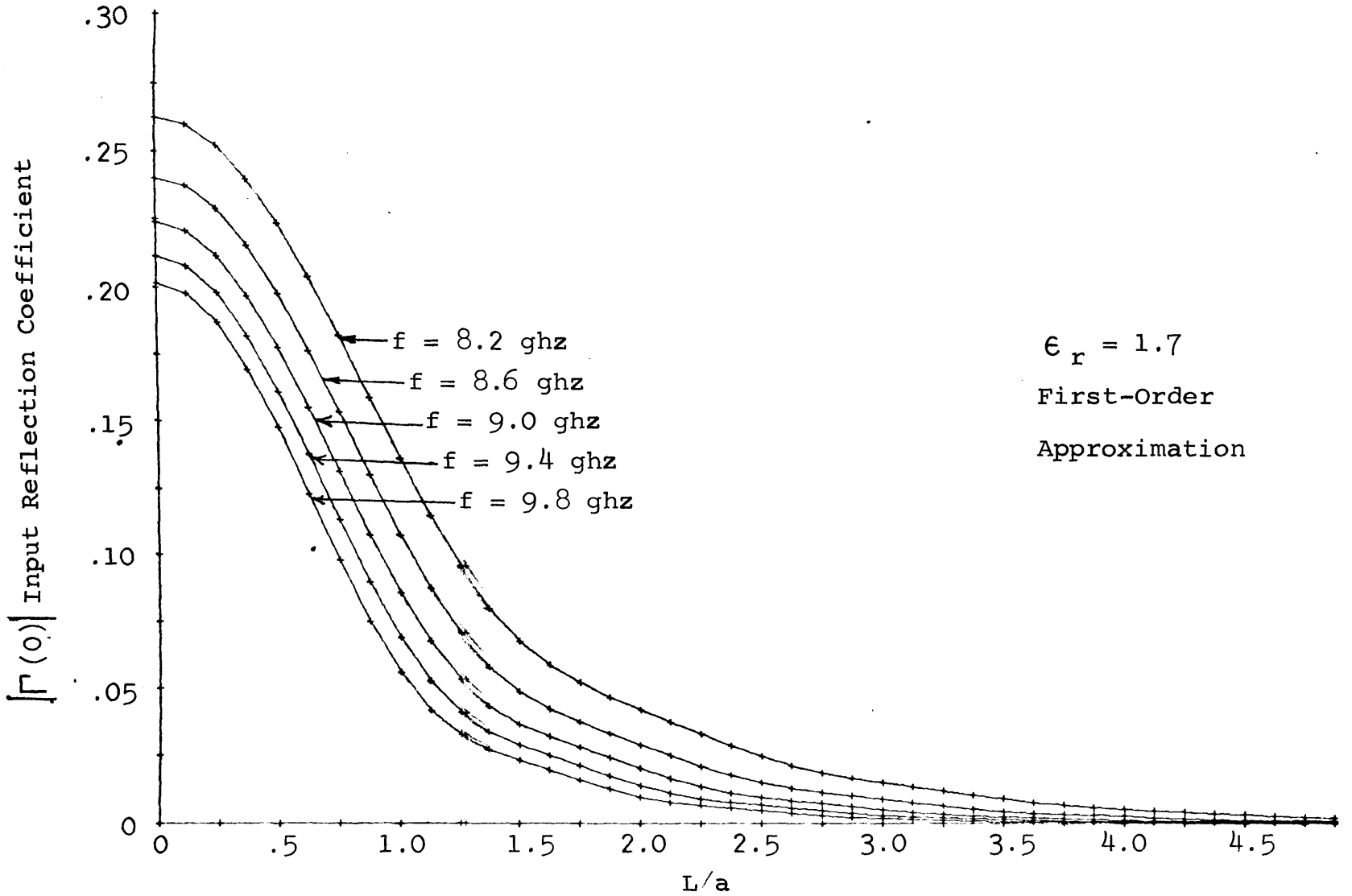

Figure 11. $|\Gamma(0)|$ Versus L/a For the Linear UCT With ω As Parameter

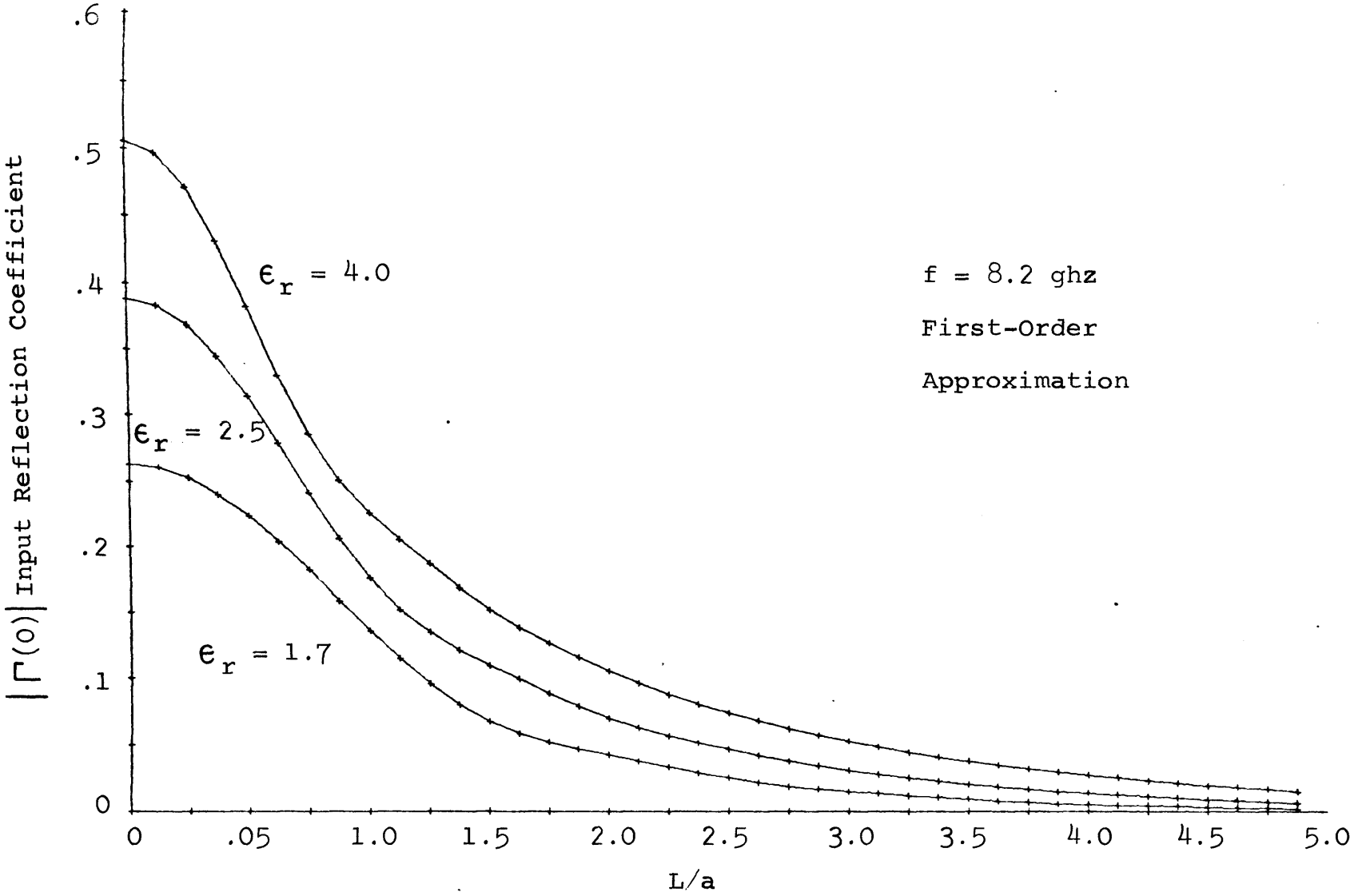

Figure 12. $|\Gamma(0)|$ Versus L/a For the Linear UCT With ϵ_r as Parameter

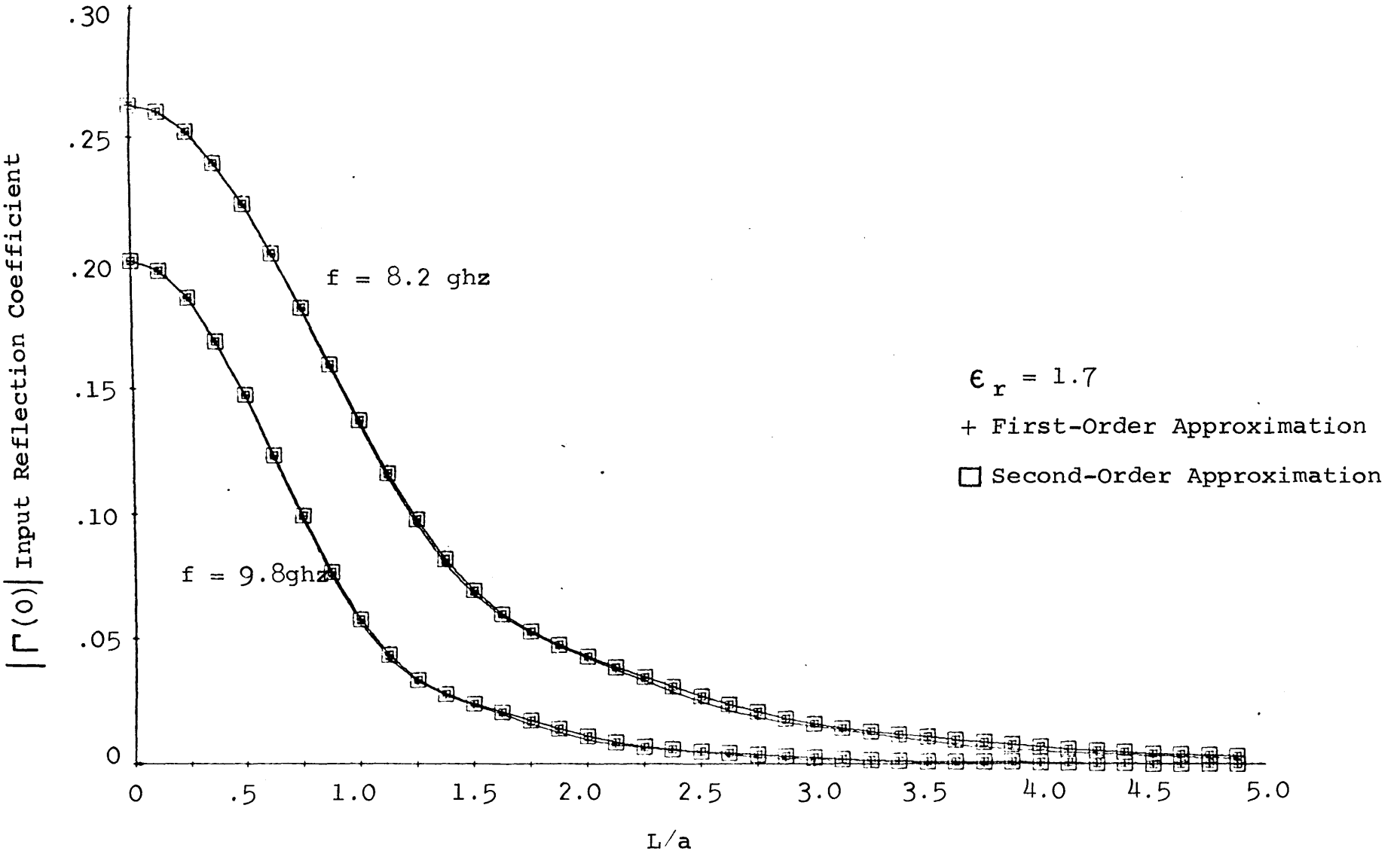

Figure 13. Comparison of First-Order and Second-Order Approximations for the Linear UCT With ω as Parameter

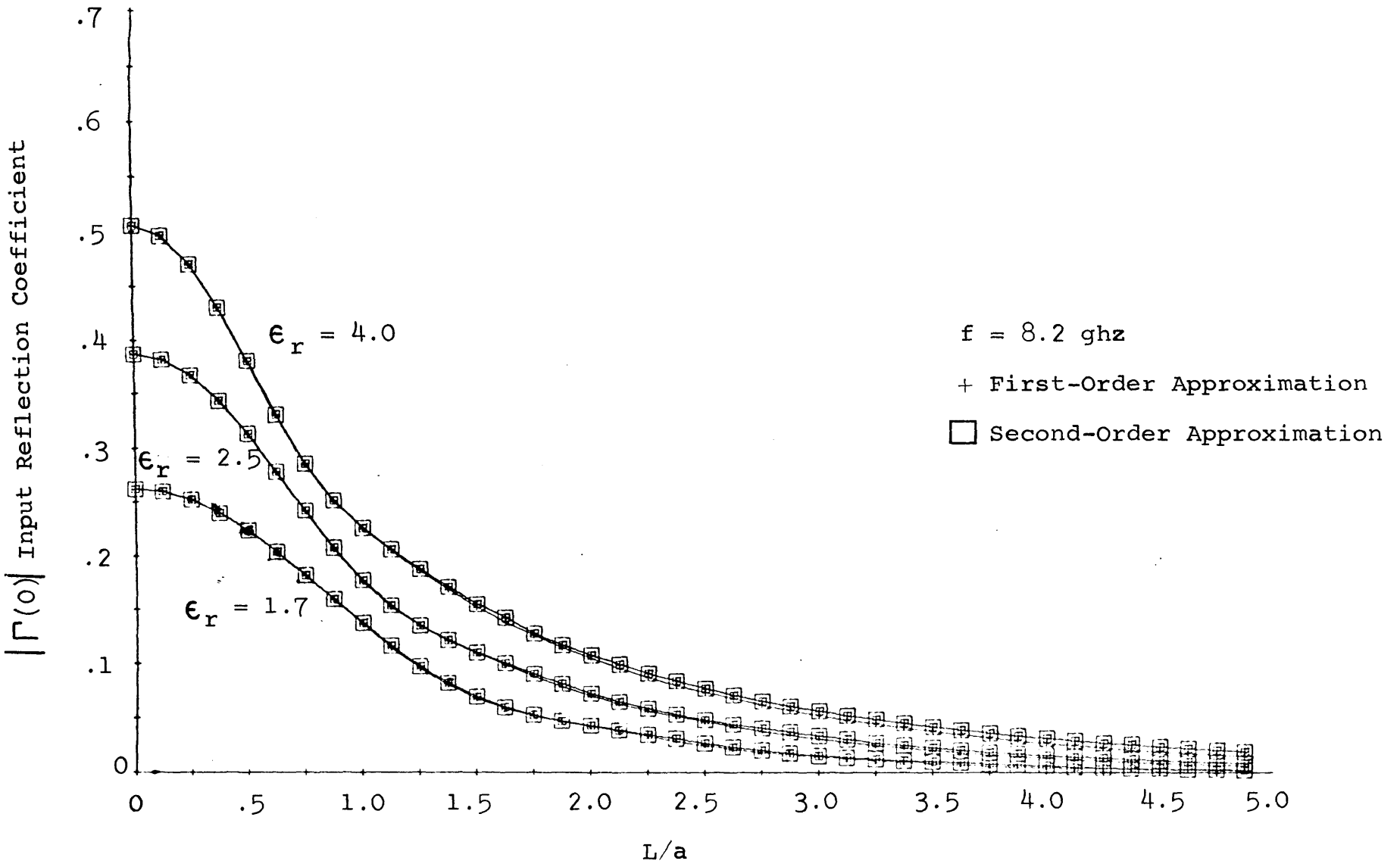

Figure 14. Comparison of First-Order and Second-Order Approximations for the Linear UCT with ϵ_r as a Parameter

$$Y_1 = \frac{k_o^2 - (\frac{\pi}{a})^2}{\omega \mu_o} + \frac{2\omega \epsilon_o (\epsilon_r - 1)}{\pi} (\frac{\pi}{2L} z - \frac{1}{2} \sin \frac{\pi}{L} z). \quad (60)$$

The derivative of Y_1 with respect to z is

$$\frac{dY_1}{dz} = \frac{\omega \epsilon_o (\epsilon_r - 1)}{L} (1 - \cos \frac{\pi}{L} z). \quad (61)$$

For this taper the derivative of Z_o with respect to z vanishes at z = 0 but is finite at z = L. No reflection then occurs at the input of the line but reflection does occur at the output of the line. The derivative of Z_o is then discontinuous at z = L since at z = L(+) the line is uniform and

$$\left. \frac{dZ_o}{dz} \right|_{z = L(+)} = 0.$$

Again the modulus of the integral of equation (36) may be written

$$\frac{1}{2} \frac{d(\ln Z_o)}{dz} = - \frac{1}{4} \frac{d(\ln Y_1)}{dz}$$

and the phase term of the integral is

$$e^{-2 \int_o^z j \sqrt{\omega \mu_o Y_1} \, d\tau}.$$

Figure 15 gives the variation of $\Gamma(0)$ versus L/a for $\epsilon_r = 1.7$ and with ω as a parameter. Figure 16 gives the variation of $\Gamma(0)$ versus L/a for f = 8.2 ghz and with ϵ_r as a parameter.

The comparison of the first-order and second-order approximations are given in Figure 17 for $\epsilon_r = 1.7$ and

f = 8.2 ghz and ϵ_r = 1.7 and f = 9.8 ghz. Figure 18 gives both approximations for f = 8.2 ghz with ϵ_r = 1.7, 2.5 and 4.0.

C. The Linear SCCT

The admittance function for the symmetrical center taper was from equation (27)

$$Y_1 = \frac{k^2 - (\frac{\pi}{a})^2}{\omega \mu_o} - \frac{2\omega \epsilon_o (\epsilon_r - 1)}{\pi} (\frac{\pi d}{a} - \frac{1}{2} \sin \frac{2\pi d}{a})$$

which may be expressed as a function of z by the substitution

$$\frac{d}{a} = \frac{1}{2} (1 - z/L).$$

Making this substitution and using trigonometric identities yields

$$Y_1 = \frac{k_o^2 - (\frac{\pi}{a})^2}{\omega \mu_o} + \frac{2\omega \epsilon_o (\epsilon_r - 1)}{\pi} (\frac{\pi z}{2L} + \frac{1}{2} \sin \frac{\pi}{L} z). \quad (62)$$

The derivative of Y_1 with respect to z is

$$\frac{dY_1}{dz} = \frac{\omega \epsilon_o (\epsilon_r - 1)}{L} (1 + \cos \frac{\pi}{L} z). \quad (63)$$

For this taper the derivative of Z_o with respect to z vanishes at z = L but is finite at z = 0. Reflection is possible from the input side of the transition. The derivative of Z_o is discontinuous at z = 0 since at z = 0(-) the line is uniform and

$$\left. \frac{dZ_o}{dz} \right|_{z = 0(-)} = 0.$$

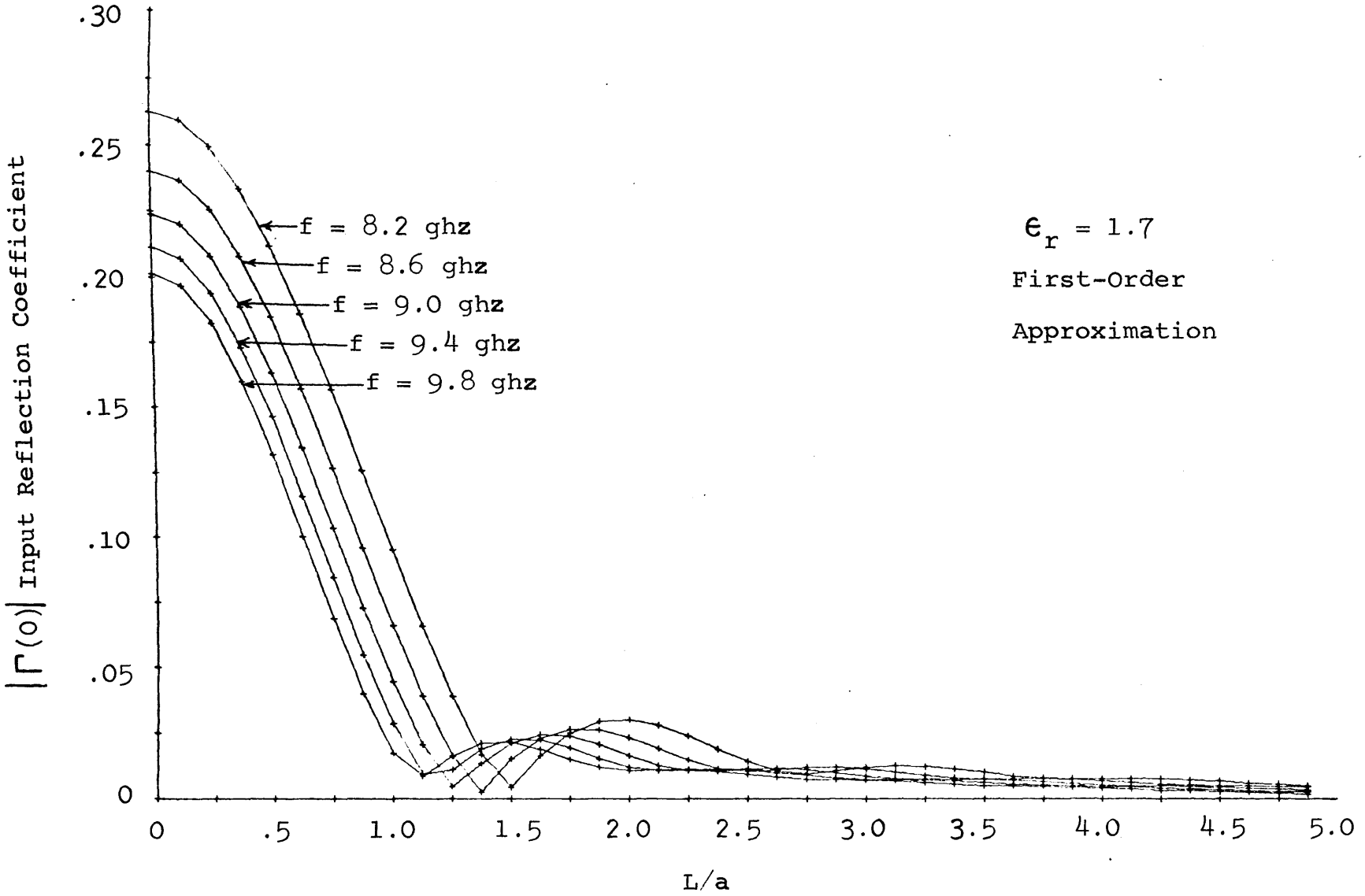

Figure 15. $|\Gamma(0)|$ Versus L/a for the Linear SSCT with ω as a Parameter

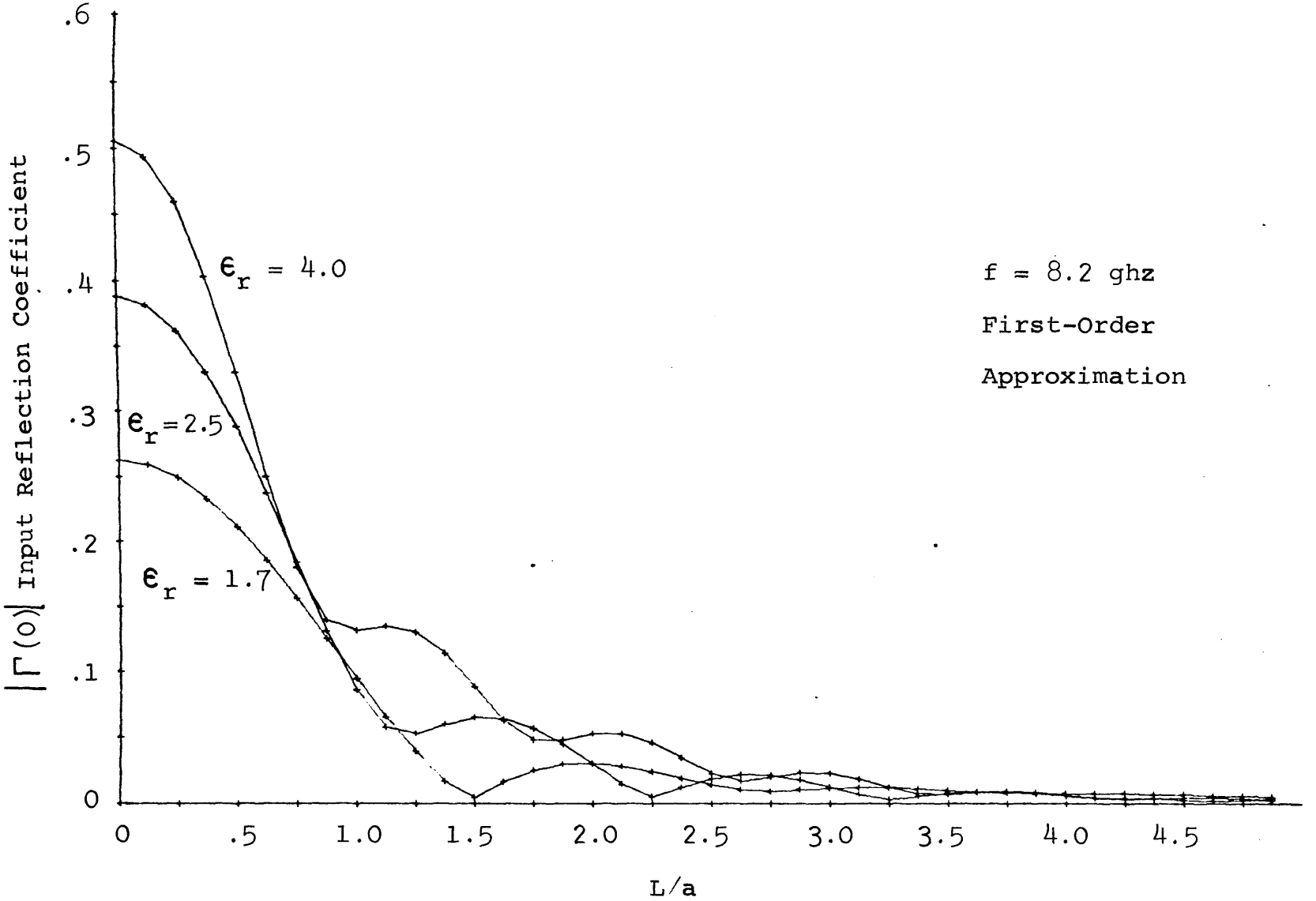

Figure 16. $|\Gamma(0)|$ Versus L/a for the Linear SSCT with ϵ_r as a Parameter

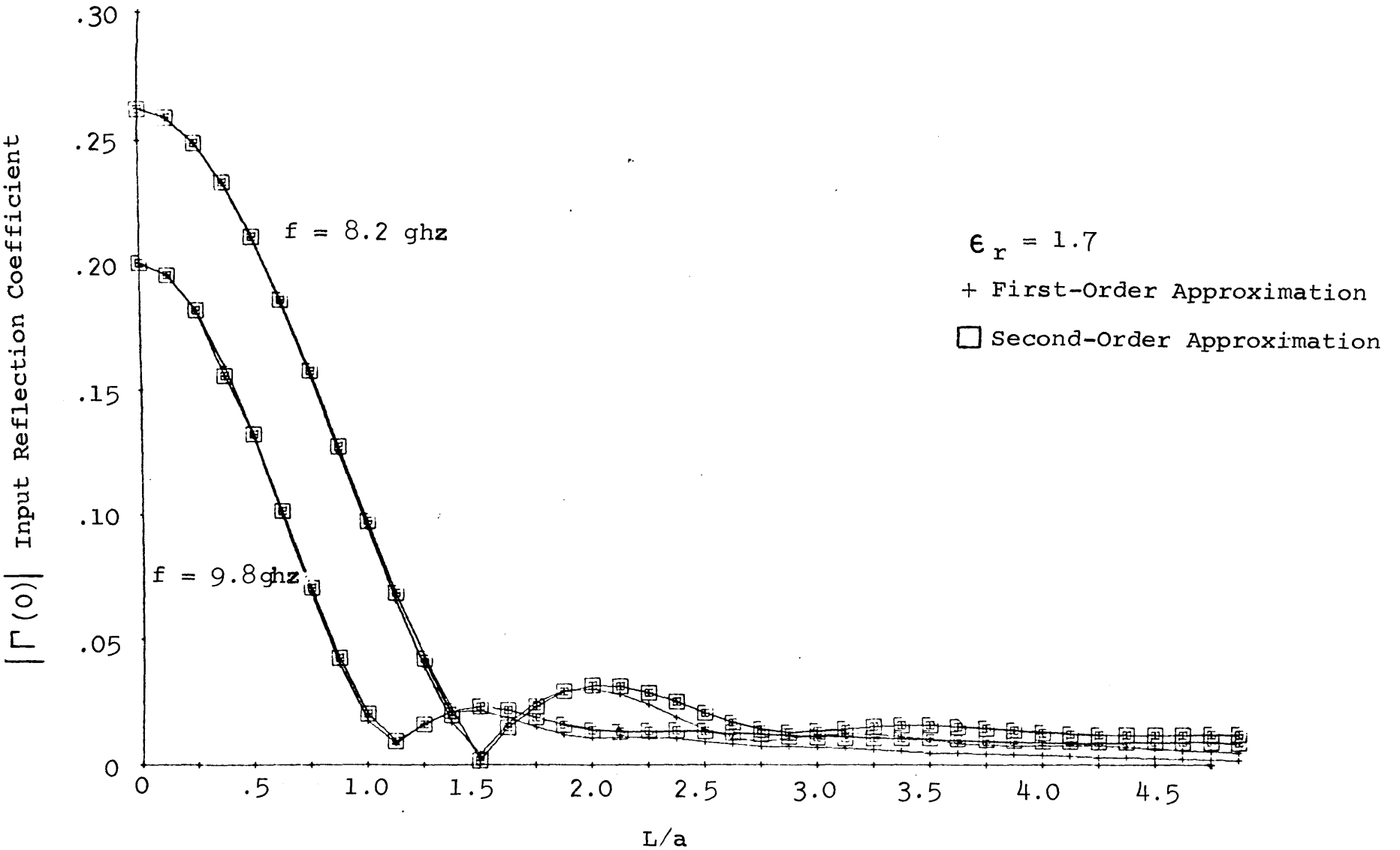

Figure 17. Comparison of First-Order and Second-Order Approximations for the Linear SSCT with ω as Parameter

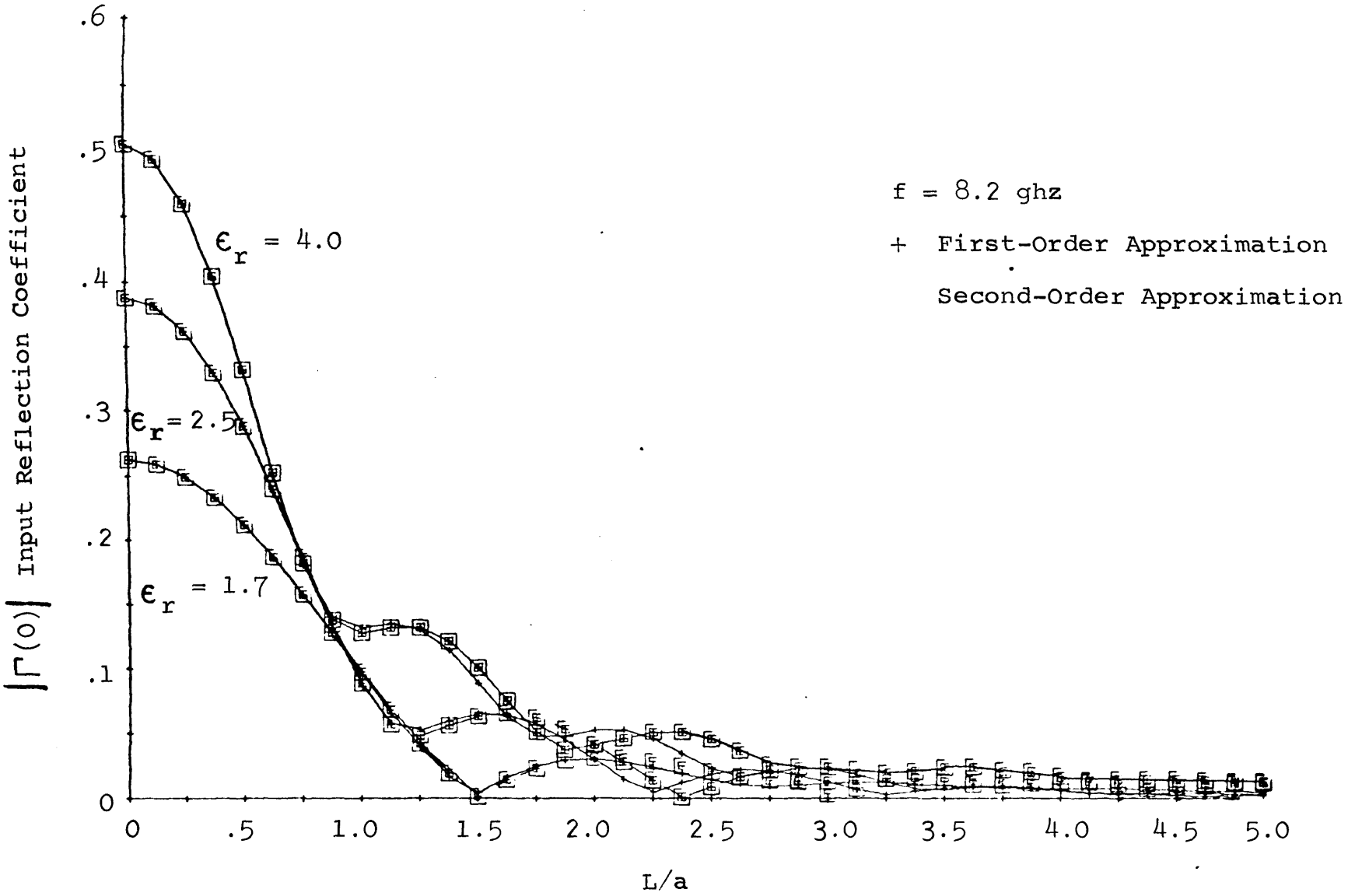

Figure 18. Comparison of First-Order and Second-Order Approximations for the Linear SSCT with ϵ_r as a Parameter

The modulus of the integral of equation (36) may again be written

$$\frac{1}{2}\frac{d(\ln Z_o)}{dz} = -\frac{1}{4}\frac{d(\ln Y_1)}{dz}$$

and the phase term of the integral is

$$e^{-2\int_o^z j\sqrt{\omega \mu_o Y_1}\, d\gamma}.$$

Figure 19 gives the variation of $\Gamma(0)$ versus L/a for $\epsilon_r = 1.7$ and with ω as a parameter. Figure 20 gives the variation of $\Gamma(0)$ versus L/a for f = 8.2 ghz and with ϵ_r as a parameter. The comparison of the first-order and second-order approximations are given in Figure 21 for $\epsilon_r = 1.7$ and f = 8.2 ghz and $\epsilon_r = 1.7$ and f = 9.8 ghz. Figure 22 gives both approximations for f = 8.2 ghz with $\epsilon_r = 1.7$, 2.5 and 4.0.

D. Comparison of Linear Continuously Tapered Transitions

The comparison of the tapers will be done using results of the first-order approximation. Figure 23 gives the variation of $\Gamma(0)$ versus L/a for the three linear tapers with $\epsilon_r = 1.7$ and f = 8.2 ghz. Figure 24 gives the variation of $\Gamma(0)$ versus L/a for the three linear tapers with $\epsilon_r = 4.0$ and f = 8.2 ghz.

The curves just described give results which are useful from a design viewpoint. In an effort to see what the characteristics of the line contribute to reflection coefficient it was decided to examine equation (36). In each case the modulus of this equation is

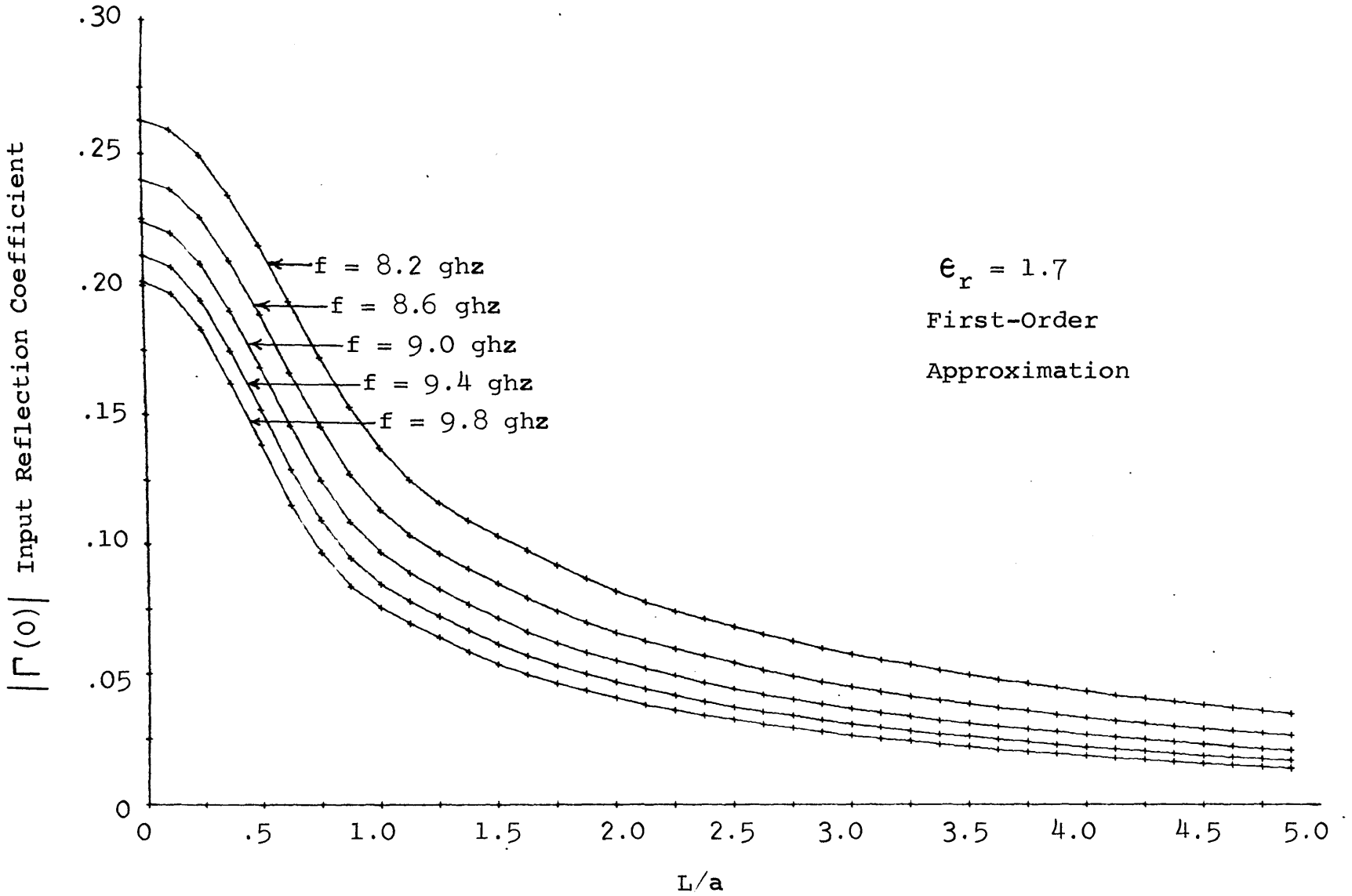

Figure 19. $|\Gamma(0)|$ Versus L/a for the Linear SCCT with ω as a Parameter

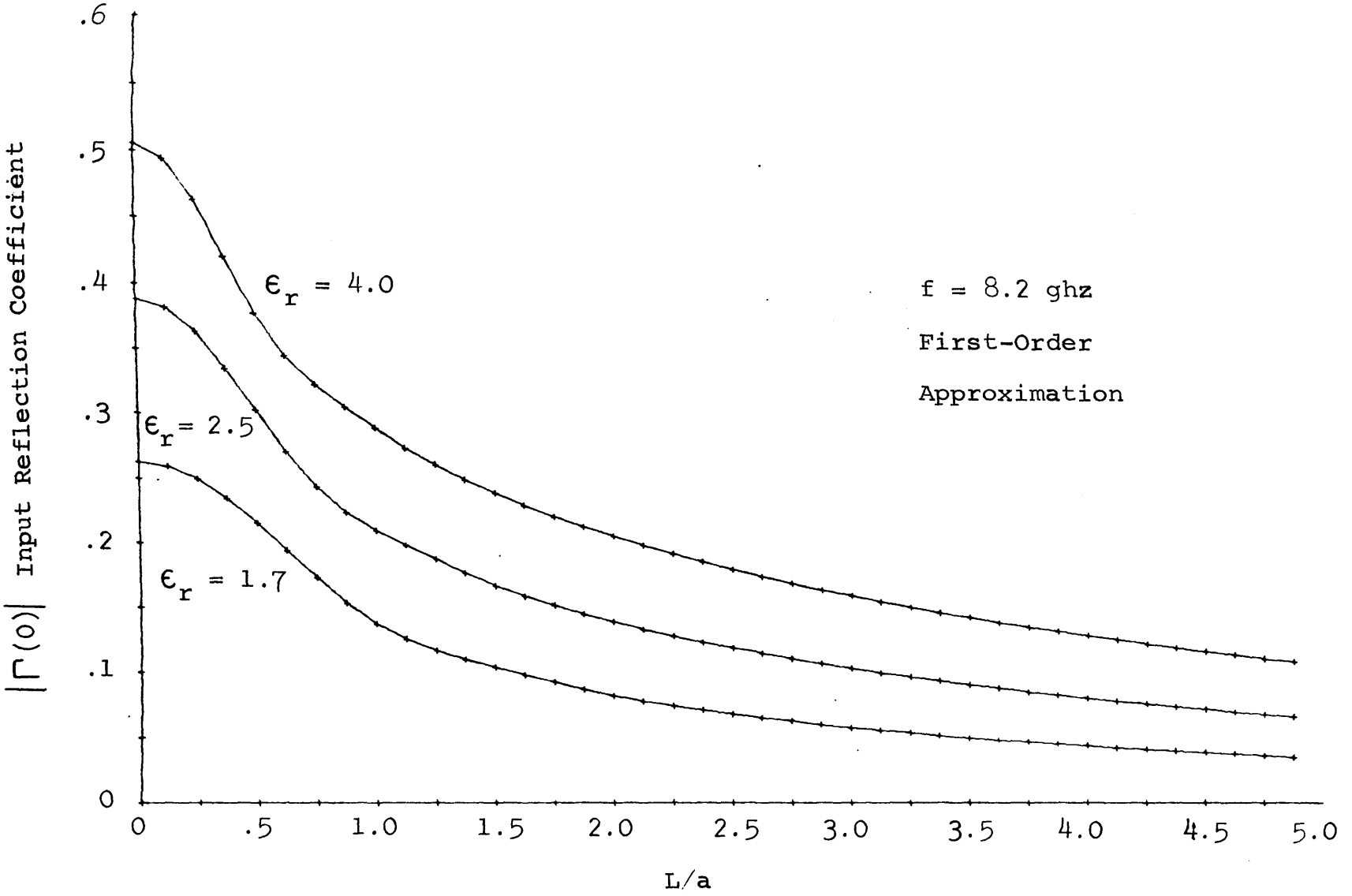

Figure 20. $|\Gamma(0)|$ Versus L/a for the Linear SCCT with ϵ_r as a Parameter

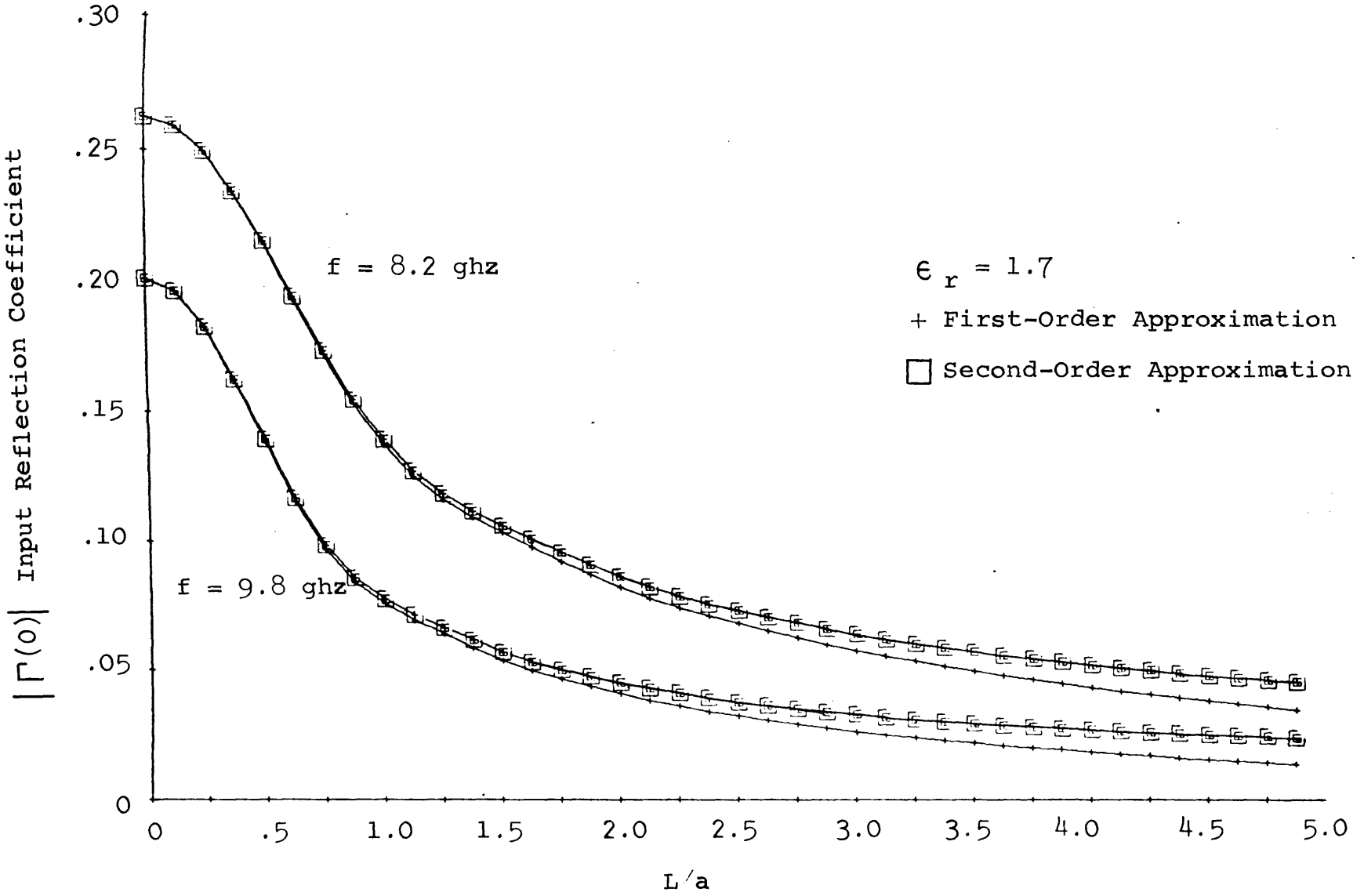

Figure 21. Comparison of First-Order and Second-Order Approximations for the Linear SCCT with ω as a Parameter

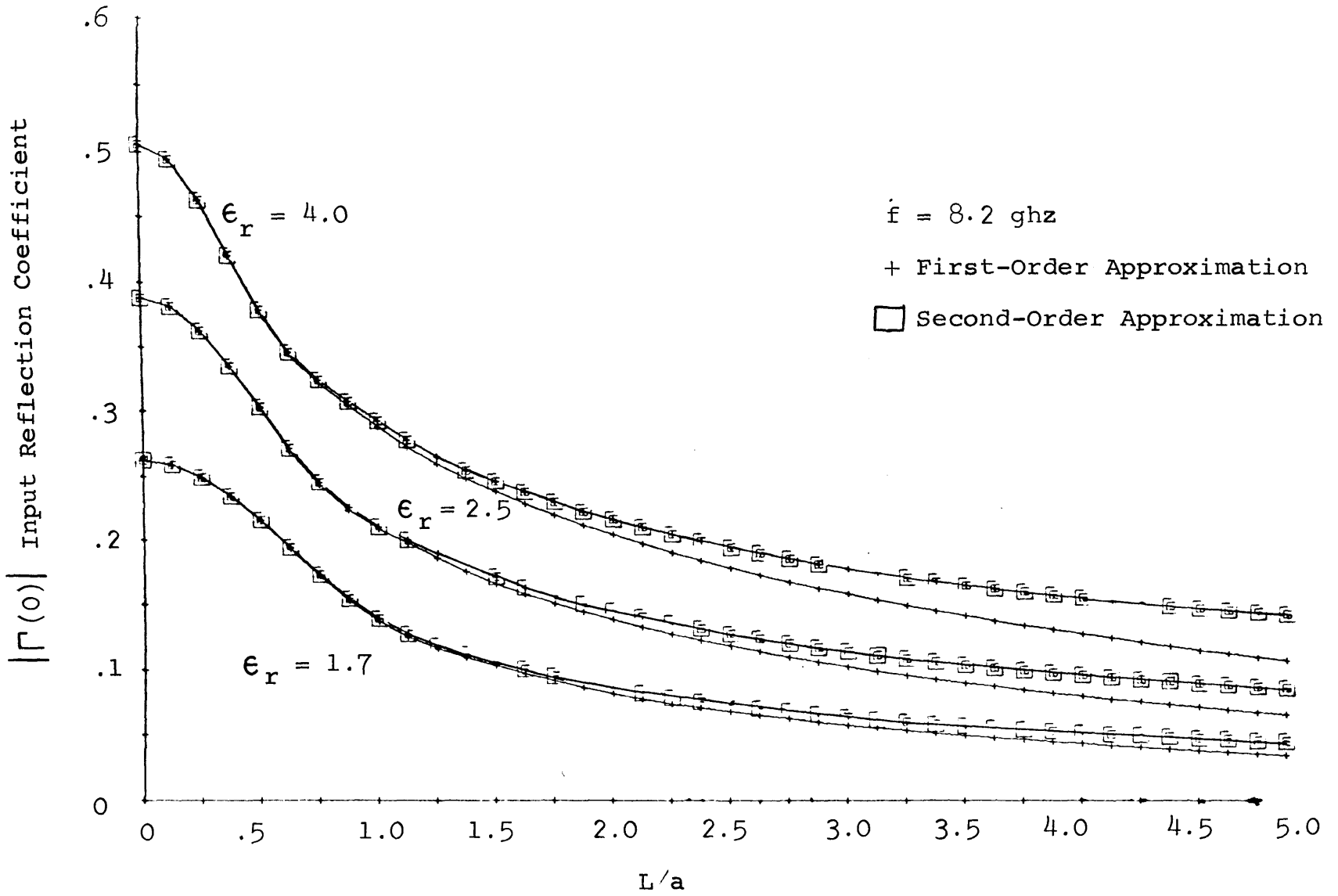

Figure 22. Comparison of First-Order and Second-Order Approximations for the Linear SCCT with ϵ_r as Parameter

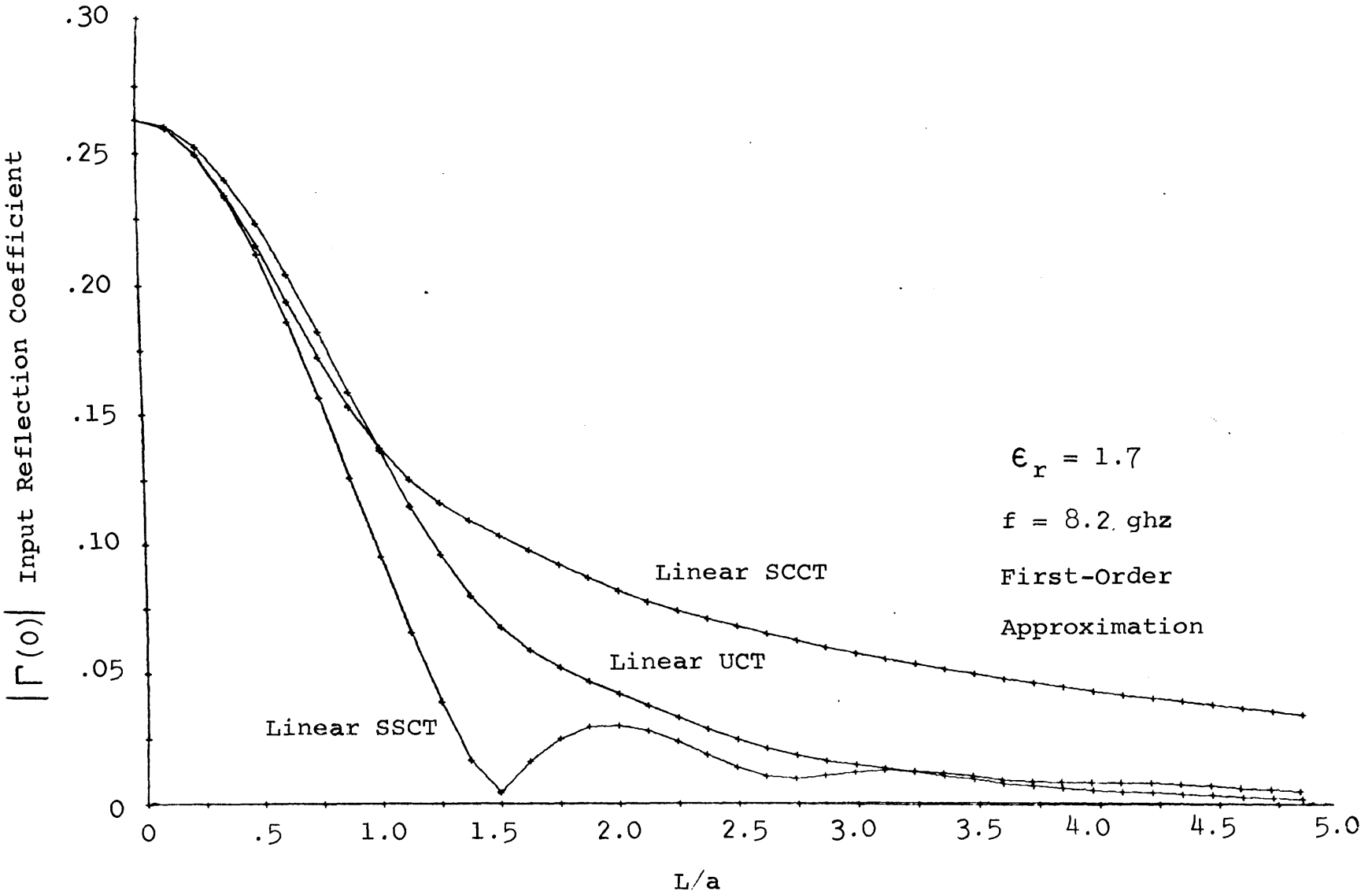

Figure 23. $|\Gamma(0)|$ Versus L/a for the Three Linear Tapers for ϵ_r = 1.7

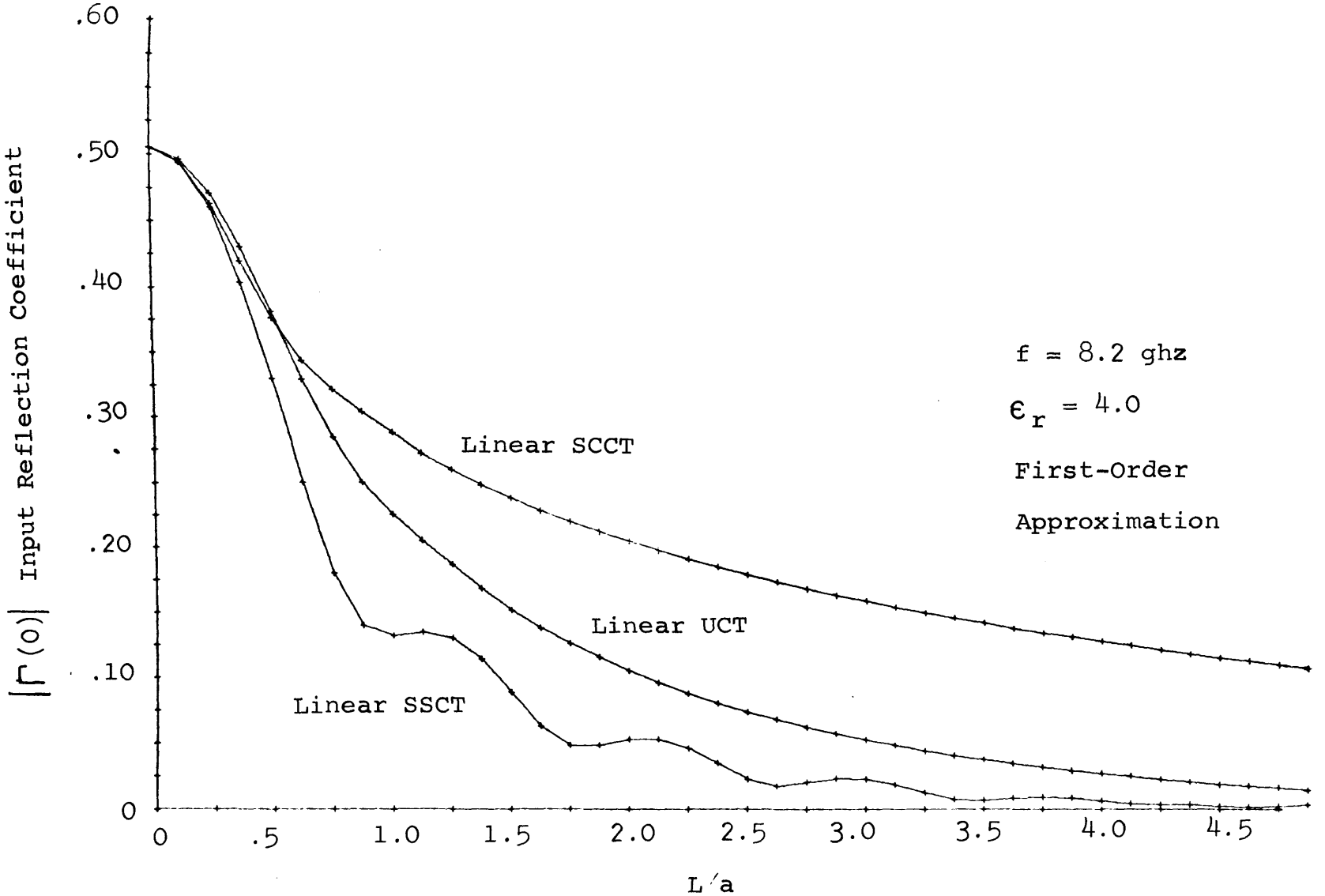

Figure 24. $|\Gamma(0)|$ Versus L/a for the Three Linear Tapers for ϵ_r = 4.0

$$-\frac{1}{4}\frac{d(\ln Y_1)}{dz}$$

and the phase is

$$-2\int_0^z \sqrt{\omega \mu_o Y_1}\; d\tau.$$

To examine the variation of these terms let L be set equal to the waveguide width. The integrand may then be plotted on the complex plane and will yield curves similar to the Nyguist plots of feedback control theory. Plots of these integrands are shown in Figures 25, 26 and 27 for the three linear tapers for the case $\epsilon_r = 1.7$ and f = 8.2 ghz. These curves are the starting point for the formidable problem of synthesizing waveguide tapers.

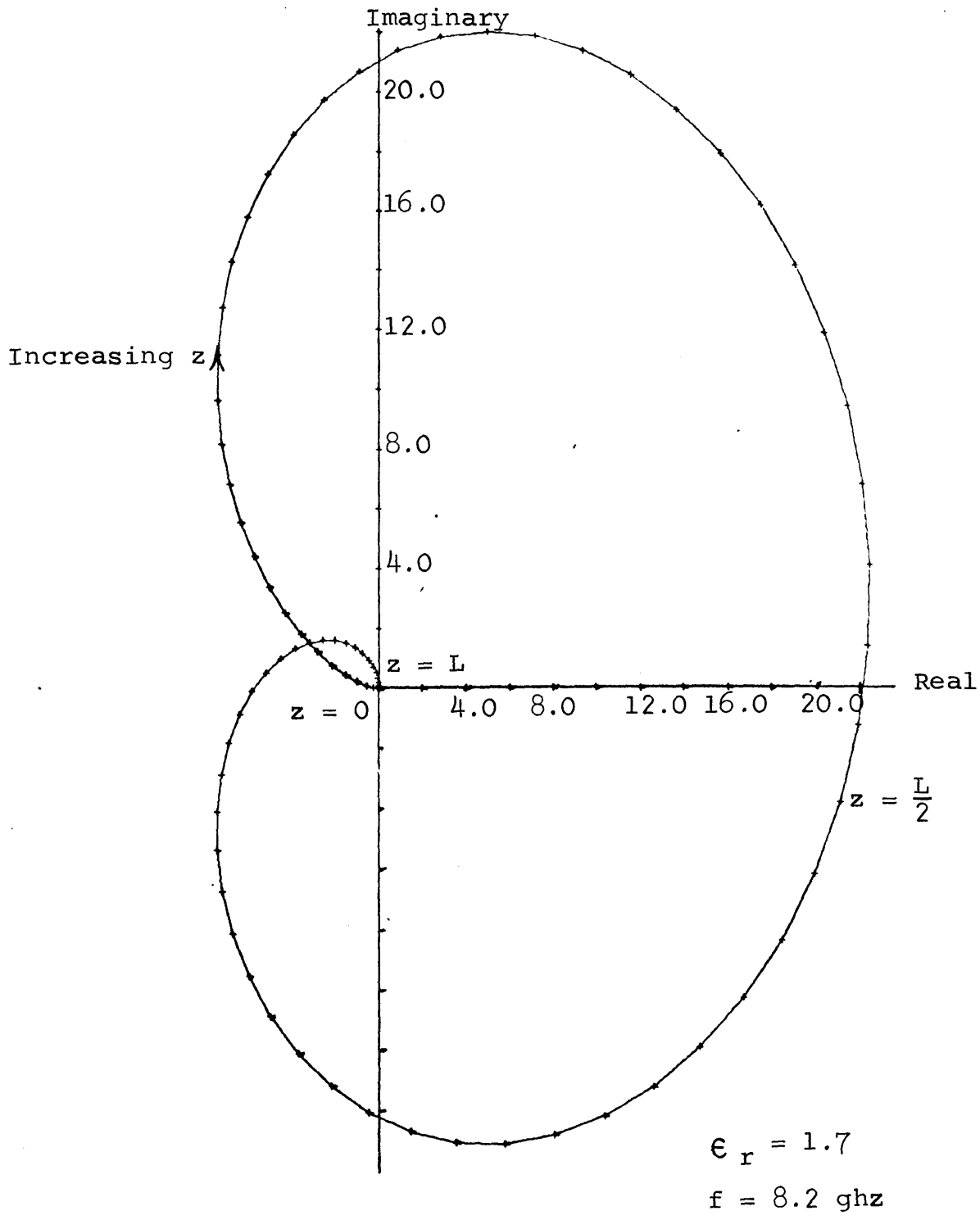

Figure 25. Plot of Complex Integrand for the Linear UCT

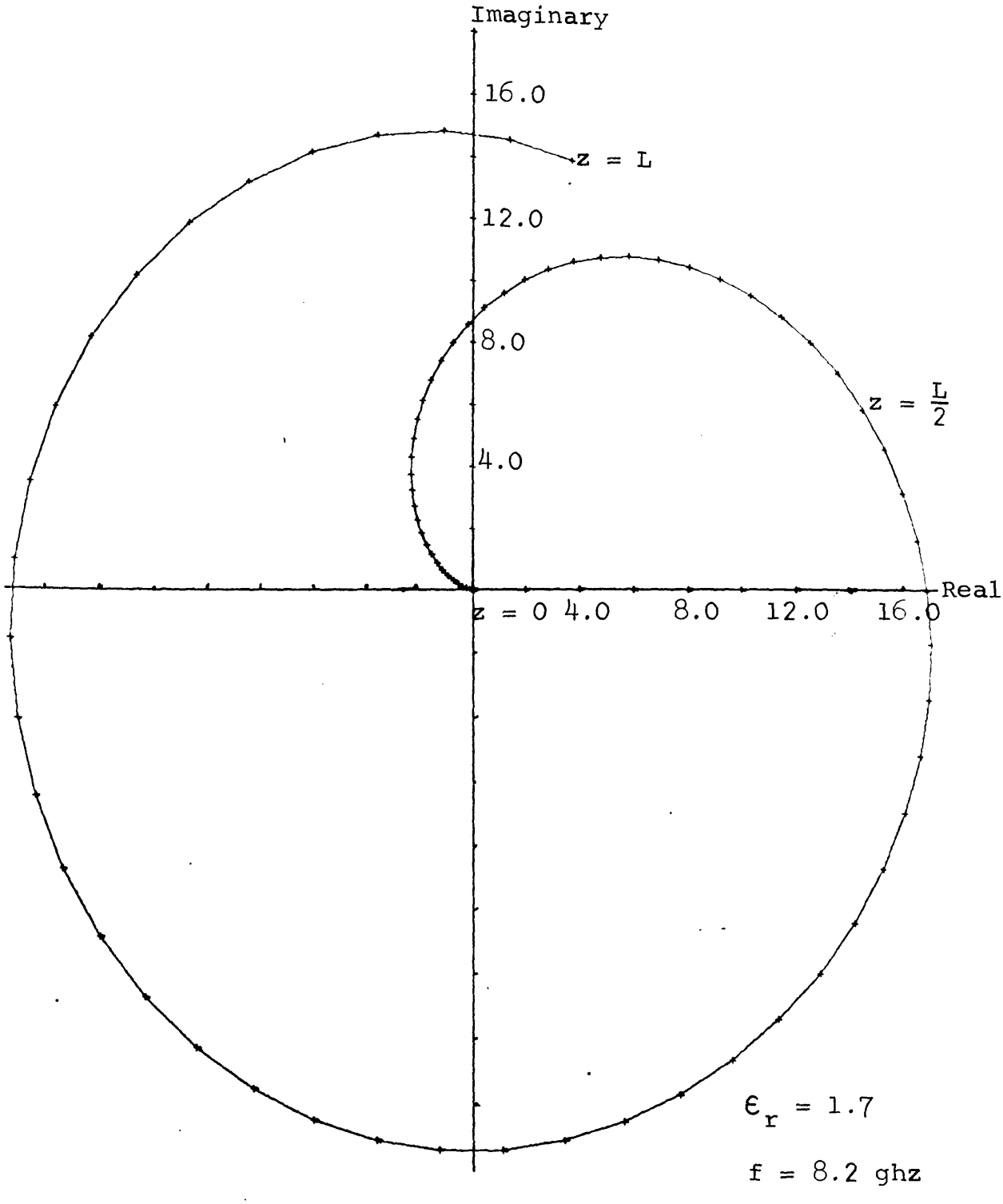

Figure 26. Plot of Complex Integrand for the Linear SSCT

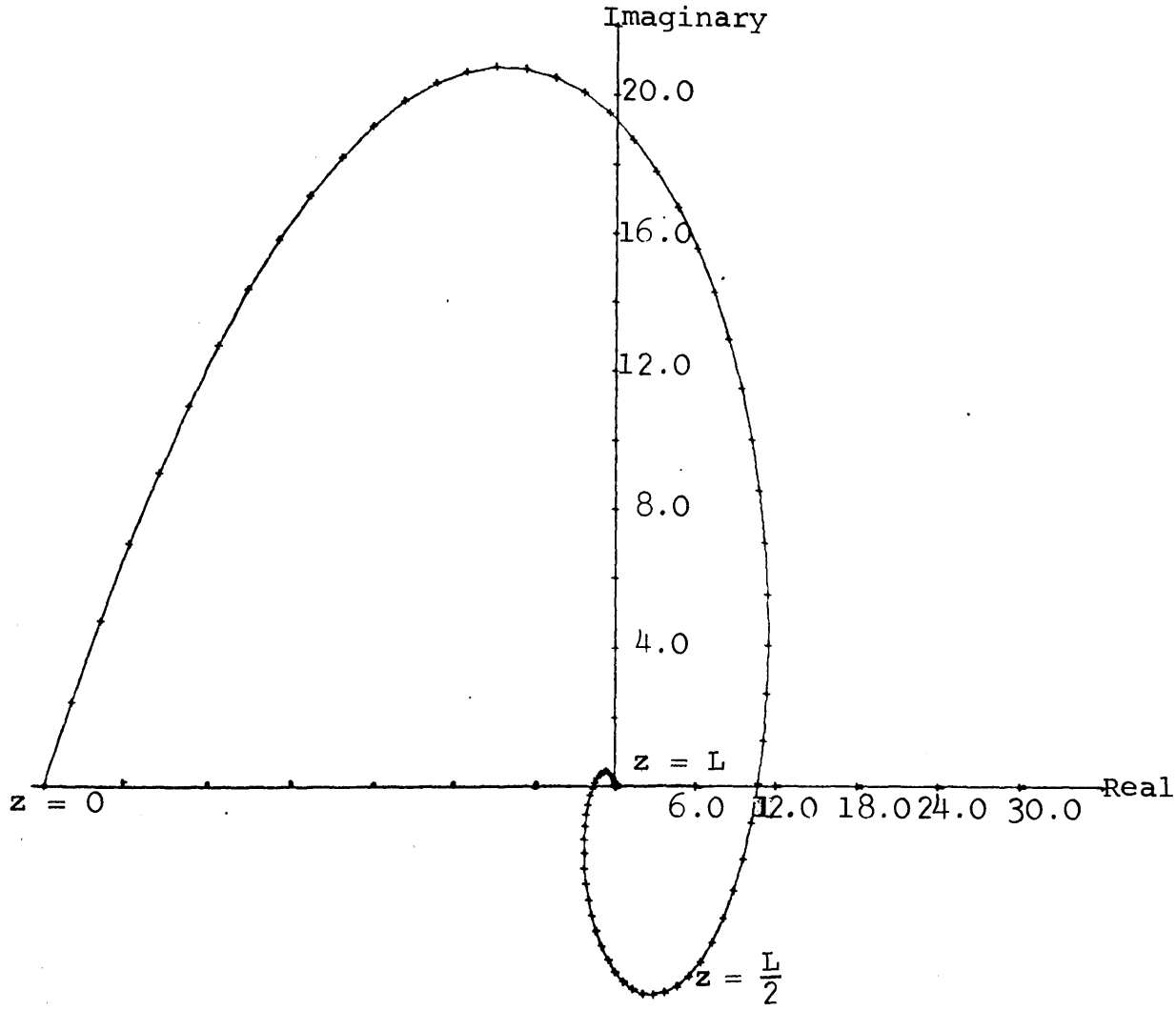

$\epsilon_r = 1.7$

f = 8.2 ghz

Figure 27. Plot of Complex Integrand for the Linear SCCT

CHAPTER V

NONLINEAR UNSYMMETRICAL CONTINUOUSLY TAPERED TRANSITIONS

There are a number of nonlinear continuously tapered dielectric transitions that could be investigated. The analysis of these tapers using the equations developed in the previous two chapters would have to deal almost exclusively with numerical solutions. Two tapers will be dealt with in this chapter. The first taper, which produces a Bessel line, was chosen since it may be treated analytically. The second taper, which produces a parabolic line, was chosen since it represents a line which has been treated quite extensively in the literature for the TEM mode.

A. Bessel Line

The first type of nonuniform transmission line to be investigated were the Bessel lines. For Bessel lines the series impedance and shunt admittances vary along the line (8) as

$$Z = j K_1 z^u \tag{64}$$

$$Y = j K_2 z^v \tag{65}$$

where K_1 and K_2 are real, positive constants. By an appropriate transformation (8) of equations (64) and (65) the transmission line equations transform into Bessel's differential equation. The variation of V and I along the z direction is proportional to Bessel functions and hence the name of the line.

To obtain results for the nonlinear tapers the first-

order approximate solution of Chapter III will be assumed valid. Equation (41) of Chapter III stated that the product of Z_o and β was constant at a particular frequency. For the Bessel line the following relations hold.

$$Z_o = \frac{K_1}{K_2} z^{\frac{u-v}{2}} \tag{66}$$

$$\beta = \sqrt{K_1 K_2}\, z^{\frac{u+v}{2}} \tag{67}$$

For the product $Z_o \beta$ to be independent of z, u must be zero. For a waveguide to be a Bessel line then the series impedance cannot vary with z. The particular transitions under study are suitable for representation a Bessel lines since the dielectric loading represents a capacitive effect. The quantity v in equation (65) may take on any value.

An exact solution of equation (36) of Chapter III may be found if it is assumed that Z_o varies linearly with z. This corresponds to v = -2 in equation (65). Specifically let

$$Z_o(z) = Z_{o1} + \frac{Z_{o2} - Z_{o1}}{L} z \tag{68}$$

where Z_{o1} is the characteristic impedance in region 1 and Z_{o2} is the characteristic impedance in region 2. L is the length of the transition section. In order to simplify the notation let

$$c = Z_{o1}$$

$$g = \frac{Z_{o2} - Z_{o1}}{L} \tag{69}$$

$$r = \ln\left(1 + \frac{g}{c} L\right)$$

By expanding the expression for r it may be shown that

$$r = \ln \left(\frac{Z_{o2}}{Z_{o1}}\right).$$

Inserting values of Z_o and β in equation (36) gives

$$\Gamma(0) = \frac{1}{2} \int_o^L \left(\frac{g}{c+gz}\right) e^{\left[-j \frac{2\omega \mu_o}{g} \ln\left(\frac{c+gz}{c}\right)\right]} dz$$

$$\Gamma(0) = \frac{1}{2} \int_o^L \left(\frac{g}{c+gz}\right) \left(\frac{c+gz}{g}\right)^{\left(\frac{-2j\ \omega\ \mu_o}{g}\right)} dz$$

$$\Gamma(0) = \frac{jg}{4\omega \mu_o} \left[\left(1 + \frac{g}{c} L\right)^{\left(\frac{-2j\ \omega\ \mu_o}{g}\right)} - (1)^{\left(\frac{-2j\ \omega\ \mu}{g}\right)}\right]$$

$$\Gamma(0) = \frac{jg}{4\omega \mu_o} \left[\cos\left(\frac{2\omega \mu_o r}{g}\right) - 1 - j \sin\left(\frac{2\omega \mu_o r}{g}\right)\right]$$

$$\Gamma(0) = \frac{g}{2\omega \mu_o} \sin\left(\frac{\omega \mu_o r}{g}\right) \left[\cos\left(\frac{\omega \mu_o r}{g}\right) - j \sin\left(\frac{\omega \mu_o r}{g}\right)\right]$$

$$\Gamma(0) = \left| \frac{g}{2\omega \mu_o} \sin \left(\frac{\omega \mu_o r}{g}\right) \right|$$

$$\Gamma(0) = \frac{1}{2} \left| \ln \frac{Z_{o2}}{Z_{o1}} \frac{\sin \frac{\omega \mu_o}{g} \ln \frac{Z_{o2}}{Z_{o1}}}{\frac{\omega \mu_o}{g} \ln \frac{Z_{o2}}{Z_{o1}}} \right|$$

$$\left|\Gamma(0)\right| = \frac{1}{2}\left|\ln \frac{Z_{o2}}{Z_{o1}} \; \frac{\sin\left(\frac{\omega \mu_o L}{Z_{o2} - Z_{o1}} \ln \frac{Z_{o2}}{Z_{o1}}\right)}{\left(\frac{\omega \mu_o L}{Z_{o2} - Z_{o1}} \ln \frac{Z_{o2}}{Z_{o1}}\right)}\right| \tag{70}$$

It is meaningful at this time to consider the differences between the problem under consideration and the problems which have been solved in the literature. The problem presented in this dissertation is a waveguide matching transition while those presented in the literature deal with structures capable of propagating TEM modes such as coaxial cables and two wire transmission lines.

For a structure which propagates TEM modes the propagation constant depends entirely upon the frequency and parameters of the material used for the line. The characteristic impedance of such structures are independent of frequency and depend only upon the geometry of the line and the material used for the line.

For the problem posed the propagation constant depends upon the propagating mode, the nonpropagating coupled modes, frequency, mode cutoff constants and materials used for dielectric in the waveguide. The characteristic impedance of a waveguide is not independent of frequency even for a uniform waveguide. A waveguide has considerably more parameters than a TEM mode structure and consequently requires many more graphs to adequately display its characteristics.

As an illustration of this, consider equation (70). For

a Bessel line matching section for a TEM mode structure all the necessary information regarding input reflection coefficient, length of transition and frequency can be specified by one graph once the characteristic impedances of the two regions are known (8). Equation (70) however contains information only on input reflection coefficient and length of transition section at a single frequency. At some other frequency the equation is not valid since the charactersitic impedance does not vary linearly with z except at one frequency. Even if the characteristic impedance does not depart too radically from a linear variation with z at other frequencies both the magnitude and the argument of the sin x/x term change with frequency and a plot of $\Gamma(0)$ versus $L/\lambda g$ is not meaningful as it is for a TEM mode structure.

Nevertheless a great deal of useful information may be gathered from the solution obtained. Comparison of this taper with other tapers may be done at a particular frequency with the results being quite useful. Generally a great deal of analysis must be done before any synthesis work is accomplished and equation (70) represents the first closed form analysis of any continuous waveguide matching section.

A plot of equation (70) is shown in Figure 28 for the case $\epsilon_r = 1.7$ and f = 8.2 ghz. Also shown in this plot is the value of reflection coefficient for the Bessel line as calculated using equation (46) of Chapter III. The number of steps for this calculation was again 20. It is seen that good accuracy is attained except at low values of L/a. The

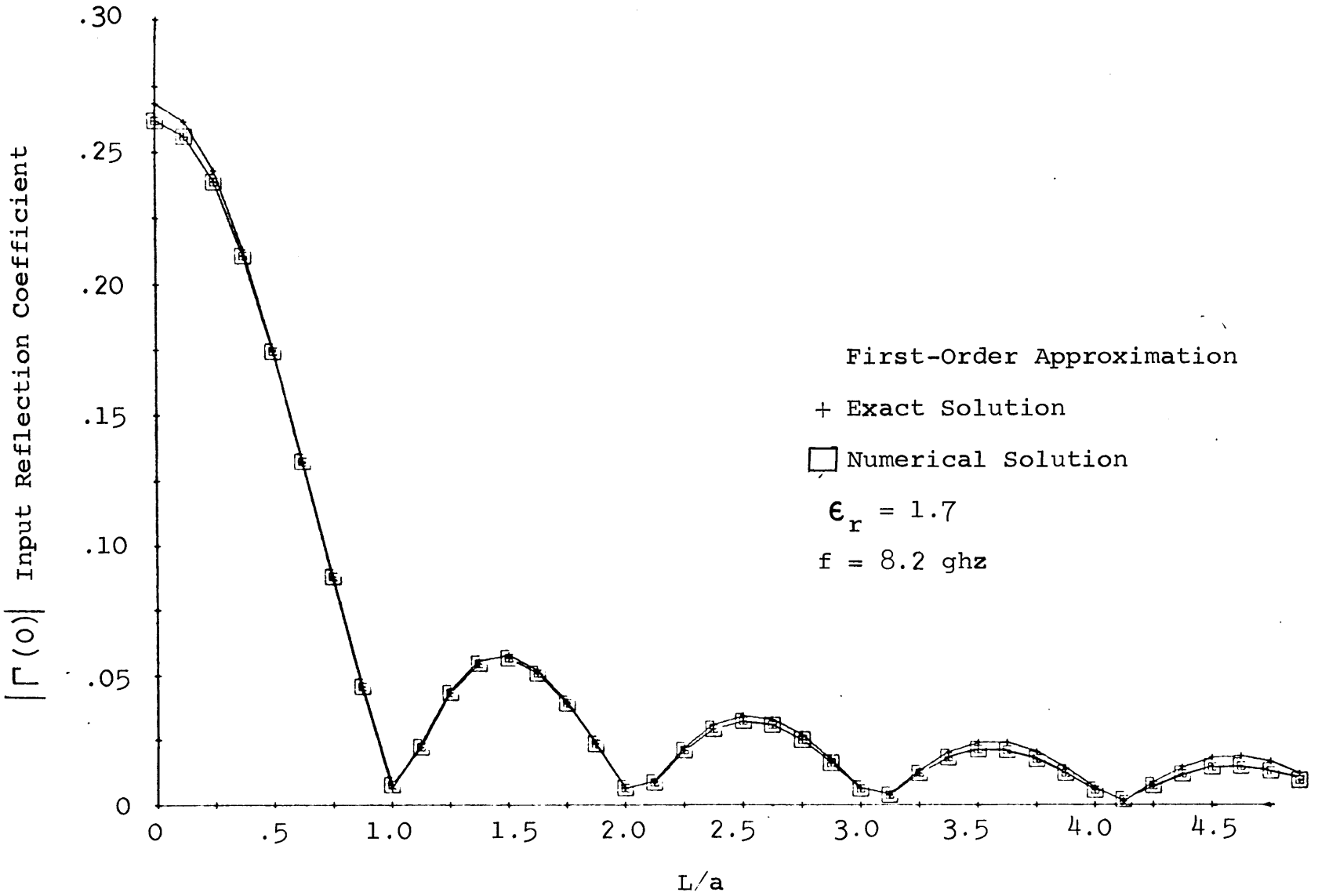

Figure 28. $|\Gamma(0)|$ Versus L/a for Bessel Line

numerical solution is actually the more accurate here since the approximation assumed to obtain equation (36), i.e. $\Gamma^2 << 1$, is not too good an assumption.

B. Parabolic Line

The parabolic line has received considerable attention in the literature (8), (12). For this line the impedance is made to vary as

$$Z_o(z) = a_o + a_1 z + a_2 z^2 + a_3 z^3. \qquad (71)$$

The constants of equation (63) are chosen so that

$$Z_o(0) = Z_{o1}$$

$$Z_o(L) = Z_{o2}$$

$$\left.\frac{dZ_o}{dz}\right|_{z=0} = 0$$

$$\left.\frac{dZ_o}{dz}\right|_{z=L} = 0.$$

Choosing the constants in this way ensures that no reflection occurs due to first-order variation of impedance at the input and output ends of the line.

Evaluating the coefficents yields the following expression for Z_o.

$$Z_o(z) = Z_{o1} + \frac{3(Z_{o2} - Z_{o1})}{L^2} z^2 + \frac{2(Z_{o1} - Z_{o2})}{L^3} z^3 \qquad (72)$$

If this equation is substitued in equation (36) a quite unworkable expression is the result. Thus numerical solutions were used to obtain results. Figure 29 gives the variation if the input reflection coefficient as a function of L/a for

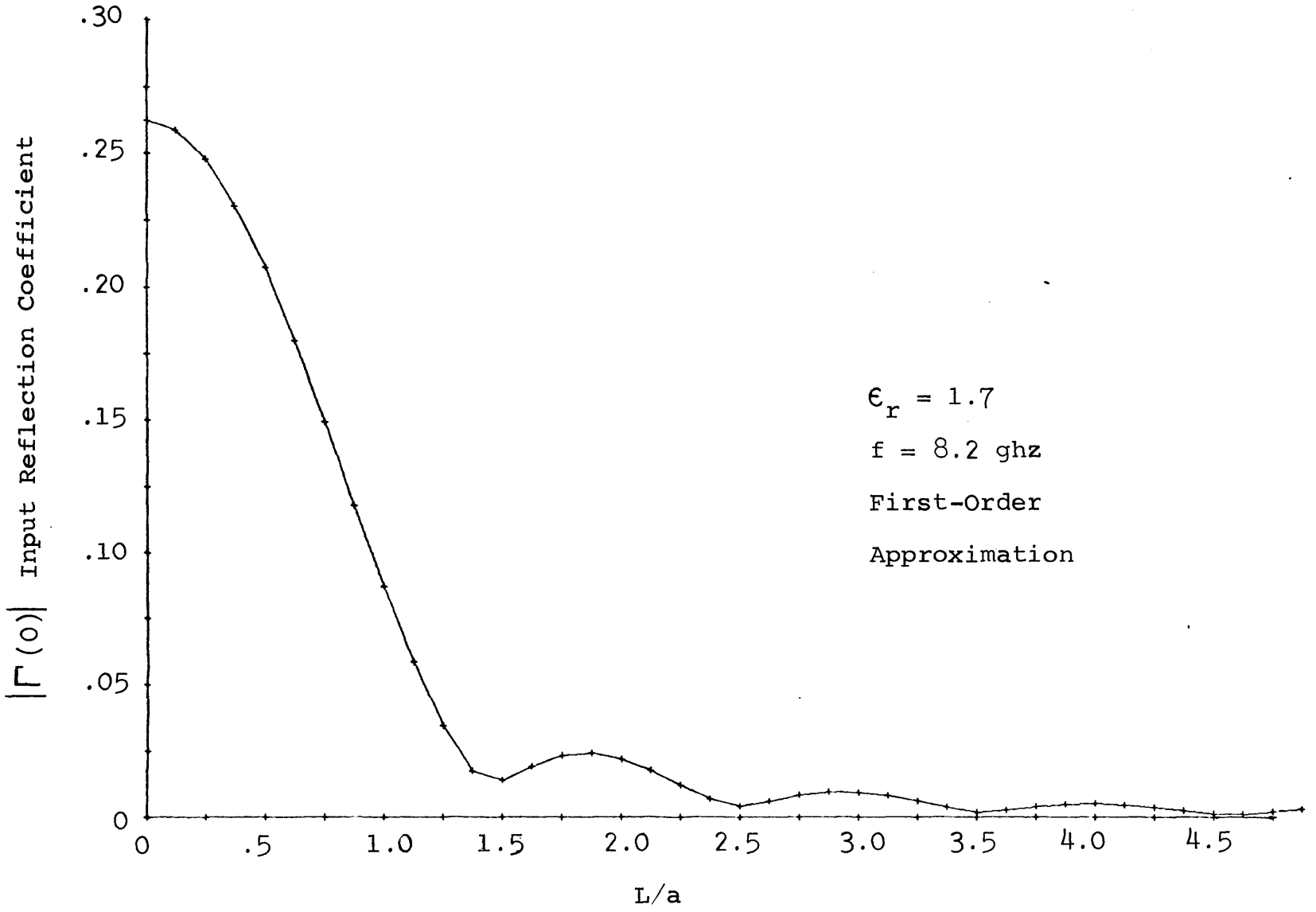

Figure 29. $|\Gamma(0)|$ Versus L/a for Parabolic Line

the case $\epsilon_r = 1.7$ and f = 8.2 ghz.

The comparison of the Bessel line, parabolic line and UCT is given in Figure 30 for the representative case $\epsilon_r = 1.7$ and f = 8.2 ghz. From this plot it is seen that the reflection coefficient of the Bessel line decreases the fastest but tends to have rather large lobes. The reflection coefficient of the parabolic line decreases faster than the UCT with relatively low lobes. If the transition section can be made long enough there is little to gain using a nonlinear taper over the linear taper. It is interesting to note that the parabolic line and symmetrical side linear taper have similar response functions.

C. Taper Shapes

To find the shape of the taper necessary to produce a given line requires the values of d which satisfy

$$Z_o(z) = \frac{\omega \mu_o}{Y_1(z)} \tag{73}$$

for any value of z in the transition length. Substitution of $Y_1(z)$ for the unsymmetrical continuously tapered dielectric matching transition into this expression gives at a general point z_1

$$d - \frac{a}{2\pi} \sin \frac{2\pi}{a} d = \frac{a}{\omega \epsilon_o (\epsilon_r - 1)} \left[\frac{\omega \mu_o}{Z_o^2(z_1)} - \frac{k_o^2 - (\frac{\pi}{a})^2}{\omega \mu_o} \right]. \tag{74}$$

The root of this equation satisfying the criterion $d/a \leq 1$ is the width of the dielectric at the point z_1. Numerical methods will have to be used to extract the roots of this transcendental

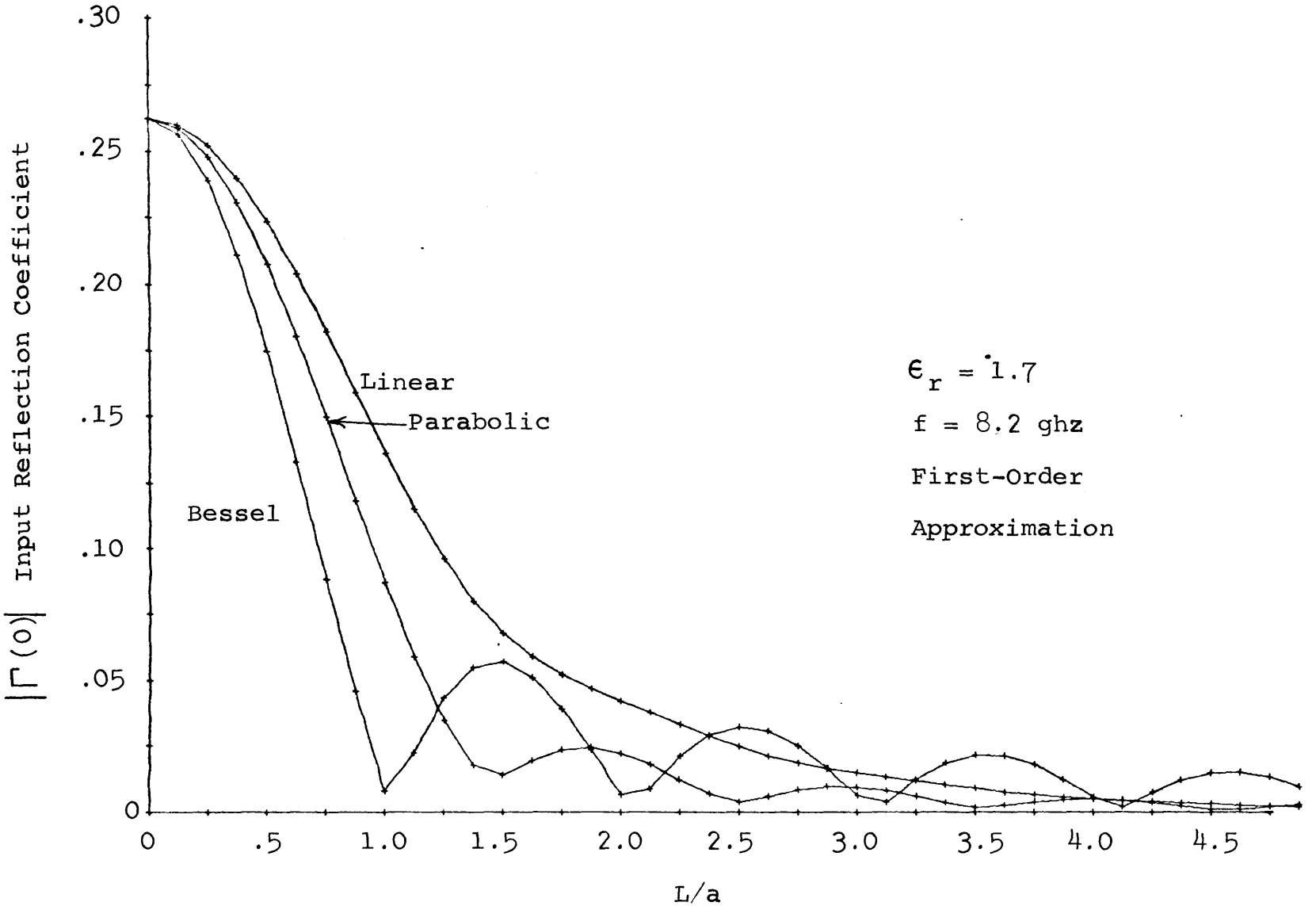

Figure 30. $|\Gamma(0)|$ Versus L/a for the Three Unsymmetrical Continuously Tapered Lines

equation. The taper shapes required for a Bessel line and a parabolic line are shown in Figure 31 for the case $\epsilon_r = 1.7$ and f = 8.2 ghz.

The variation of the characteristic impedance with z can be prescribed only at one frequency. To see the effect of frequency on characteristic impedance the curves of Figure 32 were calculated for the Bessel line. As may be see the departure from linearity with z of Z_o is not too significant and equation (70) can be used without appreciable error.

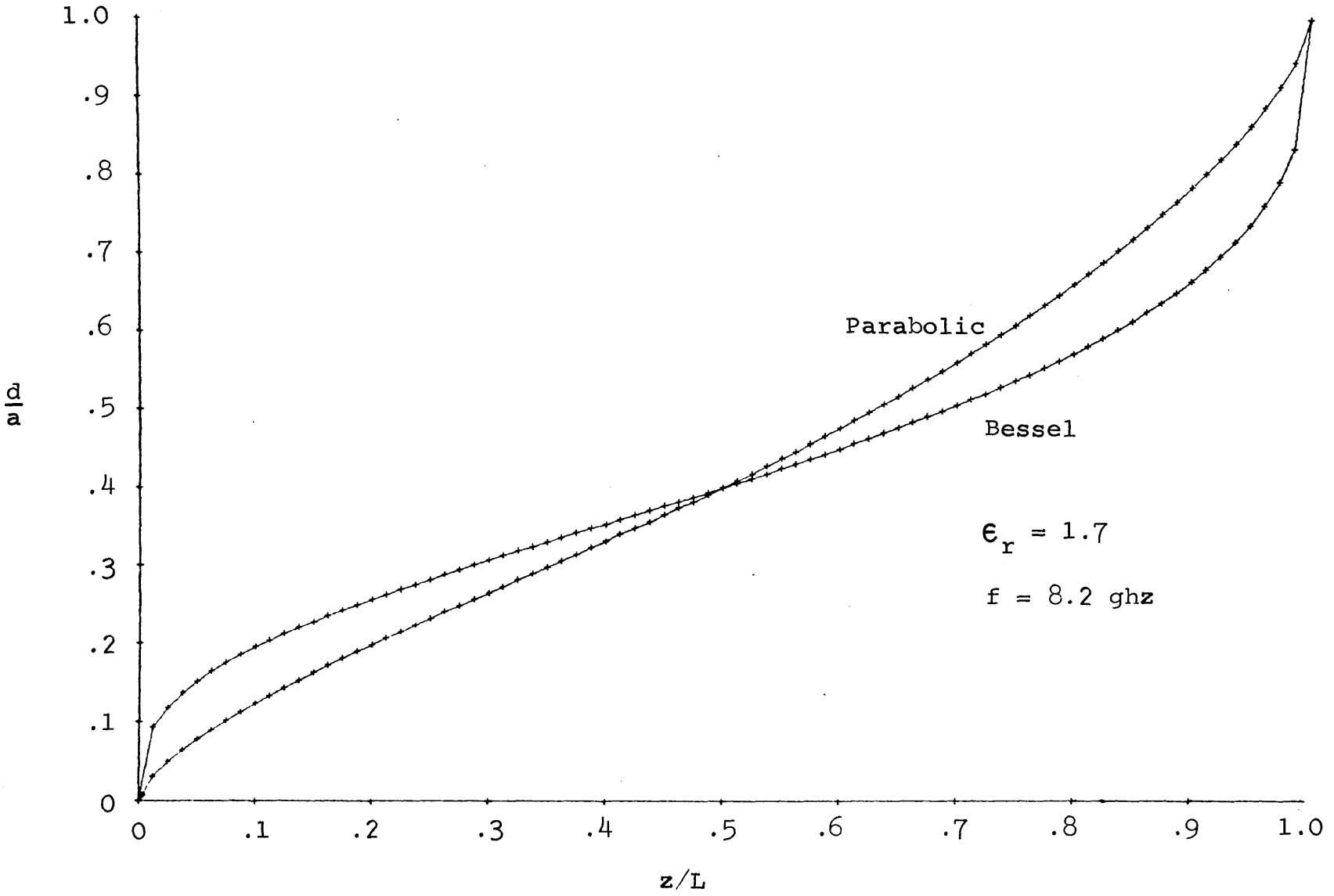

Figure 31. Taper Shape for Bessel and Parabolic Lines

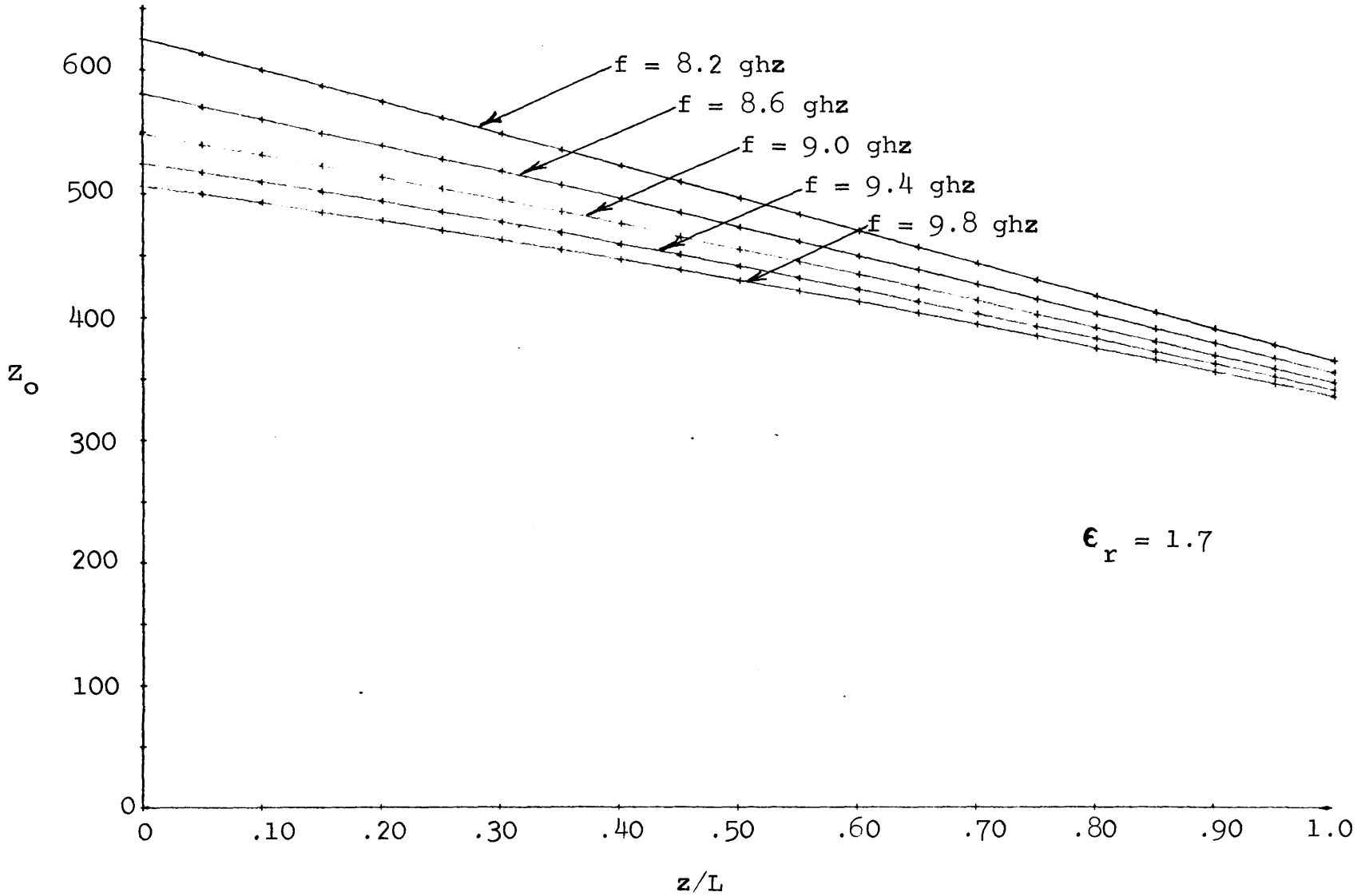

Figure 32. Variation of Z_o with Length for Bessel Line with ω as Parameter

CHAPTER VI

EXPERIMENTAL PROCEDURES AND RESULTS

A. Measuring Technique

The object of the experimental work was to verify the theory and computer curves of the preceeding chapters. A dielectric constant of 1.7 was selected for the experimental work. The dielectric used was Eccofoam which is manufactured by the Emerson-Cuming Company. This dielectric material may be cut easily by a band saw if a slow enough saw speed is used.

In microwave measurements the reflection coefficeint is almost never measured directly. The usual procedure is to measure the VSWR (voltage standing wave ratio) and calculate the reflection coefficeint from this. The measurement of VSWR is straightforward and is easily performed using slotted line techniques. There are various methods which can be used to measure VSWR of a matching transition with the slotted line. Two of these methods will be described.

For the first method the dielectric is machined into a slab which fits snugly inside the waveguide. The matching transition is machined on one end of the slab and longitudinal tapers are machined on the other end of the slab. Resistive paper is placed into the tapers. This end of the slab then represents an infinite length section and if care is taken in its design very little reflection will occur. The transition end of the slab is placed on the load end of the slotted line and the VSWR is measured. If the load has very

low reflection the VSWR is due to the matching transition and the reflection due to this may be calculated. This method will work well for dielectric material which may be cut for the longitudinal tapers. For the Eccofoam this was impossible and the method was finally rejected.

The second method also used a dielectric slab machined to fit snugly inside the waveguide. The matching transition was machined on one end of the slab and the slab was then inserted in the slotted line. The slotted line section is then a dielectric-filled waveguide as shown in Figure 33. A matched termination is then connected to the output side of the slotted line. This matched termination is built in air filled waveguide so that a dielectric-filled to air filled waveguide has been effected. The VSWR in the slotted section may now be measured and the reflection coefficient calculated.

The second method was the one used for the experimental work. The block diagram of the laboratory equipment is shown in Figure 34.

B. Experimental Results

The technique described above is easy to implement in the laboratory. However at low values of reflection coefficient inaccuracies in the dielectric slab make precise measurement of the VSWR impossible. A small nick in the dielectric may cause reflection comparable to that of the transition section. For this reason most of the measurements were made for short transition lengths where the inherent reflections of the slab will not cause as much trouble. The

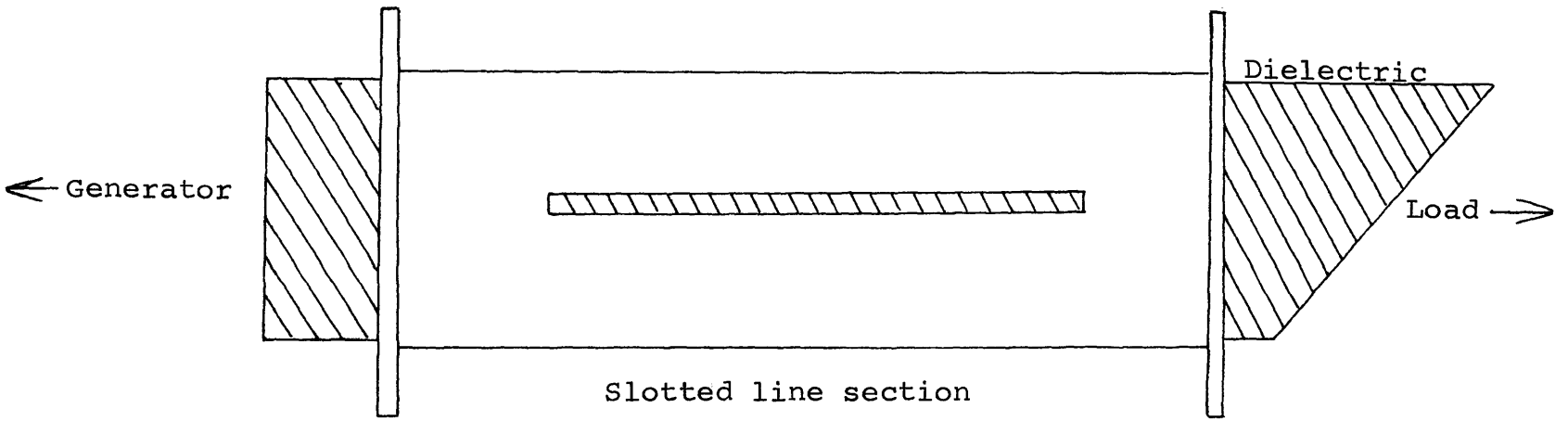

Figure 33. Dielectric Slotted Line

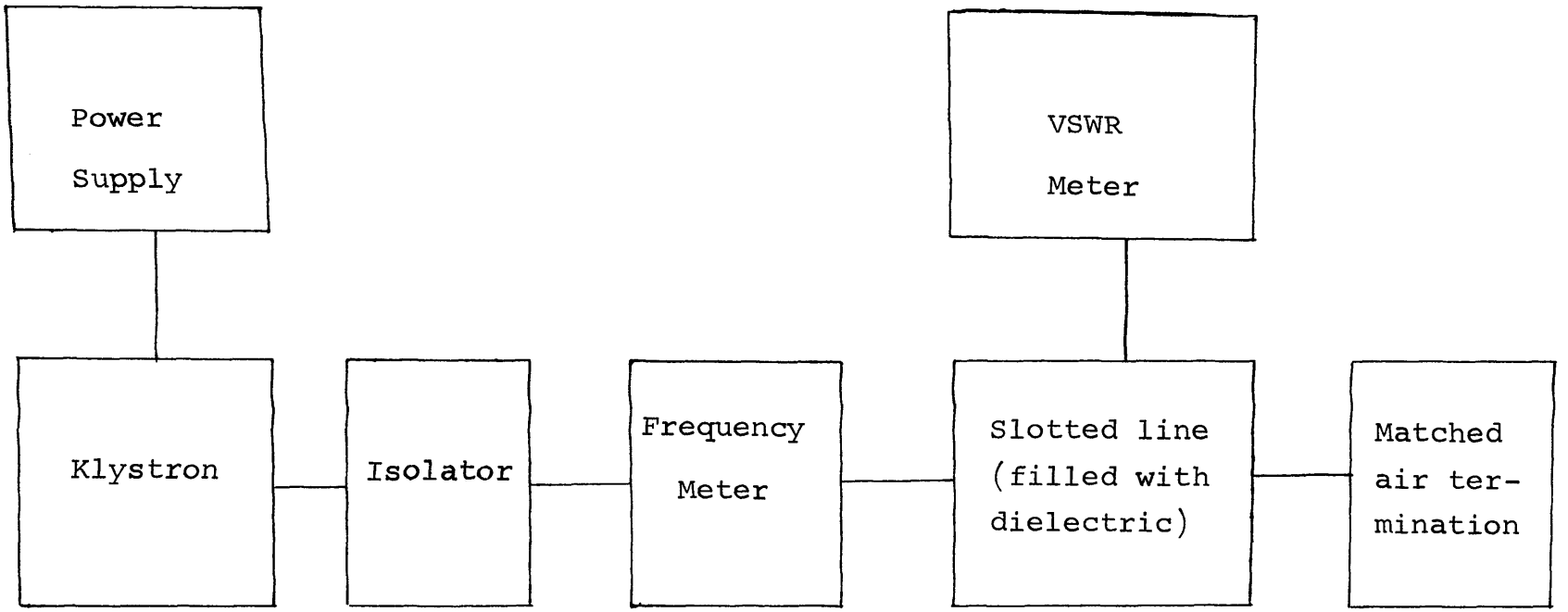

Figure 34. Block Diagram of Experimental Equipment

accuracy of the measurement of the VSWR is between 5 and 10 percent at values of VSWR above 1.20 using the standard laboratory equipment.

The following curves present the experimental points and the value of VSWR computed theoretically. The VSWR is shown instead of reflection coefficient to be consistent with the microwave literature.

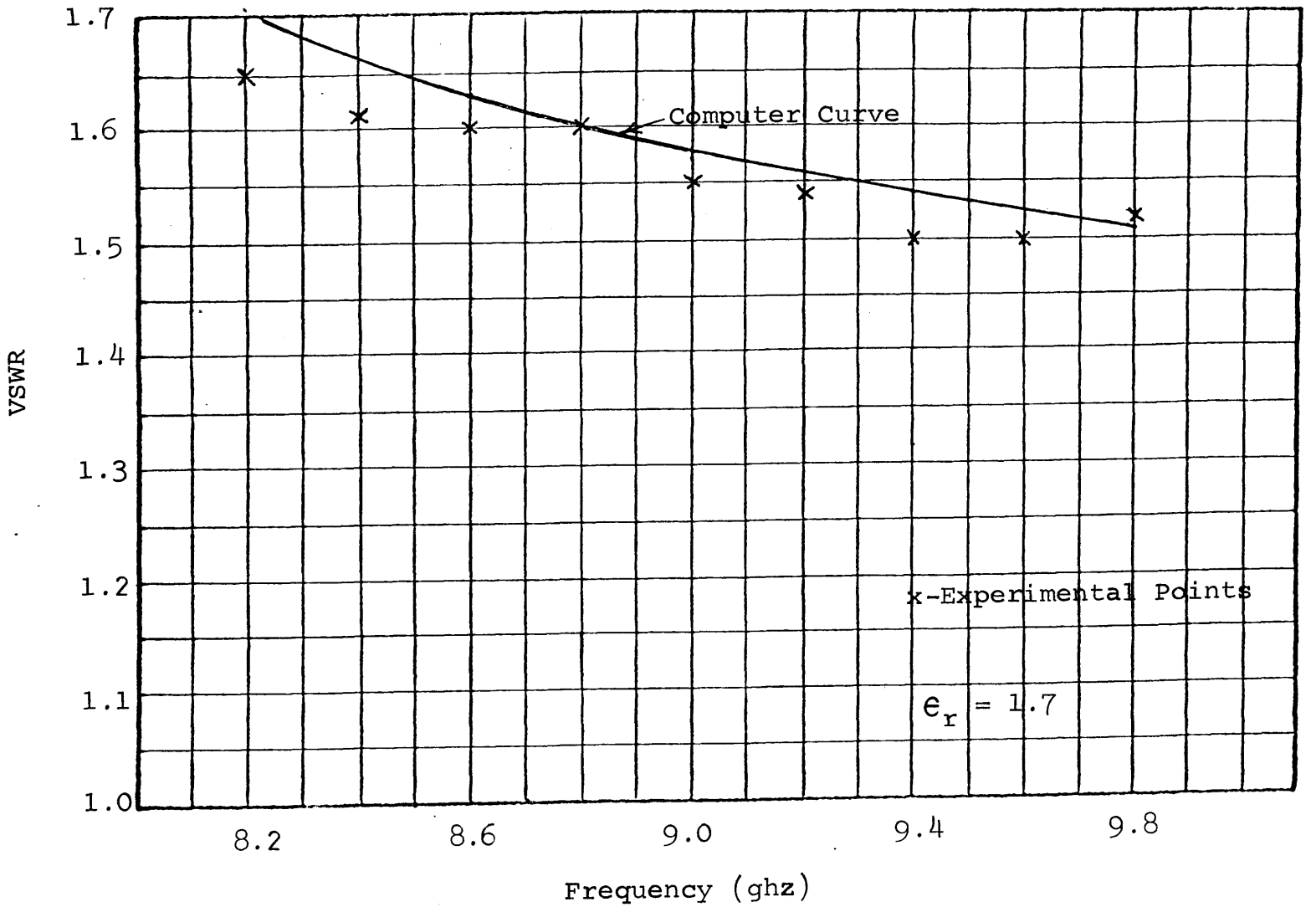

Figure 35. VSWR Versus Frequency for an Abrupt Junction (L/a = 0)

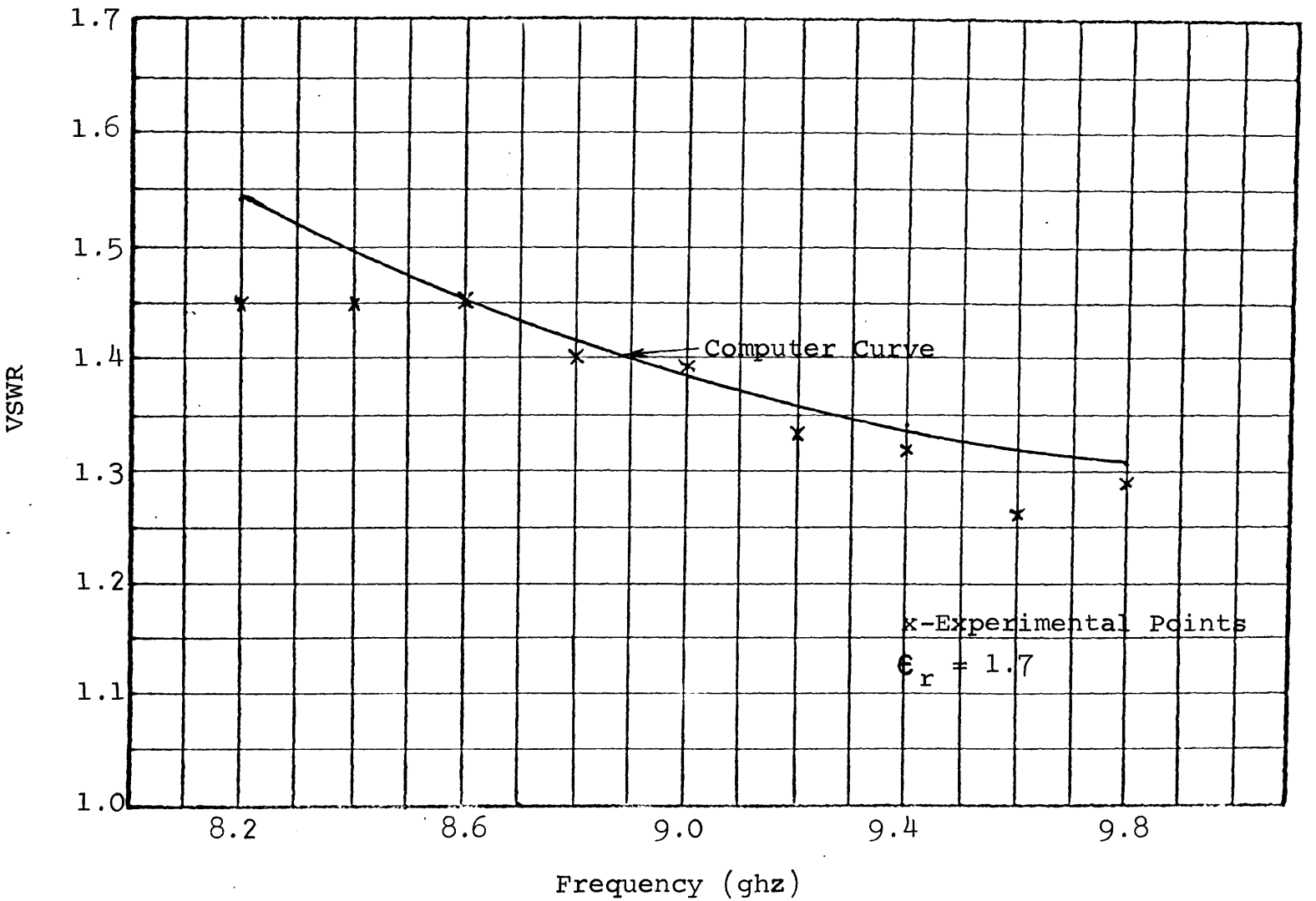

Figure 36. VSWR Versus Frequency for the Linear UCT for L/a = 0.5

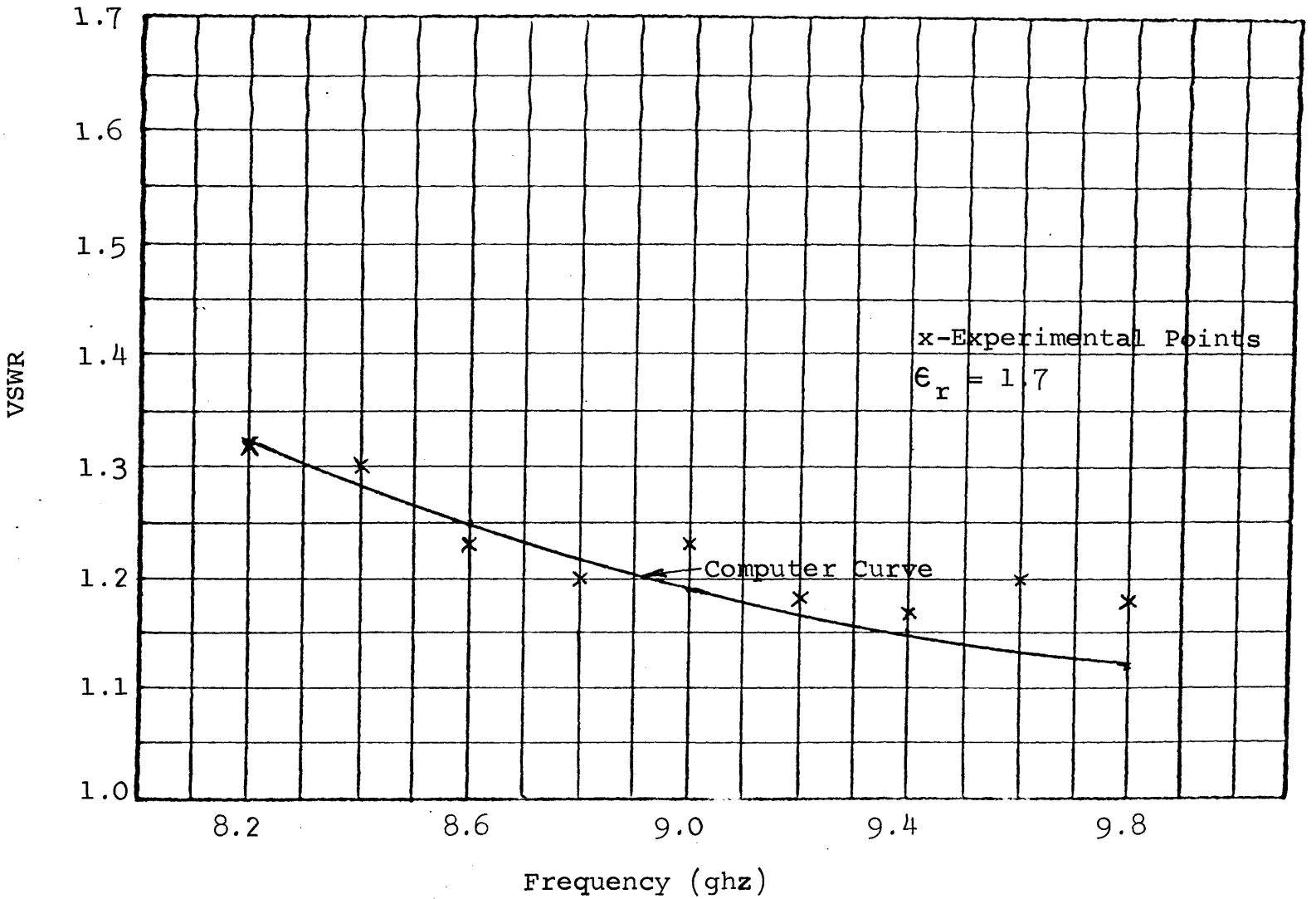

Figure 37. VSWR Versus Frequency for the Linear UCT for L/a = 1.0

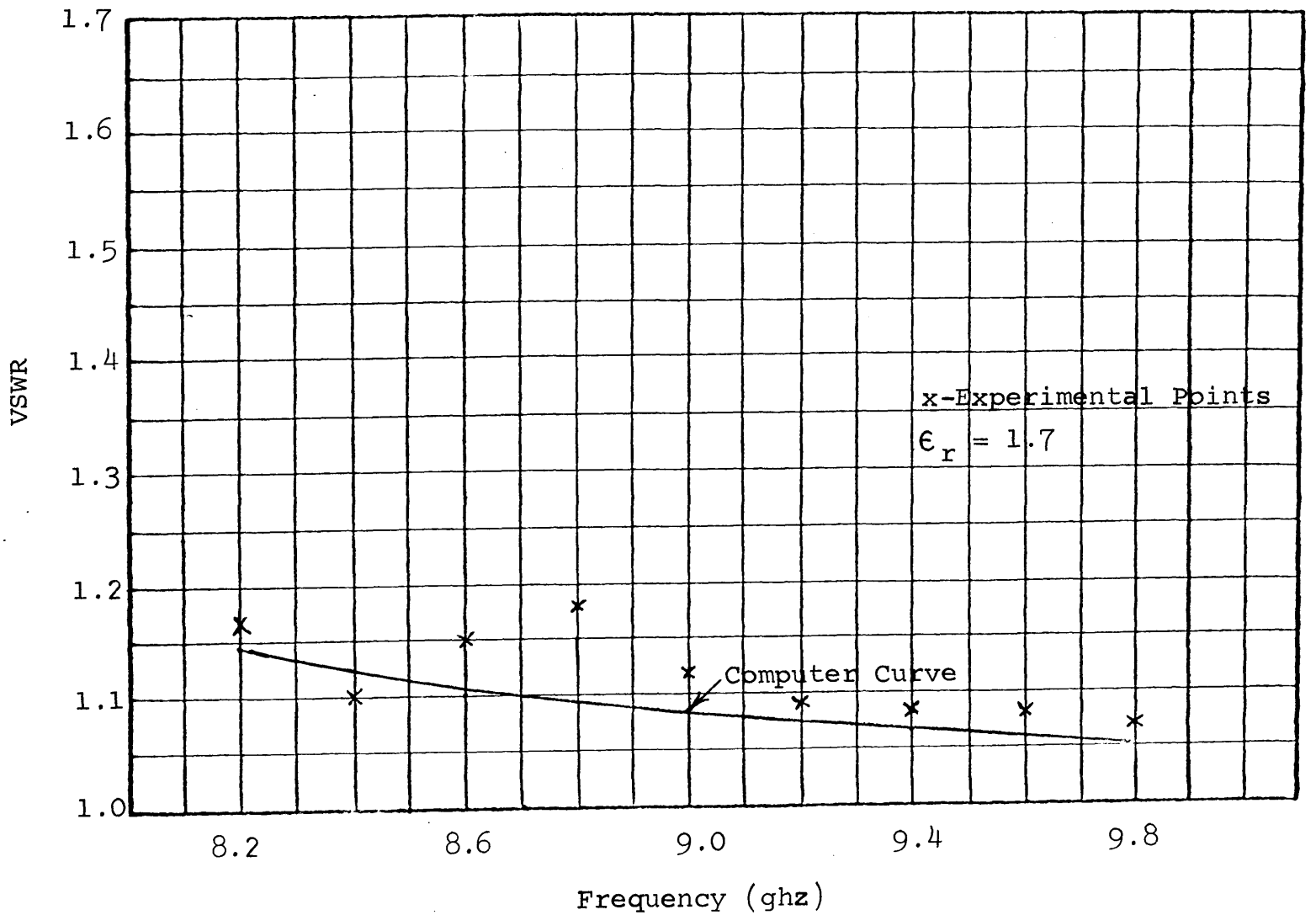

Figure 38. VSWR Versus Frequency for the Linear UCT for L/a = 1.5

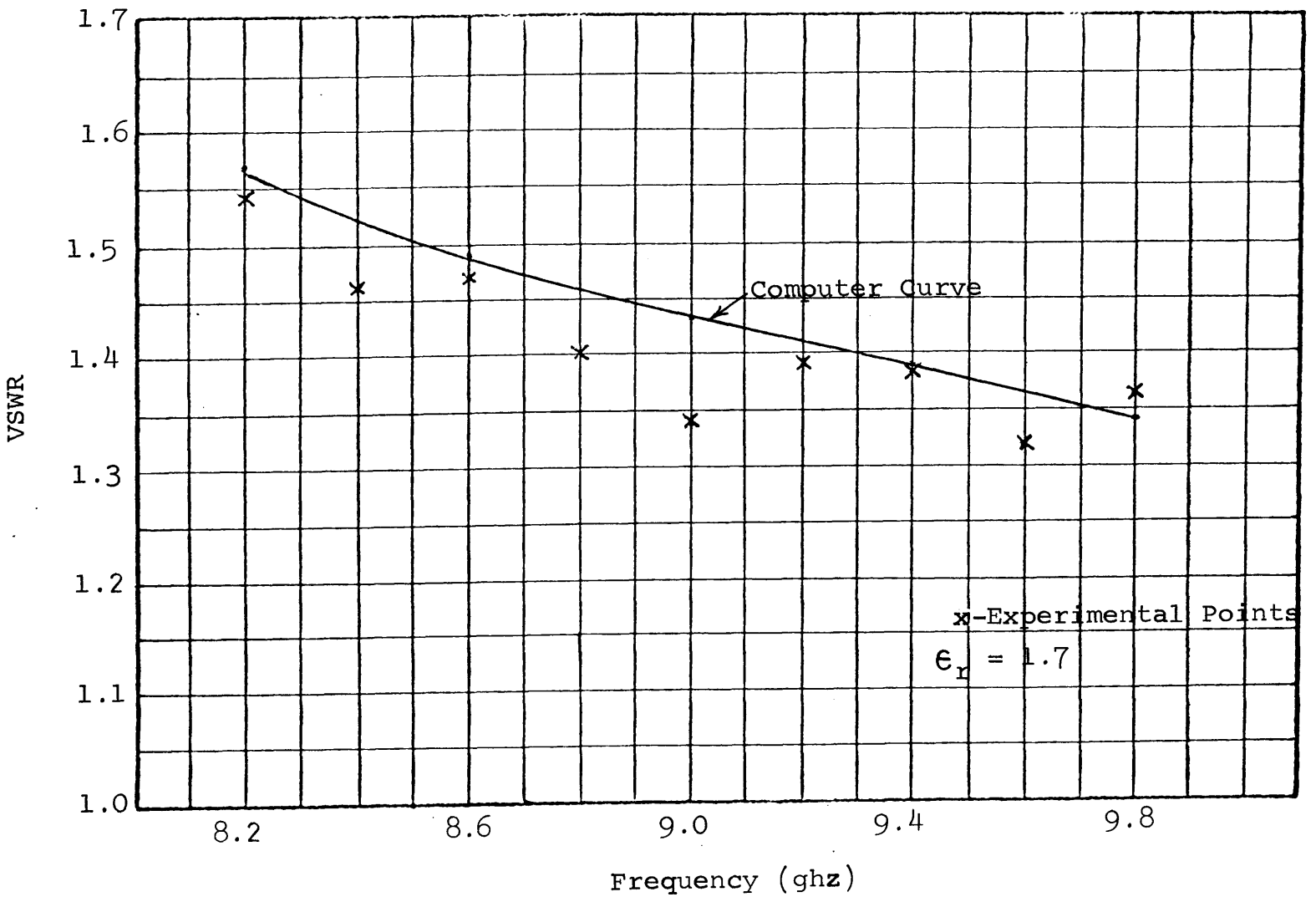

Figure 39. VSWR Versus Frequency for the Linear SSCT for L/a = 0.5

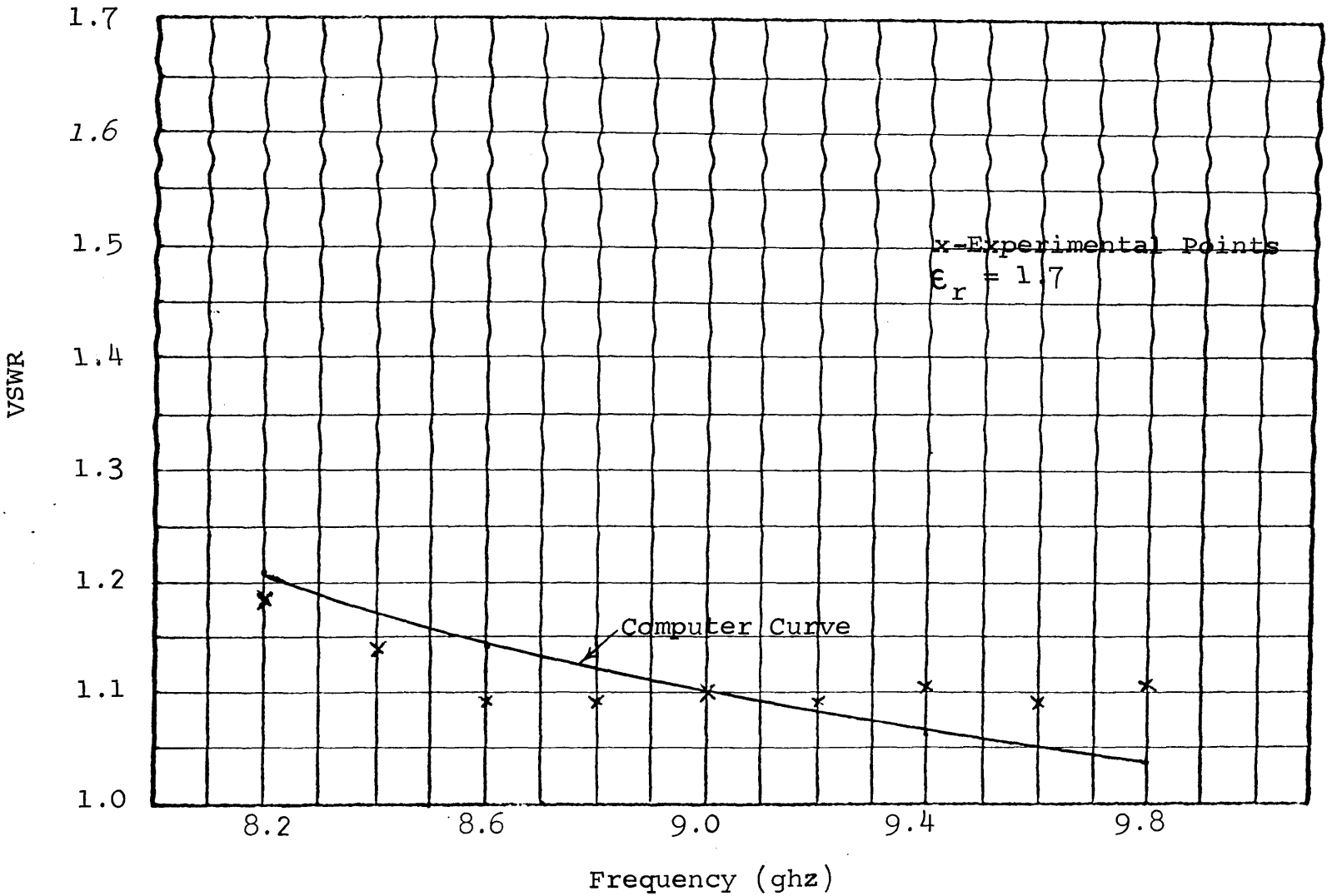

Figure 40. VSWR Versus Frequency for the Linear SSCT for L/a = 1.0

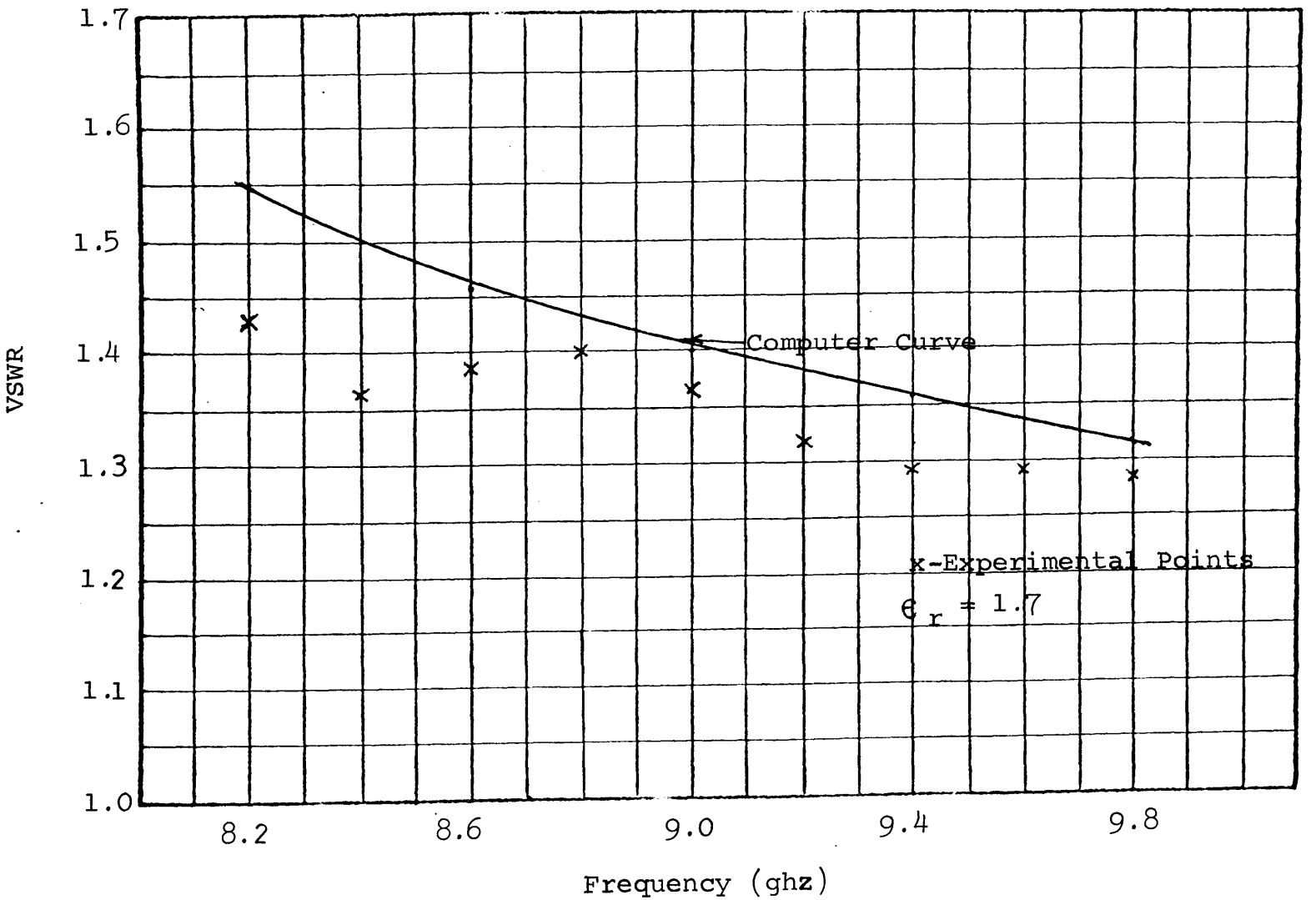

Figure 41. VSWR Versus Frequency for the Linear SCCT for L/a = 0.5

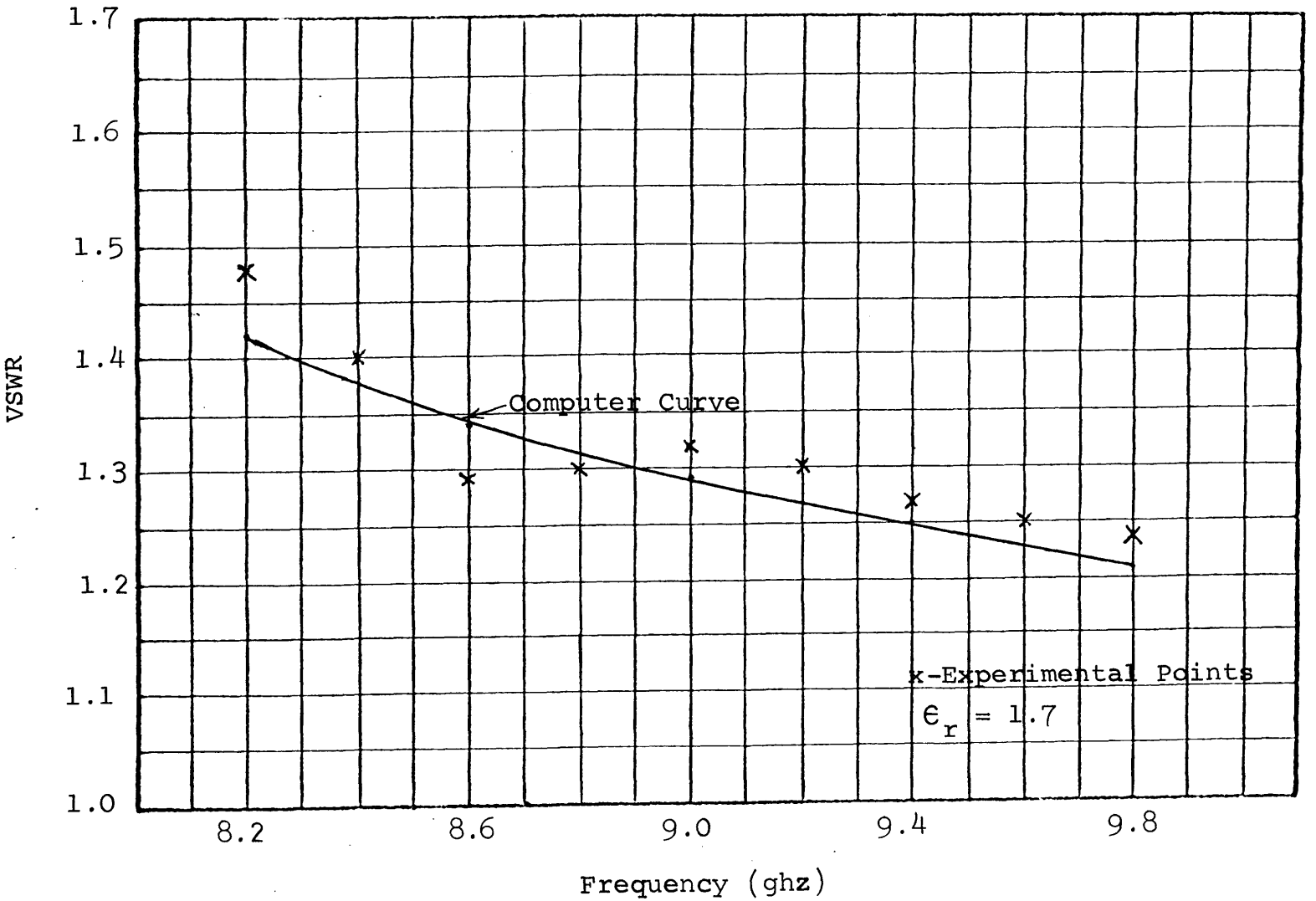

Figure 42. VSWR Versus Frequency for the Linear SCCT for L/a = 0.75

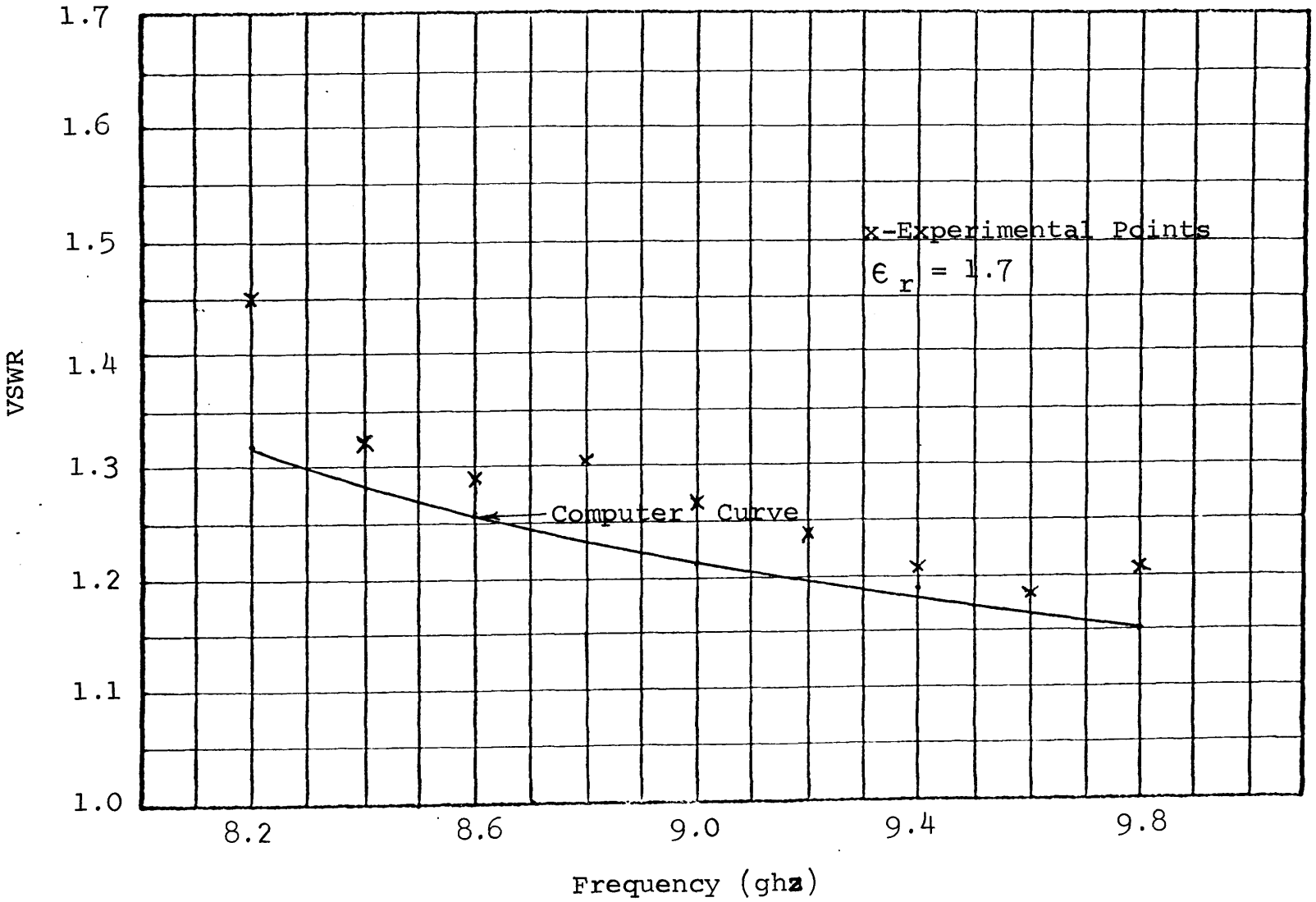

Figure 43. VSWR Versus Frequency for the Linear SCCT for L/a = 1.0

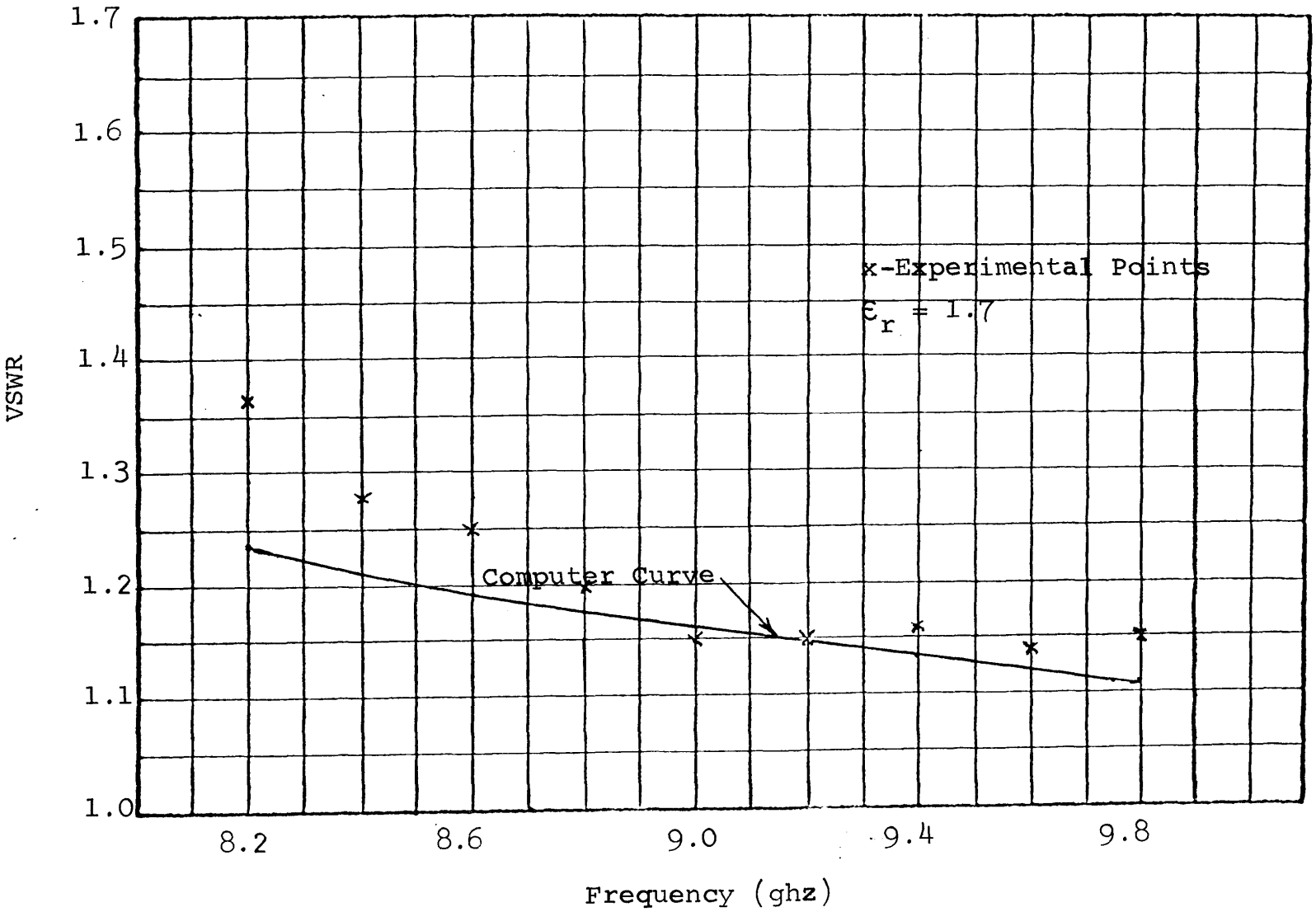

Figure 44. VSWR Versus Frequency for the Linear SCCT for L/a = 1.5

CHAPTER VII

CONCLUSIONS AND SUGGESTIONS FOR FURTHER DEVELOPMENT

A. Conclusions

A method of solving continuously tapered dielectric transitions in a waveguide of uniform cross-section has been developed. This method has been applied to dielectric matching transitions of various shapes with good results. A first-order approximate solution gives quite good accuracy from a practical viewpoint. If better accuracy is required two things must be done. The first is to use the second-order approximate solution and the second is to divide the transition section into smaller lengths. Both requirements add considerably to computer time and this should be taken into account when considering what accuracy is necessary.

The continuously tapered dielectric matching sections described in Chapter IV have improved response as the frequency is increased. There are two reasons for this. The first is that increasing the frequency increases the electrical lengths of the transition thus lowering the input reflection coefficient. The second is that the characteristic impedance changes with frequency with the overall result being to lower the reflection coefficient.

It should be mentioned that an equivalent electrical circuit could be drawn for the transition matrix from the transfer matrix.

B. Suggestions for Further Development

Much more work can be done in this area. Probably the most important is the synthesis problem for an optimum taper as mentioned earlier. This problem would have to be approached using the first-order approximate solution and optimizing the taper using the polar plots of the integrand shown in Figures 25, 26, 27. The taper could be optimized in any one of a number of ways. One possibility would be to require the reflection coefficient to fall below a prescribed minimum in the shortest transition length possible. Another possibility would be to optimize the taper so that the next highest propagating mode is minimized. These are probably the two most important possibilities.

The problem of continuous dielectric tapers in circular waveguide is another area that should prove fruitful. This could be done using the generalized telegraphist's equations and the procedure developed in this dissertation. An extension to elliptic waveguide is also possible.

The dielectric tapers could also be used for microwave devices other than matching transitions. One idea is to use linear taper to correct for the dispersive effects of the waveguide. Another possivility is to use the dielectric taper as a variable (with length) frequency cutoff device. This would have application to pulse compression (18). It may also be possible to use the tapered dielectric for filters in the microwave region. All of these possibilities may be investigated using the first-order approximate solution described in the dissertation.

BIBLIOGRAPHY

1. Goodwin, F. E. and Moss, G. E.
   Impedance Matching Into Dielectric Filled Waveguides, IEEE Transactions on Microwave Theory and Techniques, January 1963, pp 36-39.

2. Collin, R. E. and Brown, J.
   The design of Quarter-Wave Matching Layers For Dielectric Surfaces. Proceedings of the IEE, Volume 103-C, 1956, pp. 153-158.

3. Sullivan, D. J. and Parkes, D. A.
   Stepped Transformers For Partially Filled Transmission Lines, IRE Transactions on Microwave Theory and Techniques, March 1960, pp. 212-217.

4. Soohoo, R. F.
   Theeory of Dielectric-Loaded and Tapered Field Ferrite Devices, IFE Transactions on Microwave Theory and Techniques, May 1960, pp. 220-224.

5. Heaviside, Oliver
   Electromagnetic Theory, New York: Dover Publications, Inc., 1950.

6. Starr, A. T.
   The Nonuniform Transmission Line, Proceedings of the IRE, Volume 20, No. 6, June, 1932, pp. 1052-63.

7. Scott, H. J.
   The Hyperbolic Transmission Line as a Matching Section, Proceedings of the IRE, Volume 41, No. 11, November, 1953, pp. 1654.

8. Ghose, R. N.
   Microwave Circuit Theory and Analysis, New York: McGraw-Hill Book Company, Inc., 1963.

9. Klopfenstein, R. W.
   A Transmission Line Taper of Imporved Design, Proceedings of the IRE, Volume 44, No. 1, January, 1956, pp. 31.

10. Willis, J. and Sinha, N. K.
    Non-uniform Transmission Lines as Impedance Transformers, Proceedings of the IEE, Volume 103-B, 1956, pp. 166.

11. Bolinder, F.
    Fourier Transforms and Tapered Transmission Lines, Proceedings of the IRE, Volume 44, No. 4, April 1956, pp. 557.

12. Yang, R. F. H.
Parabolic Transmission Line, Proceedings of the IRE, Volume 43, No. 8, August 1955, pp. 1955.

13. Collin, R. E.
The Optimum Tapered Transmission Line Matching Section, Proceedings of the IRE, Volume 44, No. 4, April 1956, pp. 557.

14. Bertnolli, E. C.
Exact and Numerical Analyses of Distributed Parameter RC Networks, Ph.D. Dissertation, Kansas State University Bulletin, Volume 49, No. 9, September 1965.

15. Schelkunoff, S. A.
Generalized Telegraphist's Equations For Waveguides, Bell System Technical Journal, Volume 31, pp. 784-801.

16. Schelkunoff, S. A.
Electromagnetic Waves, New York: D. Van Nostrand Company, Inc., 1943.

17. Bertnolli, E. C.
Personal Communication

18. Hord, W. E.
A Pulse Compression Technique, Emerson Electric Technical Memorandum, September 1963.

APPENDIX A

PROOF OF THEOREM STATED IN TEXT

The theorem as stated in the text was:

Consider a dielectric matching transition consisting of a continuously tapered dielectric of constant permeability in a uniform rectangular waveguide. If the dielectric constant is independent of y only TE_{n0} modes where n = 1, 2, 3, . . . exist in the transition when it is excited by the dominant TE_{10} mode.

For the proof of the theorem consider the rectangular waveguide shown in Figure 1. The mode functionsof this waveguide are given in equation (8). Let the waveguide be filled with dielectric for which

$$\epsilon_r = \epsilon_r(x,z) \tag{1A}$$

$$\mu = \mu_o. \tag{2A}$$

Referring to the generalized telegraphist's equations of Chapter II it is seen that the term giving rise to coupling between TE modes in equation (1) is

$$\iint_s \mu_{zz}\, T_n^e\, T_m^e\, ds$$

which vanishes except for n = m by the first equation of set (7). Thus coupling between different TE modes cannot arise from equation (1).

Equation (2) relates only TE modes. No coupling between TE modes comes from this. Equation (3) relates coupling

between TE and TM modes but not between different TE modes. In equation (4) the term involving coupling between TE modes is

$$\iint_s \left[\mu_{xx} \frac{\partial T_n^e}{\partial x} \frac{\partial T_m^e}{\partial x} + \mu_{yy} \frac{\partial T_n^e}{\partial y} \frac{\partial T_m^e}{\partial y}\right] ds$$

which may be written

$$\mu_o \iint_s \left[\frac{\partial T_n^e}{\partial x} \frac{\partial T_m^e}{\partial x} + \frac{\partial T_n^e}{\partial y} \frac{\partial T_m^e}{\partial y}\right] ds. \qquad (3A)$$

Equation (3A) vanishes except for n = m from the third equation of set (7). No coupling between different TE modes is introduced by equation (4). Equation (6) related coupling between TE and TM modes and does not have terms involving coupling between TE modes.

Only equation (5) may give rise to coupling between TE modes. The term giving coupling between the modes is

$$\iint_s \left[-\epsilon_{xx} \frac{\partial T_n^e}{\partial y} \frac{\partial T_m^e}{\partial y} - \epsilon_{yy} \frac{\partial T_n^e}{\partial x} \frac{\partial T_m^e}{\partial x}\right] ds. \qquad (4A)$$

Substituting the mode functions in equation (4A) gives

$$N_{pq} N_{st} \int_o^b \int_o^a \epsilon_r(x,z) \frac{qt\pi^2}{b^2} \cos\frac{p\pi}{a}x \cos\frac{s\pi}{a}x \sin\frac{q\pi}{b}y \sin\frac{t\pi}{b}y \, dxdy$$

$$+ \int_o^b \int_o^a \epsilon_r(x,z) \frac{ps\pi^2}{b^2} \sin\frac{p\pi}{a}x \sin\frac{s\pi}{a}x \cos\frac{q\pi}{b}y \cos\frac{t\pi}{b}y \, dxdy$$

Since $\epsilon_r(x,z)$ is not a function of y the y integrations may

be performed and it may be shown that both integrals vanish unless t = q.

Since the integral has nonzero value only for t = q the coupling between TE modes is zero except for the modes belonging to the set

$$TE_{pq}$$

$$TE_{sq}. \tag{5A}$$

Since the incident mode on the transition was the TE_{10} mode, q = 0 in equation (5A) and coupling exists only between TE_{po} and TE_{so} modes. TM modes may still be coupled since they have not been eliminated yet.

From here on the only TE modes that need be considered are the TE_{po} modes since only they are coupled to the TE_{10} mode. For all of these modes

$$\frac{\partial T^{e}_{po}}{\partial y} = 0. \tag{6A}$$

The coupling between TE_{n0} and TM modes will now be shown to vanish. Equation (1) relates only TE modes and cannot give rise to coupling between TE and TM modes. Equation (2) relates only TM modes and does not give rise to coupling between TE and TM modes. The term in equation (3) giving rise to coupling between TE and TM modes is

$$\iint_{s} \left[\mu_{xx} \frac{\partial T^{e}_{n}}{\partial x} \frac{\partial T^{h}_{m}}{\partial y} - \mu_{yy} \frac{\partial T^{e}_{n}}{\partial y} \frac{\partial T^{h}_{m}}{\partial x}\right] ds$$

which may be written

$$\mu_o \iint_s \left[\frac{\partial T_n^e}{\partial x}\frac{\partial T_m^h}{\partial y} - \frac{\partial T_m^h}{\partial x}\frac{\partial T_n^e}{\partial y}\right] ds. \qquad (7A)$$

Equation (7A) vanishes by the fourth equation given in set (7).

In equation (4) the term giving rise to coupling between TE and TM modes is

$$\iint_s \left[\mu_{yy}\frac{\partial T_n^h}{\partial x}\frac{\partial T_m^e}{\partial y} - \mu_{xx}\frac{\partial T_m^e}{\partial x}\frac{\partial T_n^h}{\partial y}\right] ds$$

which may be written

$$\mu_o \iint_s \left[\frac{\partial T_n^h}{\partial x}\frac{\partial T_m^e}{\partial y} - \frac{\partial T_m^e}{\partial x}\frac{\partial T_n^h}{\partial y}\right] ds$$

which also vanishes from set (7).

The term giving coupling between TE and TM modes in equation (5) is

$$\iint_s \left[-\epsilon_{xx}\frac{\partial T_n^h}{\partial x}\frac{\partial T_m^e}{\partial y} + \epsilon_{yy}\frac{\partial T_n^h}{\partial y}\frac{\partial T_m^e}{\partial x}\right] ds$$

the first term vanishing because of equation (6A). The second term may be written

$$\int_o^a \int_o^b \epsilon_r(x,z)\,\frac{t\pi}{b}\,N_{st}\,\frac{p\pi}{a}\,N_{po}\,\sin\frac{s\pi}{a}x\,\cos\frac{p\pi}{a}x\,\cos\frac{t\pi}{b}y\,dxdy.$$

If this is integrated with respect to y it may be shown that it vanishes. Thus no coupling comes from equation (5).

PROOF OF COROLLARY STATED IN TEXT

The corollary of the theorem as stated in the text was: Consider a dielectric matching transition consisting of a continuously tapered dielectric of constant permeability in a uniform rectangular waveguide. If the dielectric constant is independent of y and in addition is symmetrical in x about the center of the waveguide only $TE_{2n-1,0}$ modes where n = 1, 2, 3, . . . exist in the transition when it is excited by the dominant TE_{10} mode.

For the proof of the corollary the waveguide shown in Figure 1 is used with

$$\epsilon_r(x,z) = \epsilon_r(a-x,z) \tag{8A}$$

$$\mu = \mu_o. \tag{9A}$$

Since the theorem has proven that only TE_{mO} modes may exist it is necessary to consider only equation (5) for coupling between TE_{mO} modes. The term introducing the coupling was

$$\iint_s \left[-\epsilon_{xx} \frac{\partial T_n^e}{\partial y} \frac{\partial T_m^e}{\partial y} - \epsilon_{yy} \frac{\partial T_n^e}{\partial x} \frac{\partial T_m^e}{\partial x}\right] ds.$$

The first term of this integral vanishes due to equation (6A). The second term may be written

$$\int_o^b \int_o^a \epsilon_r(x,z) \frac{nm\pi^2}{a^2} N_{nO} N_{mO} \sin \frac{n\pi}{a} x \sin \frac{m\pi}{a} x \, dxdy.$$

The y integration may be performed leaving

$$\frac{nm\pi^2}{a^2} N_{n0} N_{m0} \int_0^a \epsilon_r(x,z) \sin \frac{n\pi}{a} x \sin \frac{m\pi}{a} x \, dx$$

which may be written as the sum of two integrals

$$\frac{nm\pi^2 b}{a^2} N_{n0} N_{m0} \int_0^{\frac{a}{2}} \epsilon_r(x,z) \sin \frac{n\pi}{a} x \sin \frac{m\pi}{a} x \, dx$$

$$+ \int_{\frac{a}{2}}^a \epsilon_r(x,z) \sin \frac{n\pi}{a} x \sin \frac{m\pi}{a} x \, dx \quad .$$

In the second integral let

$$x = a - x'$$

so that it becomes

$$- \int_{\frac{a}{2}}^0 \epsilon_r(a-x',z) \sin \frac{n\pi}{a} (a-x') \sin \frac{m\pi}{a} (a-x') \, dx'. \qquad (10A)$$

Now

$$\sin \frac{k\pi}{a} (a-x') = \sin k\pi \cos \frac{k\pi}{a} x' - \cos k\pi \sin \frac{k\pi}{a} x'$$

$$\sin \frac{k\pi}{a} (a-x') = -(-1)^k \sin \frac{k\pi}{a} x'.$$

The integral of (10A) is then

$$\int_0^{\frac{a}{2}} \epsilon_r(a-x',z)(-1)^n(-1)^m \sin \frac{n\pi}{a} x' \sin \frac{m\pi}{a} x' \, dx'.$$

The variable of integration x' may be replaced by x giving

$$(-1)^{n+m} \int_{o}^{\frac{a}{2}} \epsilon_r(a-x,z) \sin \frac{n\pi}{a} x \sin \frac{m\pi}{a} x \, dx$$

However $\epsilon_r(a-x) = \epsilon_r(x)$ by hypothesis. The integral is then

$$(-1)^{n+m} \int_{o}^{\frac{a}{2}} \epsilon_r(x,z) \sin \frac{n\pi}{a} x \sin \frac{m\pi}{a} x \, dx.$$

Adding this to the first integral then gives the coupling term

$$\frac{nm\pi^2 b}{a^2} N_{nO} N_{mO} \left[1 + (-1)^{n+m}\right] \int_{o}^{\frac{a}{2}} \epsilon_r(x,z) \sin \frac{n\pi}{a} x \sin \frac{m\pi}{a} x \, dz.$$

Substitution of m = 1 then gives zero value for any n even. This proves the corollary.

APPENDIX B

```
    INPUT REFLECTION COEFFICIENT FOR SYMMETRICAL SIDE
    TAPER USING FIRST ORDER APPROXIMATION (W FIXED,
    ER VARIABLE)
    DIMENSION ZO1(6),ZO2(6),BETA(6,30),ZO(6,30),ZI(50)
    DIMENSION THETA(50)
    A=.0229
    AU=4.*3.14159*1.0E-7
    PI=3.14159
    EP=8.854E-12
    OMEGA=2.*3.14159*8.2E9
    DO 419 L=1,3
    READ 456, ER
    Z=1.0-.025
    DO 4 J=1,20
    ETA=OMEGA**2*AU*EP
    ZETA=ETA*(ER-1.0)/PI
    CHI=ETA-(PI/A)**2+2.*ZETA*(PI*Z/2.-0.5*SINF(PI*Z))
    BETA(L,J)=SQRTF(CHI)
    ZO(L,J)=OMEGA*AU/BETA(L,J)
  4 Z=Z-0.05
    ZO1(L)=OMEGA*AU/(SQRTF(ETA-(PI/A)**2))
    ZO2(L)=OMEGA*AU/(SQRTF(ER*ETA-(PI/A)**2))
    DO 403 K=1,40
    M=20
    R=M
    S=K-1
    D=S*A/8.
    DEL=D/R
    ZI(1)=ZO2(L)
    THETA(1)=0.000000
    DO 99 N=1,M
    RENUM=ZI(N)*COSF(BETA(L,N)*DEL)*COSF(THETA(N))
    G1=ZI(N)*COSF(BETA(L,N)*DEL)*SINF(THETA(N))
    AIMAG=G1+ZO(L,N)*SINF(BETA(L,N)*DEL)
    G2=ZO(L,N)*COSF(BETA(L,N)*DEL)
    REDEN=G2-ZI(N)*SINF(BETA(L,N)*DEL)*SINF(THETA(N))
    BIMAG=ZI(N)*SINF(BETA(L,N)*DEL)*COSF(THETA(N))
    SS=SQRTF(RENUM**2+AIMAG**2)
    P=ATANF(AIMAG/RENUM)
    TT=SQRTF(REDEN**2+BIMAG**2)
    Q=ATANF(BIMAG/REDEN)
    ZI(N+1)=ZO(L,N)*SS/TT
 99 THETA(N+1)=P-Q
    U=ZI(M+1)*COSF(THETA(M+1))
    V=ZI(M+1)*SINF(THETA(M+1))
    TOP=SQRTF((U-ZO1(L))**2+V**2)
    DOWN=SQRTF((U+ZO1(L))**2+V**2)
    GAMMA=TOP/DOWN
    PUNCH 123,GAMMA,D
403 PRINT 123,GAMMA,D
419 CONTINUE
```

```
      CALL EXIT
  456 FORMAT(1E18.8)
  123 FORMAT(4E18.8)
      END
```

```
      INPUT REFLECTION COEFFICIENT FOR UNSYMMETRICAL TAPER
      USING SECOND ORDER APPROXIMATION (W FIXED, AND ER
      VARIABLE)
      DIMENSION AR(4,4),AI(4,4),BR(4,4),BI(4,4),CR(4,4),CI(4,4)
      A=.0229
      PI=3.14159
      AU=4.*PI*1.E-7
      EP=8.854E-12
      W=2.*PI*8.2E9
      READ 456,ER
      DO 993 M=1,40
      S=M-1
      T=S*A/8.
      DZ=T/20.
      Z=DZ
      A2=(W**2*AU*EP-(PI/A)**2)/(W*AU)
      A3=W*EP*(ER-1.)/PI
      A4=((3.*PI/A)**2-W**2*AU*EP)/(W*AU)
      A5=W*AU*DZ
      B=(A2+A3*(PI*Z/T-0.5*SINF(2.*PI*Z/T)))*DZ
      C=(A3*(SINF(PI*Z/T)-SINF(3.*PI*Z/T)/3.))*DZ
      D=(A4-(A3/2.)*(2.*PI*Z/T-0.5*SINF(4.*PI*Z/T)))*DZ
      DO 3 I=1,4
    3 AR(I,I)=1.0
      DO 4 I=2,4
    4 AR(1,I)=0
      AR(2,1)=0
      AR(2,3)=0
      AR(2,4)=0
      AR(3,1)=0
      AR(3,2)=0
      AR(3,4)=0
      DO 5 I=1,3
    5 AR(4,I)=0
      DO 6 I=1,4
    6 AI(I,I)=0
      AI(1,2)=A5
      AI(1,3)=0
      AI(1,4)=0
      AI(2,1)=B
      AI(2,3)=0
      AI(2,4)=0
      AI(3,1)=0
      AI(3,2)=0
      AI(3,4)=A5
      AI(4,1)=C
      AI(4,2)=0
      AI(4,3)=D
      DO 213 N=1,19
      Z=Z+DZ
      B=(A2+A3*(PI*Z/T-0.5*SINF(2.*PI*Z/T)))*DZ
```

```
      C=(A3*(SINF(PI*Z/T)-SINF(3.*PI*Z/T)/3.))*DZ
      D=(A4-(A3/2.)*(2.*PI*Z/T-0.5*SINF(4.*PI*Z/T)))*DZ
      DO 13 I=1,4
   13 BR(I,I)=1.0
      DO 14 I=2,4
   14 BR(1,I)=0.
      BR(2,1)=0
      BR(2,3)=0
      BR(2,4)=0
      BR(3,1)=0
      BR(3,2)=0
      BR(3,4)=0
      DO 15 I=1,3
   15 BR(4,I)=0
      DO 16 I=1,4
   16 BI(I,I)=0
      BI(1,2)=A5
      BI(1,3)=0
      BI(1,4)=0
      BI(2,1)=B
      BI(2,3)=0
      BI(2,4)=0
      BI(3,1)=0
      BI(3,2)=0
      BI(3,4)=A5
      BI(4,1)=C
      BI(4,2)=0
      BI(4,3)=D
      DO 31 I=1,4
      DO 31 K=1,4
      CR(I,K)=0
      CI(I,K)=0
      DO 31 J=1,4
      CR(I,K)=CR(I,K)+AR(I,J)*BR(J,K)-AI(I,J)*BI(J,K)
   31 CI(I,K)=CI(I,K)+AR(I,J)*BI(J,K)+AI(I,J)*BR(J,K)
      DO 11 I=1,4
      DO 11 J=1,4
      AR(I,J)=CR(I,J)
   11 AI(I,J)=CI(I,J)
  213 CONTINUE
      ZO1L=W*AU/SQRTF(W**2*AU*EP*ER-(PI/A)**2)
      ZO10=W*AU/SQRTF(W**2*AU*EP-(PI/A)**2)
      IF(W**2*AU*EP*ER-(2.*PI/A)**2)30,39,39
C     FOR TE20 MODE CUTOFF
   30 AA=AR(1,1)*ZO1L+AR(1,2)
      AB=AI(1,1)*ZO1L+AI(1,2)
      BB=AR(2,1)*ZO1L+AR(2,2)
      BA=AI(2,1)*ZO1L+AI(2,2)
      AC=SQRTF(AA**2+AB**2)
      AD=SQRTF(BB**2+BA**2)
      T1=ATANF(AB/AA)
      T2=ATANF(BA/BB)
      VI=AC/AD
      ANG=T1-T2
```

```
      GO TO 43
C     FOR PROPAGATION OF TE20 MODE
   39 AC=AR(3,4)+AR(3,3)*ZO2L
      AD=AI(3,4)+AI(3,3)*ZO2L
      AE=AR(3,1)*ZO1L+AR(3,2)
      AF=AI(3,1)*ZO1L+AI(3,2)
      ZO2L=W*AU/SQRTF(W**2*AU*EP*ER-(2.*PI/A)**2)
      RI2=-1.0*(AE*AC+AF*AD)/(AC**2+AD**2)
      EI2=-1.0*(AC*AF-AD*AE)/(AC**2+AD**2)
      G1=AR(1,1)*ZO1L+AR(1,2)+AR(1,3)*ZO2L*RI2
      VIR=G1+AR(1,4)*RI2-AI(1,3)*ZO2L*EI2-AI(1,4)*EI2
      G2=AI(1,1)*ZO1L+AI(1,2)+AI(1,3)*ZO2L*RI2
      VII=G2+AI(1,4)*RI2+AR(1,3)*ZO2L*EI2+AR(1,4)*EI2
      G3=AR(2,1)*ZO1L+AR(2,2)+AR(2,3)*ZO2L*RI2
      EIR=G3+AR(2,4)*RI2-AI(2,3)*ZO2L*EI2-AI(2,4)*EI2
      G4=AI(2,1)*ZO1L+AI(2,2)+AI(2,3)*ZO2L*RI2
      EII=G4+AI(2,4)*RI2+AR(2,3)*ZO2L*EI2+AR(2,4)*EI2
      VI=SQRTF(VIR**2+VII**2)/SQRTF(EIR**2+EII**2)
      ANG=ATANF(VII/VIR)-ATANF(EII/EIR)
   43 BBB5=VI*COSF(ANG)+ZO10
      AAA5=VI*COSF(ANG)-ZO10
      AAA6=VI*SINF(ANG)
      TOP=SQRTF(AAA5**2+AAA6**2)
      DOWN=SQRTF(BBB5**2+AAA6**2)
      GAMMA=TOP/DOWN
      PUNCH 100,GAMMA,T
  993 PRINT 100,GAMMA,T
  888 CONTINUE
  456 FORMAT (1E18.8)
  100 FORMAT (4E18.8)
      CALL EXIT
      END
```

```
      EVALUATION OF INTEGRAND FOR SYMMETRICAL SIDE TAPER
      DIMENSION F(30)
      N=20
      PI=3.14159
      W=2.*PI*8.2E9
      EP=8.854E-12
      ER=1.7
      AU=4.*PI*1.E-7
      A=.0229
      D=A
      Z=0.0
      DO 103 I=1,81
      G1=(W*EP*(ER-1.)/D)*(1.-COSF(PI*Z/D))
      G2=(W**2*AU*EP-(PI/A)**2)/(W*AU)
      G3=(2.*W*EP*(ER-1.)/PI)*(.5*PI*Z/D-.5*SINF(PI*Z/D))
      T=(-.25*G1)/(G2+G3)
      R=N
      H=Z/R
      R1=W**2*AU*EP-(PI/A)**2
      DO 33 J=1,21
      R2=(2.*W**2*AU*EP*(ER-1.)/PI)*(.5*PI*Z/D
      -.5*SINF(PI*Z/D))
   33 F(J)=SQRTF(R1+R2)
      FO=F(2)+F(4)+F(6)+F(8)+F(10)+F(12)+F(14)+F(16)
      +F(18)+F(20)
      FE=F(3)+F(5)+F(7)+F(9)+F(11)+F(13)+F(15)+F(17)+F(19)
      PHI=(-2.*H/3.)*(F(1)+4.*FO+2.*FE+F(21))
      X=T*COSF(PHI)
      Y=T*SINF(PHI)
      PRINT 100,X,Y
      PUNCH 100,X,Y
  103 Z=Z+D/80.
  100 FORMAT (2E18.8)
      CALL EXIT
      END
```

```
    CALCULATION OF TAPER SHAPE FOR PARABOLIC LINE
    A=.0229
    PI=3.14159
    W=2.*PI*8.2E9
    AU=4.*PI*1.E-7
    EP=8.854E-12
    ER=1.7
    Z01=625.483
    Z02=365.438
    ETA=(W**2*AU*EP-(PI/A)**2)/(W*AU)
    Z=.0125
    DO 3 J=1,79
    Z0=Z01+3.*(Z02-Z01)*(Z**2)+2.*(Z01-Z02)*(Z**3)
    XA=.1*A
    XB=.9*A
 40 T=(A/(W*EP*(ER-1.)))*(W*AU/(Z0**2)-ETA)
    FA=XA-(.5/PI)*SINF(2.*PI*XA/A)*A-T
    FB=XB-(.5/PI)*SINF(2.*PI*XB/A)*A-T
    XC=(FB*XA-FA*XB)/(FB-FA)
    FC=XC-(.5/PI)*SINF(2.*PI*XC/A)*A-T
    IF(FC)30,20,10
 10 IF(ABSF(XC-XB)-5.E-7)20,60,60
 60 XB=XC
    GO TO 40
 30 IF(ABSF(XC-XA)-5.E-7)20,80,80
 80 XA=XC
    GO TO 40
 20 PRINT 100,XC,Z
    PUNCH 100,XC,Z
  3 Z=Z+.0125
    CALL EXIT
100 FORMAT (2E18.8)
    END
```

```
      THE VARIATION OF ZO WITH FREQUENCY FOR THE BESSEL LINE
      DIMENSION D(21),Z(21)
      ER=1.7
      PI=3.14159
      EP=8.854E-12
      AU=4.*PI*1.E-7
      A=.0229
      W=2.*PI*8.2E9
      READ 100,(D(J),Z(J),J=1,21)
      DO 4 I=1,5
      ETA=(W**2*AU*EP-(PI/A)**2)/(W*AU)
      CHI=(W*EP*(ER-1.))/PI
      DO 5 J=1,21
      Y1=ETA+CHI*(PI*D(J)/A-0.5*SINF(2.*PI*D(J)/A))
      ZO=SQRTF(W*AU/Y1)
      PUNCH 100,ZO,Z(J)
    5 PRINT 100,ZO,Z(J)
    4 W=W+2.*PI*.4E9
  100 FORMAT(2E18.8)
      CALL EXIT
      END
```

```
C       PLOT GAMMA
        CALL PENPOS (2.0)
        CALL PLOT(1,0.0,5.0,15.0,.25,0.0,0.7,10.0,0.050)
        DO 30 J=1,3
        DO 10 I=1,40
        READ 100, Y,D
        X=D/.0229
   10   CALL PLOT (0,X,Y)
   30   CALL PLOT (99)
        DO 40 J=1,3
        DO 20 I=1,40
        READ 100, Y,D
        X=D/.0229
        CALL PLOT (0,X,Y)
   20   CALL SYMBOL (4)
   40   CALL PLOT (99)
        CALL PLOT (7)
        CALL PLOT (7)
        CALL EXIT
  100   FORMAT (2E18.8)
        END
```

VITA

The author was born October 17, 1938 in Leola, South Dakota. He received his elementary education at Warsaw Grade School and his secondary education at Warsaw High School both in Warsaw, Illinois. In September 1955 he entered the Missouri School of Mines and Metallurgy from which he was graduated with a Bachelor of Science Degree in Electrical Engineering in June 1959.

In September 1960 he was appointed Instructor of Electrical Engineering and began his graduate work at the Missouri School of Mines and Metallurgy. He recieved the Master of Science Degree in Electrical Engineering in June 1963.

The author was employed by Sperry Gyroscope Company from June 1959 until September 1960. He also worked for Speery during the summers of 1961 and 1962. He was employed by the Emerson Electric Company of St. Louis during the summers of 1963 and 1964.

He is married to the former Reva Sallee and is the father of two children; Diana Lynn and Robert.